Université de Lille

CRIStAL
Centre de Recherche en Informatique,
Signal et Automatique de Lille

Curve Based Approach for Shape Reconstruction of Continuum Manipulators

PhD THESIS
to obtain the title of

Doctor from Université de Lille
Speciality : Robotics

Defended by

Inderjeet Singh

prepared at
CRIStAL CNRS-UMR 9189

defended on September 24, 2018
at Polytech Lille

Jury

Reviewers :	Pr. Véronique Perdereau	-	University of Paris-Sorbonne
	Pr. Ian Walker	-	University of Clemson, USA
Examiners :	Dr. Christian Duriez	-	INRIA Lille
	Dr. Falotico Egidio	-	Scuola Superiore Sant'Anna, Italy
	Pr. Geneviève Dauphin-Tanguy	-	Ecole Centrale de Lille
	Pr. Taha Chettibi	-	Ecole Militaire Polytechnique, Algeria
Supervisor :	Pr. Rochdi Merzouki	-	University of Lille

Modélisation par des Courbes pour la Reconstruction des Formes de Manipulateurs Continuums

THÉSE

soumise à l'Université de Lille pour le degré de

Doctorat

Spécialisation : Robotique

par

Inderjeet Singh

préparée au laboratoire

CRIStAL CNRS-UMR 9189

soutenue le September 24, 2018

à Polytech Lille

Jury

Reviewers :	Pr. Véronique Perdereau	-	University of Paris-Sorbonne
	Pr. Ian Walker	-	University of Clemson, USA
Examiners :	Dr. Christian Duriez	-	INRIA Lille
	Dr. Falotico Egidio	-	Scuola Superiore Sant'Anna, Italy
	Pr. Geneviève Dauphin-Tanguy	-	Ecole Centrale de Lille
	Pr. Taha Chettibi	-	Ecole Militaire Polytechnique, Algeria
Supervisor :	Pr. Rochdi Merzouki	-	University of Lille

Curve Based Approach for Shape Reconstruction of Continuum Manipulators

Abstract

This work provides a new methodology to reconstruct the shape of continuum manipulators using a curve based approach. Pythagorean Hodograph (PH) curves are used to reconstruct the optimal shape of continuum manipulators using minimum potential energy (bending and twisting energy) criteria. This methodology allows us to obtain the optimal kinematics of continuum manipulators. The models are applied to a continuum manipulator, namely, the Compact Bionic Handling Assistant (CBHA) for experimental validation under free load manipulation. The calibration of the PH-based shape reconstruction methodology is performed to improve its accuracy to accommodate the uncertainties due to the structure of the manipulator. The proposed method is also tested under the loaded manipulation after combining it with a qualitative Neural Network approach. Furthermore, the PH-based methodology is extended to model multi-section heterogeneous bodies. This model is experimentally validated for a closed loop kinematic chain formed using two CBHAs manipulating jointly a rope.

Keywords: Continuum manipulators, Shape reconstruction, Pythagorean Hodograph curves, Continuum kinematics.

Modélisation par des courbes pour la reconstruction des formes de manipulateurs continuums

Résumé

Ce travail de thèse propose une nouvelle méthode de modélisation et de reconstruction de la forme d'une classe de manipulateurs continuum, basée sur la géométrie des courbes. Les Hodographes Pythagoriens (courbes HP) sont utilisées pour reconstruire des formes optimales pour ce type de robots, par une optimisation des énergies potentielles de flexion et de torsion. Cette méthode nous permis de déduire la cinématique optimale des bras manipulateurs continuum. La validation de la méthode proposée a été réalisée sur le robot dit trompe d'éléphant 'Compact Bionic Handling Assistant (CBHA)'. Une calibration a été réalisée sur la méthode de reconstruction afin d'améliorer les performances en terme de précision et de prendre en considération les incertitudes dues à la structure du bras manipulateur. La méthode proposée est également testée dans le cas de la préhension, en s'appuyant sur une approche qualitative à base de réseaux de neurones. De plus, l'approche HP est étendue à la modélisation des structures de robots hétérogènes avec plusieurs sections. Ce dernier a été validé pour une chaîne cinématique fermée, composée de deux manipulateurs CBHA, manipulant conjointement une corde flexible.

Mots clés: Manipulateurs continuums, Reconstruction des formes, Pythagorean Hodograph Courbes, Cinématiques continuums.

This thesis is dedicated to my parents, Parminder Singh and Jagmeet Kaur, and my sister, Manpreet Kaur, for their love, endless support and encouragement.

Acknowledgments

Contents

List of Figures

List of Tables

Introduction

Contents

1.1 General Introduction

Advances in technology introduce the concept of robotics in the human world. This technology is growing rapidly according to human needs. Today, there are many types of robot systems under development or in use. For most of the applications, a robotic arm (manipulator) is necessary (e.g., supplying food or handling objects, etc.). In the beginning, rigid robotic manipulators were developed to perform specific applications (e.g., industrial, military, medical, space and electronics). With the technology developments since last decade on actuators, sensors, and structures based on 3D printing, a new type of manipulators with soft behavior have been born. These manipulators are used to reproduce bio-inspired tasks. A spreading number of industries and researchers are viewing to the soft manipulators as an exciting and new technology because it has many notable advantages. The most pronounced one is the safety provided by their compliant parts. Whenever there is a need for human-robot interaction (e.g., the interaction of workers with robots, guides in museums, etc.), soft manipulators serve as an additional safety layer. Also, there are some applications where soft manipulators are required (e.g., in the agricultural application: to pick fruits and vegetables, in the medical field: lifting and carrying patients, minimally invasive surgery, etc..). Figure 1.1 shows an evolution from rigid robotic manipulators to the soft manipulators. To get flexible motion, rigid manipulators are evolved to soft manipulators with a transition phase of hyper-redundant manipulators. Soft manipulators have the following properties:
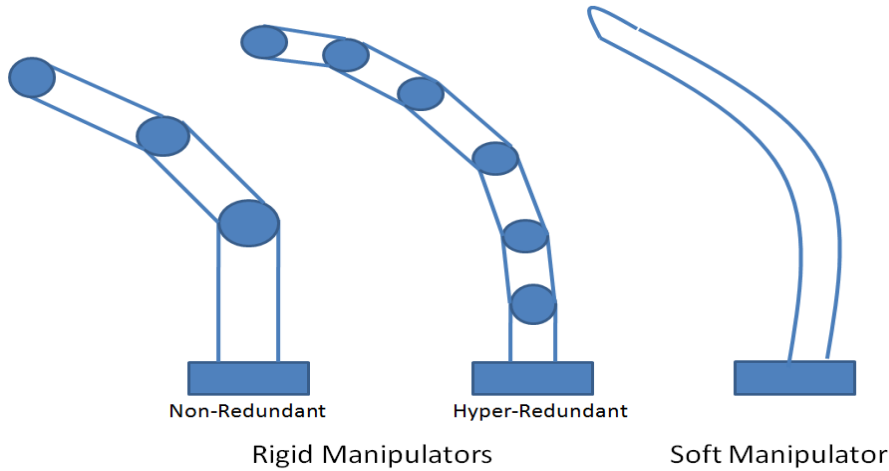
Figure 1.1: Evolution from rigid to soft manipulators

- Mechanical structure made by rapid manufacturing;

- Low cost because of the use of soft materials (e.g., polyamides, silicon, carbon fibers, etc.);

- Bionic gripper which makes them to interact with the delicate environment;

- Lightweight structure

These properties made them more challenging these days, where various research topics are launched.

Many decades have been passed involving the research in the field of modeling and controlling of soft manipulators. Still, to get an accurate model for such type of manipulators is an open problem. Development of a generic algorithm to model each type of soft manipulators is not an easy task. The main reason behind this is the bio-inspiration to develop the soft manipulators. Nature offers tremendous shapes and motion mechanisms from which we gather information to design such manipulators. To reach the main goal to control the soft manipulators accurately, it is essential to reconstruct their behavior precisely. As per the application, the behavior can be kinematic or dynamic. With continuum structure, these manipulators are described by an infinite number of degrees of freedom. This makes it complex to model such manipulators without considering assumptions. Thus, it is possible to limit the number of degrees of freedom but keeping it high to converge to hyper-redundant manipulators. The other main problem in case of such manipulators is their inherent hyper-redundancy due to their soft material which makes them possible to reach a particular position in their workspace with different possible postures. Therefore, along with the kinematic models, the optimal shape approximation of these manipulators is equally important. Figure 1.2 shows the manipulators in the order of the increase in the degrees of freedom.

Increase in degrees of freedom

Dof=6	Dof~10-15	Dof~20-30	Dof=infinite
Rigid Manipulators	Redundant Manipulators	Hyper-redundant Manipulators	Continuum Manipulators
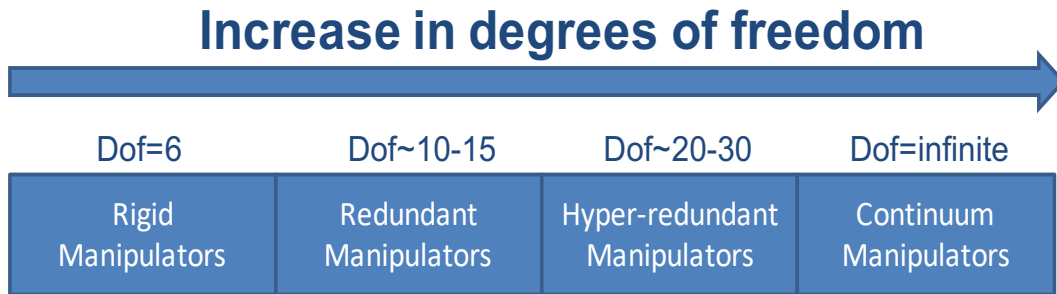
Figure 1.2: Increase in the degrees of freedom in the manipulators

1.2 Framework and Context of the Thesis

This Ph.D. thesis is prepared in the research group "Méthodes et Outils pour la Conception Intégrée de Systémes (MOCIS)"[1], of the laboratory "Centre de Recherche en Informatique, Signal et Automatique de Lille (CRIStAL) (UMR CNRS 9189)"[2]. This work has been developed in the framework of a joint collaborative research project between CNRS in France and DST (Department of Science & Technology)[3] in India (PRC CNRS-DST 2016-2018). This project aims to develop a dynamic model for collaborative mobile bionic robots. The robot under consideration is 'Robotino XT' developed by FESTO-DIDACTIC [fes 2018]. This robot consists of a soft bionic arm called Compact Bionic Handling Assistant (CBHA), attached to an omni-directional mobile base, called Robotino. The present work focuses on determining the behavior (shape) as well as kinematic models of the soft-continuum manipulators. This work is developed under the supervision of Mr. Rochdi Merzouki, Professor at Ecole Polytechnique Universitaire de Lille.

1.3 Thesis Objective

Soft-continuum manipulators are very popular these days due to the possibility of their interaction with biological environments (medical and treatment applications etc...). Due to the need for accurate models for these manipulators, there are continuous advancements in this research field. The present work proposes a novelty in the area of soft-continuum manipulators.
The main goal of this Ph.D. work is the development of an optimal model to approximate the shape of the soft-continuum manipulators using Pythagorean Hodograph (PH) curves [Farouki 2008], leading to the calculation of their kinematic models (forward and inverse). This work has been applied to the open loop kinematic of the Compact Bionic Han-

---

[1] https://www.cristal.univ-lille.fr/?rubrique27&eid=24
[2] https://www.cristal.univ-lille.fr
[3] https://www.dst.gov.in

dling Assistant (CBHA) manipulator and closed loop heterogeneous kinematic chain for experimental validation.

The purpose of this model is to approximate the shape of the manipulator which can be further used for future applications (e.g., obstacle avoidance, dynamics, etc..).

1.4 Research Problem Statement

Soft-continuum manipulators are increasingly used in scientific research in the last decade. They are inspired from biological entities like elephant trunk [Zhao 2010], octopus [Zheng 2014] etc... To improve the closed-loop control of soft-continuum manipulators, it is essential to develop accurate models, starting from the optimal shape modeling, kinematic models and converging to the dynamic models.

The hyper-redundant nature of soft-continuum manipulators allows them to have multiple postures for a single pose in the task space. If $r(h)$ is the curve representing the shape of a single soft-continuum manipulator, reconstructed using the four known variables P_s (position vector at the base of the manipulator), d_s (direction vector at the base point P_s), P_f (position vector at the tip of the manipulator) and d_f (direction vector at the tip point P_f) as shown in Fig. 1.3, the problem statement to model the n number of links in a kinematic chain using n number of curves $r_n(h)$ is stated as

$$P_{s_n}(x_{s_n}, y_{s_n}, z_{s_n}), d_{s_n}(d_{xs_n}, d_{ys_n}, d_{zs_n}) \overset{r_n(h)}{\rightarrow} \atop P_{f_n}(x_{f_n}, y_{f_n}, z_{f_n}), d_{f_n}(d_{xf_n}, d_{yf_n}, d_{zf_n}) \tag{1.1}$$

where h represents the curvilinear coordinate along the curve. In our case, the problem of reconstructing the optimal posture of soft-continuum manipulators, having length L and potential energy E, is formulated as follows:

$$minimize \quad E = \int (\omega^2(L)) dL \tag{1.2}$$

$$\omega = \sqrt{\kappa^2 + \tau^2} \tag{1.3}$$

$$subject\ to \quad L_{min} \leq L \leq L_{max} \tag{1.4}$$

Where ω is the total bending of the soft-continuum manipulator, it is the combination of its bending and twisting energy. The curvature and the torsion are represented by κ and τ respectively.

Kinematic modeling of soft-continuum manipulators can be classified into two approaches: quantitative and qualitative. Quantitative approaches are model-based approaches while the qualitative approaches are learning-based approaches. Due to their soft materials and complex structures, modeling of continuum manipulators is a cumbersome task.

Generally, the forward kinematic model imposes a specific posture to the manipulator according to the known joint coordinates $L(h)$ to calculate the end-effector position. h represents the curvilinear coordinate along the curve.

$$P_f = g[L(h)] \tag{1.5}$$

In the case of the soft-continuum manipulators, the joint space consists of the
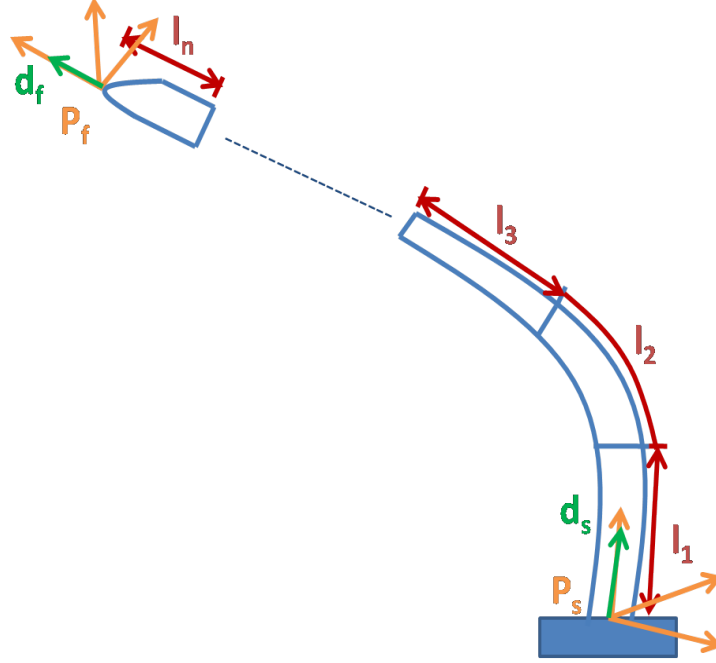
Figure 1.3: Soft-continuum manipulator

achievable lengths of the various sections of the manipulator as shown in Fig. 1.3. Therefore, by fixing the values of the input lengths, the tip position (P_f) of the manipulator can be determined. The inverse kinematics model of a soft-continuum manipulator is stated as:

$$L(h) = g^{-1}[P_f] \tag{1.6}$$

In this model, we need to compute the joint lengths of the manipulator for a particular tip position in its workspace. But the continuum manipulators can have infinite solutions (postures) to reach the tip position due to their inherent hyper-redundancy. Therefore, at first, it is an essential task to compute the optimal posture of the soft-continuum manipulators.

Then, it is possible to answer the Golden Circle questions: Why, How, What related to the contributions of this Ph.D. thesis:

Why this research? Real-time optimization of the posture and kinematics of soft-continuum manipulators.

How to model? Geometrical curve-based modeling for the shape reconstruction and the kinematics computation of the soft-continuum manipulators.

What approach? PH polynomial curves reconstruct the posture, based on an optimal solution of the potential energy, with a low computational cost.

1.5 Contribution Positioning in the Framework of the Group Activities

The present work is performed for a class of soft-continuum manipulators named Compact Bionic Handling Arm 'CBHA'. The latter has been studied in previous research works developed in our group: Since 2012, the MOCIS group has been working on the kinematic modeling of a class of soft manipulator in open chain and with a continuum behavior. These robot structures, issued from 3D printing are lightweight, flexible and have compliant material properties. However, by their hyper-redundant characteristics with an unusually high number of degrees of freedom, it is difficult to achieve control performance described by a rigid manipulator. Thus, the work of the group in recent years has focused on the development of kinematic models of CBHA, optimized for real-time applications, using different approaches: quantitative using arc geometry methods [Escande 2015] under the assumption of constant curvature; qualitative using learning approximation of neural network for both modeling and control [Melingui 2015]; hybrid using quantitative method to approximate the behavior of the CBHA, emulated by a succession of serial-parallel robot-section, with a qualitative neural network-based approach to approximate the solving of the kinematic model [Lakhal 2016]. Finally, computational mechanics using the finite element method [Bieze 2018].

1.6 Main Contributions

The main contributions of the present work are:

1. The shape of the soft-continuum manipulators is modeled using PH curves. PH curves approximate the optimal shape using minimum potential energy (bending as well as twisting energy) criteria. Further, the PH reconstructed shape is improved to accommodate the uncertainties due to the structure of the manipulator.

2. PH shape reconstruction allows to calculate the optimal inverse kinematic solution for the purpose of control at the task space. Further, the forward kinematic model is deduced in the free-load case and performed in case of loaded manipulator after combining with a qualitative neural network approach.

3. The PH approach is extended to model multi-section heterogeneous bodies.

4. Experimental validation of the presented approach is done on a class of soft-continuum manipulators called CBHA. Then a closed loop heterogeneous kinematic chain is formed with two CBHA manipulators holding a rope (a passive link) which illustrates the application of skipping rope. This chain is built to validate the model of multi-section heterogeneous bodies.

1.7 Disseminated Results

The results are disseminated through the following publications:

Journal

1. Inderjeet Singh, Yacine Amara, Achille Melingui, Pushparaj Mani Pathak, Rochdi Merzouki. Modeling of Continuum Manipulators using Pythagorean Hodograph Curves. Soft Robotics Journal. Mary Ann Liebert, Inc. DOI: 10.1089/soro.2017.0111.

International Conferences

1. Inderjeet Singh, Yacine Amara, Rochdi Merzouki. PH Model-based Shape Reconstruction of Heterogeneous Continuum Closed Loop Kinematic Chain: An Application to skipping Rope. In Intelligent Robots and Systems (IROS), 2018 IEEE/RSJ International Conference.

2. Inderjeet Singh, Yacine Amara, Manarshhjot Singh, Rochdi Merzouki. Towards Accurate Shape Reconstruction of Compact Bionic Handling Arm. IEEE/ASME International Conference on Advanced Intelligent Mechatronics (AIM 2018), July 2018, Auckland, New Zealand.

3. Inderjeet Singh, Othman Lakhal, Yacine Amara, Vincent Coelen, Pushparaj Pathak, Rochdi Merzouki. Performances Evaluation of Inverse Kinematic Models of a Compact Bionic Handling Assistant. IEEE Conference on Robotics and Biomimetics (ROBIO) 2017, pp. 264-269.

4. Inderjeet Singh, Manarshhjot Singh, Pushparaj Pathak, Rochdi Merzouki. Optimal Work Space of Parallel Continuum Manipulator Consisting of Compact Bionic Handling Arms. IEEE Conference on Robotics and Biomimetics (ROBIO 2017), pp. 258-263. Selected among the finalists of best student paper award.

5. Mulu Girmay, Inderjeet Singh, Pushparaj Mani Pathak, A.K. Samantaray, Rochdi Merzouki, Belkacem Ould Bouamama. Dynamic Modelling of Cooperative Planar Bionic Manipulator. 3rd International and 18th National Conference on Machines and Mechanisms (iNaCoMM 2017), Dec 2017, Mumbai, India.

6. Inderjeet Singh, Othman Lakhal, Rochdi Merzouki. Towards Extending Forward Kinematic Models on Hyper-Redundant Manipulator to Cooperative Bionic Arms. 13th European Workshop on Advanced Control and Diagnosis (ACD 2016). Journal of Physics: Conference Series (vol. 783, No.1, p. 012056), IOP Publishing.

1.8 Manuscript Organization

The document is organized in the following five chapters:

- The second chapter summarizes the state of the art in the area of shape as well as kinematic models developed for the soft-continuum manipulators. This chapter allows to make a concrete positioning of our work compared to the existing literature in the field of modeling soft-continuum manipulators.

- The third chapter presents the shape reconstruction of soft-continuum manipulators using different curve formulations. This chapter discusses the theory of different curves for the shape reconstruction and their application to the CBHA. Also, the improvement in the reconstructed shape is performed using experimental data issued from the external tracking system.

- The fourth chapter deals with the kinematics of the soft-continuum manipulators based on PH-curves approach. Forward, as well, Inverse kinematics are presented using PH curves for both freeload and loaded manipulators. Further, the experimental validation of the discussed approach is done for the CBHA manipulator.

- The fifth chapter expands the proposed PH-based approach for overall shape reconstruction of multi-section heterogeneous continuum manipulators. The experimental validation is presented for a closed loop heterogeneous kinematic chain formed using two CBHA manipulators holding a passive segment described by a rope.

- Finally, the sixth chapter summarizes the conclusion of the main contributions and the future prospects of the work.

State of the Art on Soft-continuum Manipulators: Shape & Kinematics

Contents

2.1 Introduction

Soft-continuum manipulator robots present a rapidly growing research field. Various research works are developed in this area to overcome the problems of modeling and control of this class of robots. In this chapter, the soft-continuum manipulators are defined in the context of our work. The State of the art concerns the shape reconstruction and kinematic modeling of soft-continuum manipulators. It allows to make a positioning of our work in the framework of the current literature.

2.2   Soft-continuum Manipulator

2.2.1   Definition

It is better to start with the conventional rigid manipulators to reach to the concept of soft-continuum manipulators. The conventional rigid manipulators are composed of serially connected rigid links joined by specific joints. In these manipulators, by knowing the lengths of the links, the relative positions of the joints can be deduced w.r.t. a reference frame [Siciliano 2016]. Let us consider that we begin adding more rigid links to the rigid manipulators until our manipulator will have more degrees of freedom [1] than the ones required to place an object in the space. This type of manipulators are known as hyper-redundant manipulators in the literature [Hirose 2004] (Fig. 2.1). If we are further adding more links to the manipulator till the point, the number of links approaches to infinite, and their length approaches to zero, the robot will finally approach to what is known as continuum manipulator. The continuum manipulators made up of soft material are known as soft or soft-continuum manipulators. There are manipulators which are not made up of soft material but are continuum, e.g. a continuum manipulator used for endoscopy purpose (Fig. 2.2).

The definition provided may imply that all of the degrees of freedom in

(a)   (b)   (c)
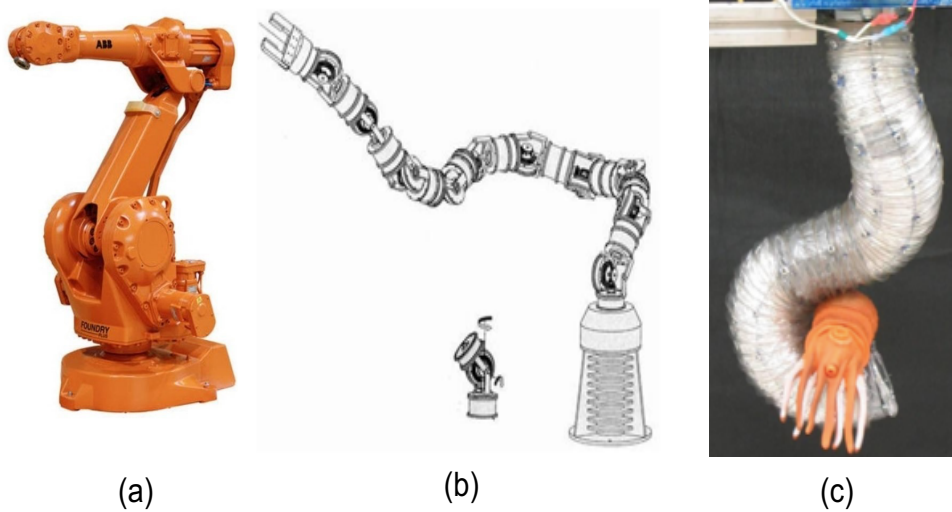
Figure 2.1: (a) A rigid industrial manipulator (ABB IRB 2400L), (b) A hyper-redundant robot, the transition phase between rigid and continuum manipulators [Vujović 2016], (c) A soft-continuum Air-Octor manipulator [Walker 2013]

---

[1]In robotics, two types of degrees of freedom exist; active and passive. Passive degrees of freedom cannot be directly controlled and conform passively to the motion of the robot, while active degrees of freedom are controlled to provide the required forces to move the manipulator.
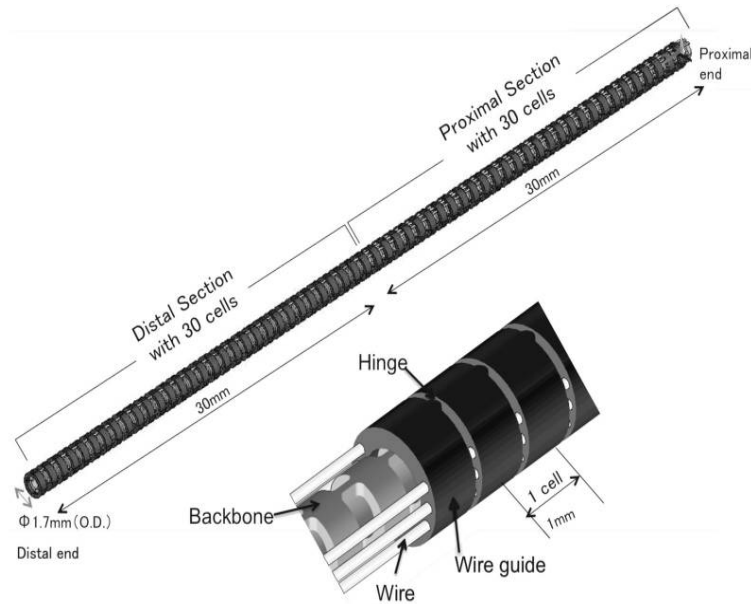
Figure 2.2: Two section continuum robot design for endoscopy [Kato 2013]

a continuum manipulator are controllable; generally, it is not the case. Often the continuum manipulators are bio-inspired by the functionality of biological limbs, octopus tentacles [Zheng 2014] [Zhao 2010], elephant trunk [Behrens 2012], and the other mammals. Continuum manipulators have a long structure without any identifiable joints, which can continuously bend via elastic deformation [Robinson 1999].

2.2.2   Soft-continuum Robot Applications

Soft-continuum manipulators are becoming more popular nowadays. The very first prototype of the continuum manipulator [Anderson 1967] suggested their use in the inspection [Tonapi 2014], search and the rescue tasks [Li 2017] [Bajo 2010].
The characteristics of soft-continuum manipulators, their compact structure, compliant nature, light-weight structure, make them suitable for many applications. The profound use of soft-continuum manipulators is in the work environment where humans have to interact with the robots. This involves the application of continuum robots in the medical field. Applications, such as, endoscopy [Fraś 2015] [Conrad 2013] [Cianchetti 2013], skeleton trauma treatment [Alambeigi 2017] [Wilkening 2017] and minimally invasion surgery [Orekhov 2016] [Qu 2016] [Mahoney 2016] have proved the use of continuum manipulators in the medical field [Burgner-Kahrs 2015].

2.2.3   Classification

Continuum manipulators can be broadly classified according to the type of backbone they possess. Therefore, they are classified as single or multi-backbone manipulators. Single backbone manipulators (Fig. 2.4 (left)) use to have a central structure along the manipulator which supports the passage of the actuation system along the body of the manipulator [Burgner-Kahrs 2015]. Many single backbone manipulators have tendons along their structure, which are spaced by the discs attached to the backbone as a way of transmission. The end-points of the tendons define the length of the bending section. Fig. 2.4 (right) shows a multi-backbone continuum manipulator. These manipulators normally consist of a parallel arrangement of the elastic elements constrained in a way.

Soft-continuum robots are bio-inspired robots. The classification of bionic manipulators is shown in Fig. 2.3.
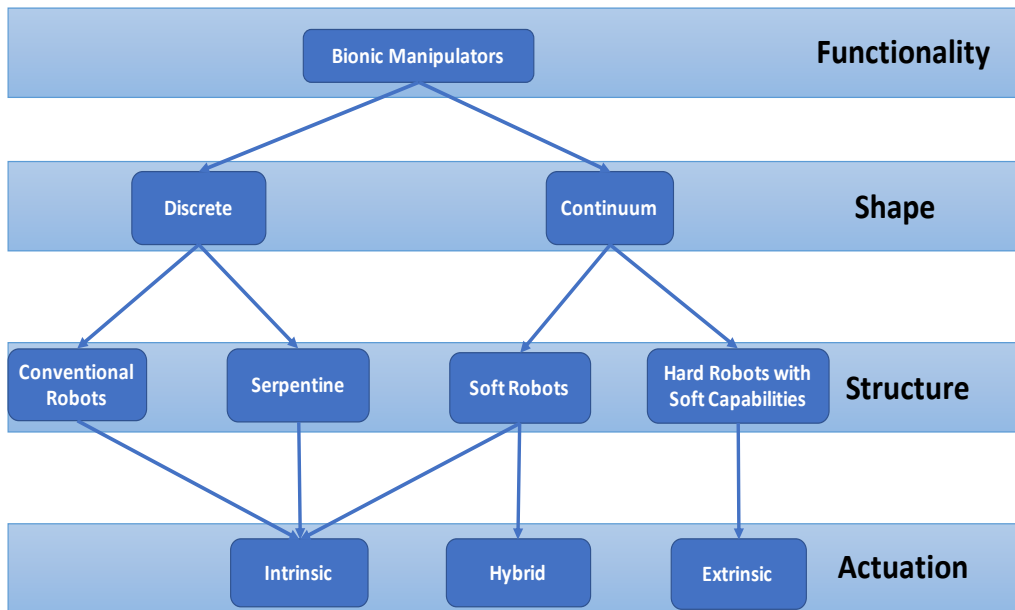
Figure 2.3: Classification of bionic manipulators

Our work deals with the continuum manipulators having soft structure. Therefore another classification of the continuum manipulators is based on the actuation used. It can be intrinsic, extrinsic or hybrid. As per classification (Fig. 2.3), the soft-continuum manipulators can have either intrinsic or hybrid actuation. When the actuation system is embedded in the structure of the continuum manipulator and applies force to the backbone directly, it is called intrinsic actuation system. The BHA manipulator (Fig. 2.5(b)) is an intrinsic pneumatically actuated manipulator.
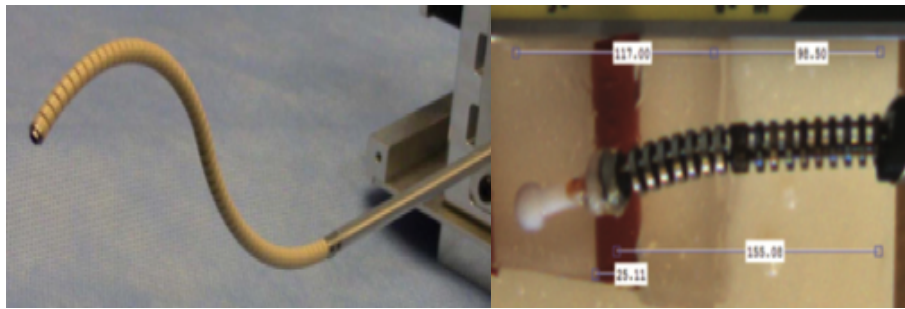
Figure 2.4: Single and multi backbone continuum robots: (left) A single backbone tendon-drive steerable catheter [Kato 2016]. (right) Multi backbone manipulator [Bajo 2016]
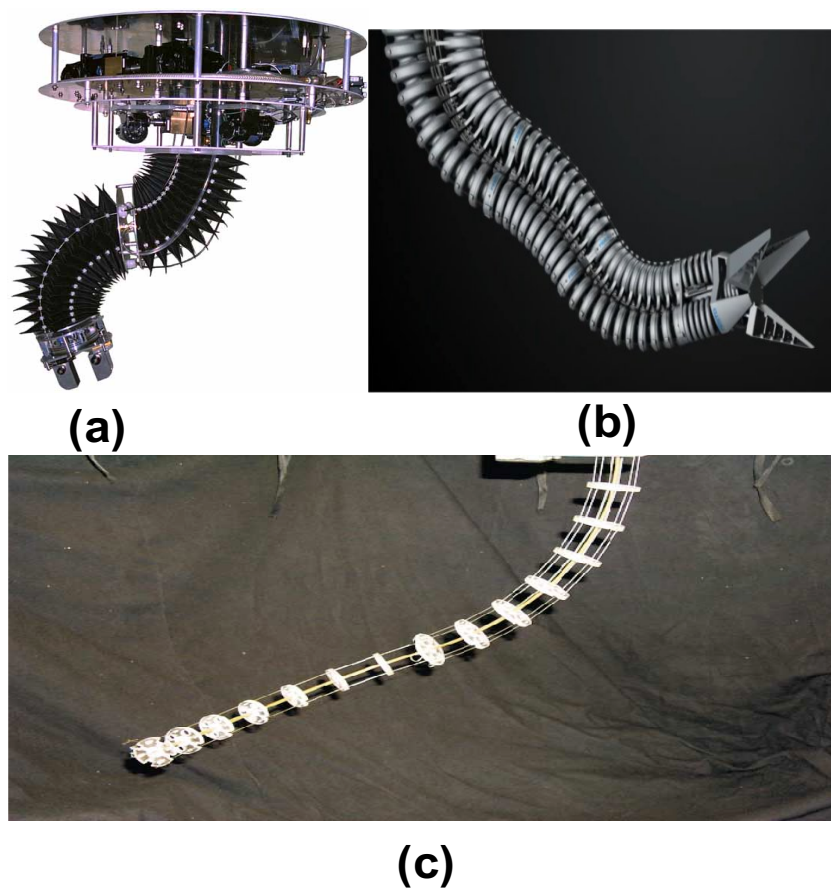
Figure 2.5: Different types of actuations: (a) Hybrid actuation- The KSI manipulator [Immega 1995], (b) The BHA intrinsic type actuated manipulator [Rolf 2012], (c) The Clemson tentacle-extrinsic actuated manipulator [Gravagne 2001]

Extrinsic actuation is defined as the actuation which applies torque and force to the backbone of the manipulator from outside of the structure of the robot. They apply localized force via a mechanical link to the backbone (Fig. 2.5(c)).

Hybrid actuation is the actuation which has both intrinsic and extrinsic actuation. Generally, the central cavity of the manipulators having extrinsic actuation is actuated by an actively controlled actuator. The example of a hybrid actuated KSI manipulator is shown in Fig. 2.5(a). Many designs of hybrid actuated manipulators have pneumatic actuation in the cavity of the structure [Chirikjian 2015], [Ataollahi 2017].

2.3   Shape Estimation of Soft-continuum Manipulators

Soft-continuum manipulators have enormous advantages which enable their use in many applications. Their ability to manipulate through confined spaces is extensively used in many applications like medical, military, and nuclear, etc. Many research works are devoted to model kinematics and dynamics of the soft-continuum manipulators and are continuously developing to enhance their accuracies, for the purpose of control strategy development. Shape estimation of soft-continuum manipulators still has very limited literature. The classification of the shape estimation approaches for the soft-continuum manipulators is as shown in Fig. 2.6.

2.3.1   Sensor Based Approaches

Most of the literature regarding shape estimation of the soft-continuum manipulators covers sensor based approaches. They need to install the specific sensors to measure and estimate the shape of the robots. Therefore, the placement and the dimension of these sensors is important according to the type of the robot. Also, these approaches request associated investments. Following existing works using different types of sensors are discussed as follows:

2.3.1.1   Fiber Bragg Gratings (FBGs)

FBG sensors are commonly used sensors in the field of shape estimation. A small sized sensor is introduced in [Araújo 2001] which can be embedded in any layer of a composite material. The configuration of this sensor is based on the intrinsic bend sensitivity of Bragg gratings written in D-type fibers. The sensor gives the information of the curvature of the manipulator at the points at which the sensors are embedded. Further, curvature information is used for the shape reconstruction of the soft-continuum manipulators. These sensors are suitable to use in smart structures due to their small size. For the first time, [MacPherson 2006] used the multiplexed Fiber Bragg grating sensors
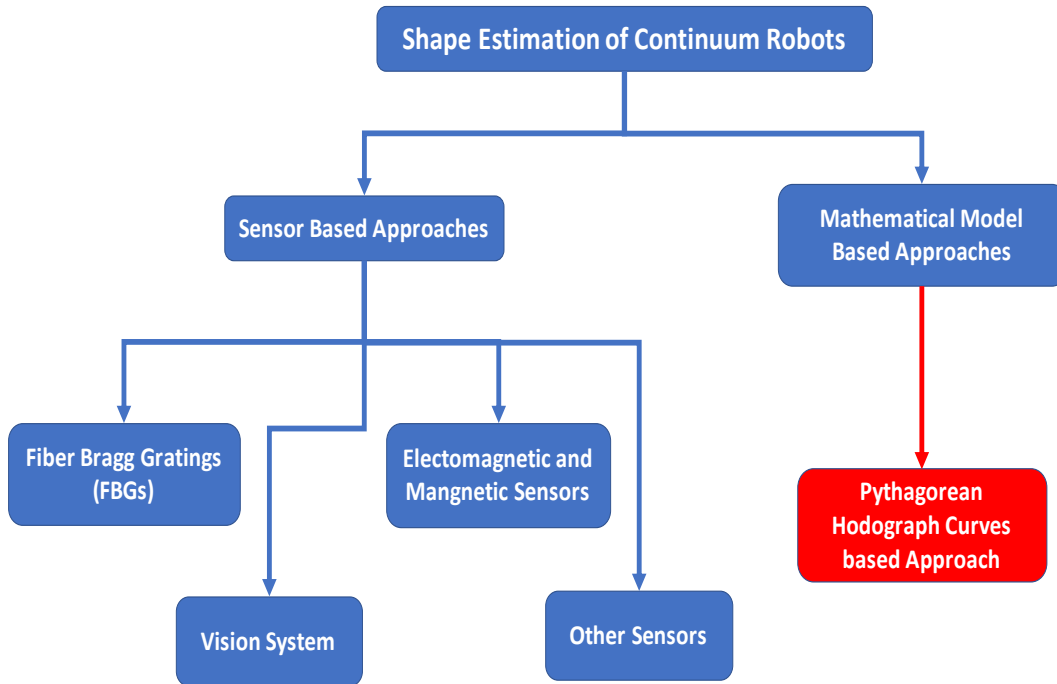
Figure 2.6: Positioning of our work to reconstruct the shape of the soft-continuum manipulators

into a multi-core fiber for the shape estimation. This work is demonstrated for the application to the structural monitoring process. In the medical field, [Yi 2007] proposed the shape estimation of the colonoscope while it is proceeding inside the colon. The design of the sensor is discussed along with its positioning. The sensor provides the information of the curvature and torsion, and further, the principle based on differential geometry is used for curve-based shape reconstruction. A Bragg gratings based optical fiber bend sensor is used in an eccentric core polymer optical fiber [Chen 2010]. This sensor provides high bend sensitivities and the wide range of curvature measurements. In medical, for the MRI process, 3-D shape of the needle and its deflection is estimated using FBG sensors. The needle is used with a fixture, and the fixture has the grooves to accommodate the optical fibers. The sensors provide the curved profile and the deflection of the tip of the needle once it is inserted into the tissues. Three FBG sensors are used, and the placement of the sensors is discussed. The work of [Roesthuis 2014] provides a prototype of a continuum nitinol needle embedded with 12 FBG sensors. FBG sensors provide the axial strain in the needle which gives the curvature of the needle. Further, the 3-D shape of the needle is estimated using kinematic and mechanics based model. The shape estimation of Dexterous Continuum Manipulators (DCMs) is proposed by sensing their curvatures using FBGs in

[Liu 2015]. Fig. 2.7 shows the shape estimation of the DCM used for minimally invasive surgery. While advancing in this direction, [Farvardin 2016]
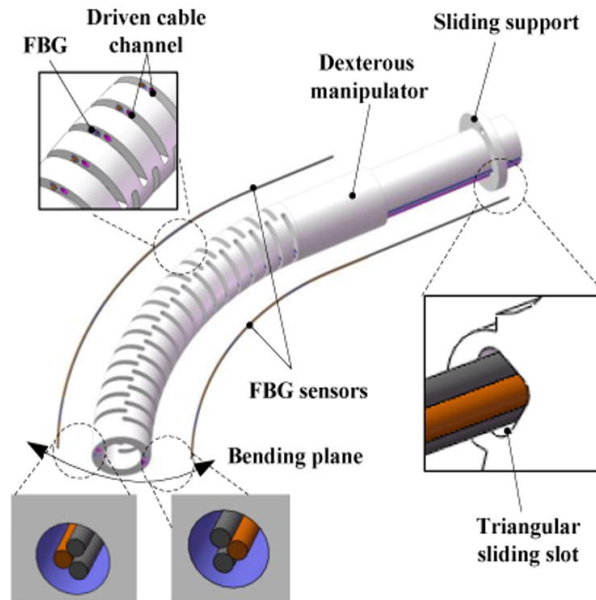
Figure 2.7: Shape sensing for osteolysis dexterous manipulator [Liu 2015]

tested the FBGs based shape estimation of soft-continuum manipulators with free bending and also in the presence of obstacles.

2.3.1.2 Vision System

There are some works which deal with the shape estimation of the soft-continuum manipulators using the vision system as an external sensor.
[Hannan 2005] used external camera based shape reconstruction of the continuum manipulators. The image processing is used from a high-speed camera. This work computes the constant curvature of each section of the elephant trunk manipulator. Further, serial concatenation of shapes gives the estimation of the full shape of the manipulator (Fig. 2.8).

[Vandini 2017] proposes a novel approach of shape estimation of concentric tube robots using vision systems for fluoroscopic images. Optical markers are used for tracking the efficient shape of a soft-continuum pneumatic manipulator. The vision system is used to track the attached markers to the manipulator (Fig. 2.9). This approach works regardless of the effect of the unknown forces and the kinematics uncertainties. Continuous detection of the shape estimation of the soft-continuum manipulator is provided by [Fraś 2017] using depth images provided by a Kinect based sensor. This vision system detects the central axis of the soft-continuum manipulator to reconstruct its
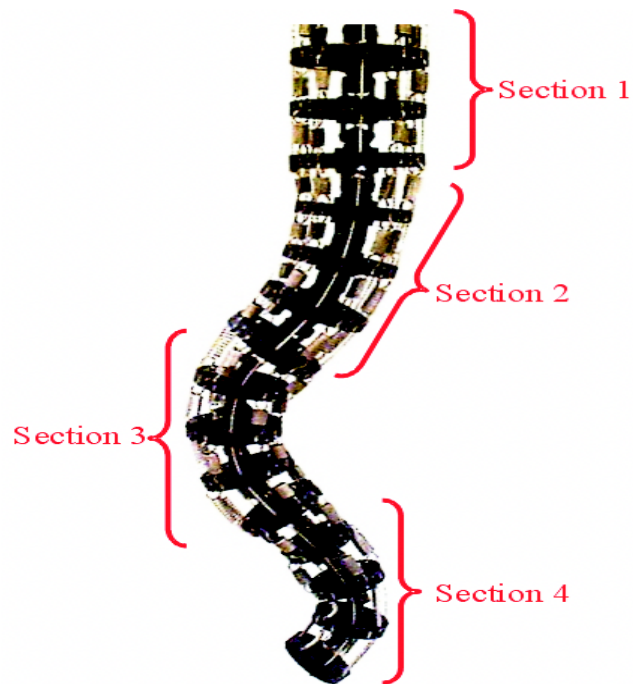
Figure 2.8: Elephant's trunk robotic manipulator [Hannan 2005]

3-D shape and also approximates the orientation of each point that lies on it. The numerical representation of the surface is also generated. This approach is used for a cylindrical manipulator named STIFF-FLOP manipulator (Fig. 2.10). But in this case, sometimes the type of material of the continuum manipulators creates the problem in detection. Also, the data is not completely retrieved from the edges of the objects.
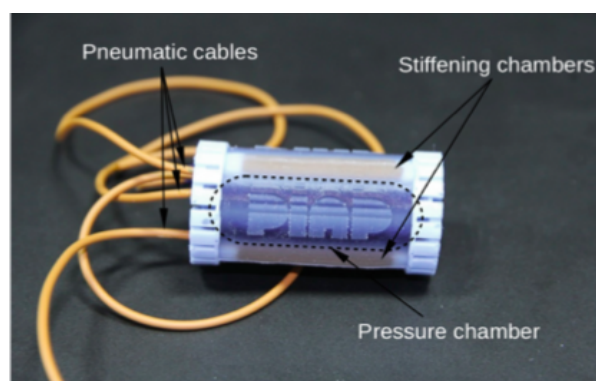
Figure 2.10: The STIFF-FLOP manipulator [Fraś 2017]
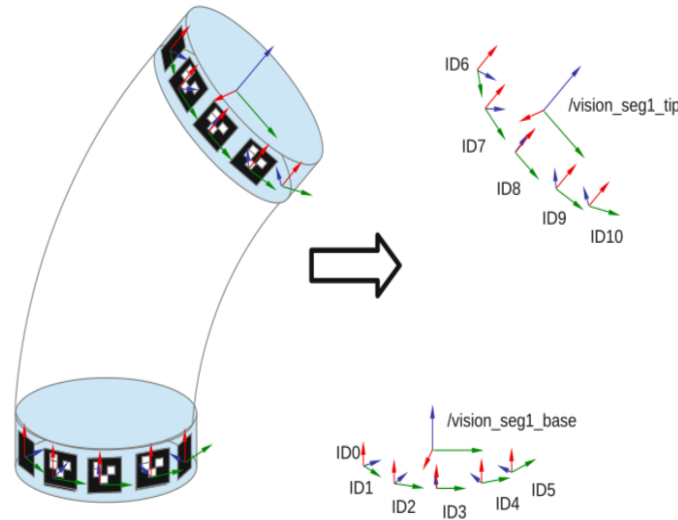
Figure 2.9: Marker tracking using vision system [Fraś 2016]

2.3.1.3 Electromagnetic and Magnetic Sensors

[Song 2015a] presents a new approach to model the shape of the multiple bending sections of wire driven soft-continuum manipulators. The information of the joints of the soft-continuum manipulator is gathered by using the Electromagnetic Tracking Method (ETM). Electromagnetic sensors are used at the joints to notice the position and the orientation information. Consequently, using this information, quadratic Bezier curves are used to reconstruct the shape of the soft-continuum manipulator section by section. Fewer sensors are used as compared to FBG sensors. Further, this work is extended in [Song 2015b] and cubic Bezier curves are used. The work of [Wang 2017] involves the mounting of the magnets at the end of each joint of the concentric tube continuum manipulator, and its pose is estimated by using a magnetic positioning system. Then third order Bezier curves are used to reconstruct the shape of the soft-continuum manipulator using the sensor data.

2.3.1.4 Other Sensors

[Searle 2013] proposes the design of a novel optical sensor to measure the bending curvatures of the soft-continuum manipulators based on light intensity modulation. [Trivedi 2014] presents the three methods to sense the shape of the soft-continuum manipulators based on geometrically exact models. The three cases are: 1) The mounting of load cells at the base of the manipulator. 2) The use of cable encoders running through along the manipulator. 3) Inclinometers mounted at the end of each section. This work uses OctArm VI for experimental validation. A low cost twisted coil sensor

is presented in [Abbas 2017] which can leverage the shape reconstruction of the soft-continuum robots. This sensor gives resistance as an output, and a model is discussed to predict the external force and the displacement of the manipulator from this resistance.

2.3.2 Mathematical Model-Based Approaches

There is less work in case of mathematical models to reconstruct the shape of the soft-continuum manipulators without using sensors.

In [Gravagne 2000], a relationship is established between the shape of a hyper-redundant planar manipulator and its actuators. This is achieved by mapping the curvature functions of the backbone curve with the lengths of tendon cables, using a wavelet decomposition method. The redundancy is handled using the minimum bending of the manipulator. This method uses a 2-D tendon driven manipulator. In [Mochiyama 1998], a correspondence between a hyper-redundant robotic manipulator (Fig. 2.11) and a geometric curve has been established by solving a non-linear optimization problem called 'shape inverse problem'. In this work, the ill conditions and the shortcut problem is solved as shown in Figs. 2.12, 2.13.
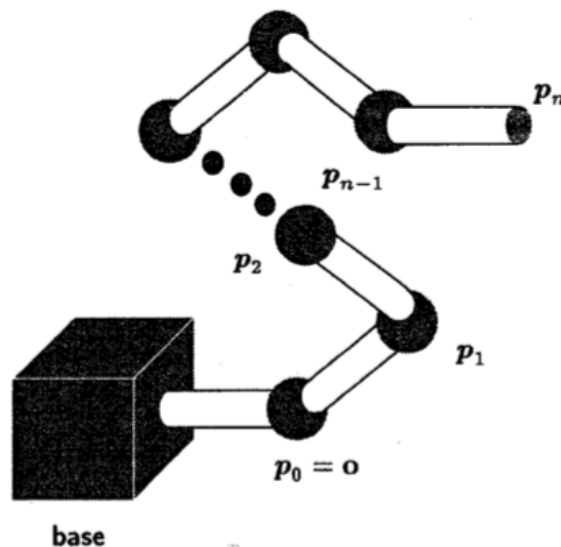
Figure 2.11: Hyper-redundant manipulator [Mochiyama 1998]
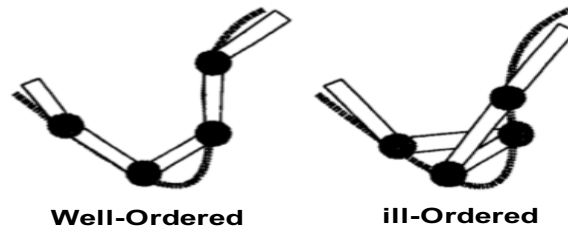
Figure 2.12: Ill Order [Mochiyama 1998]
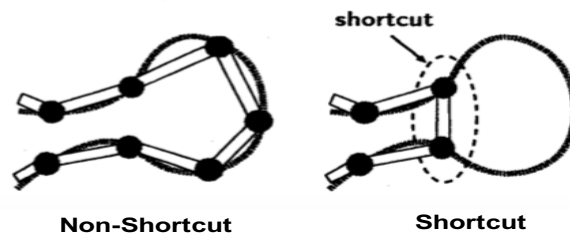
Figure 2.13: Shortcut [Mochiyama 1998]

The backbone shape of a hyper-redundant manipulator has also been solved using the modal approach and thereby using a fitting algorithm to join the various sections of a discrete 30 DOF manipulator [Chirikjian 1994]. The backbone curve is solved to compute the inverse kinematic of the hyper-redundant manipulator (Fig. 2.14). Hyper-redundancy resolution is performed to select one optimal solution.
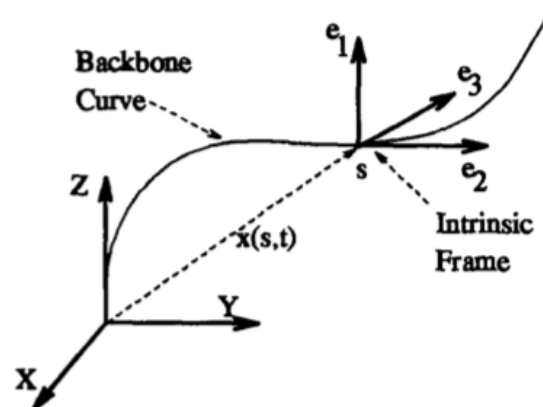
Figure 2.14: Backbone reference frame [Chirikjian 1994]
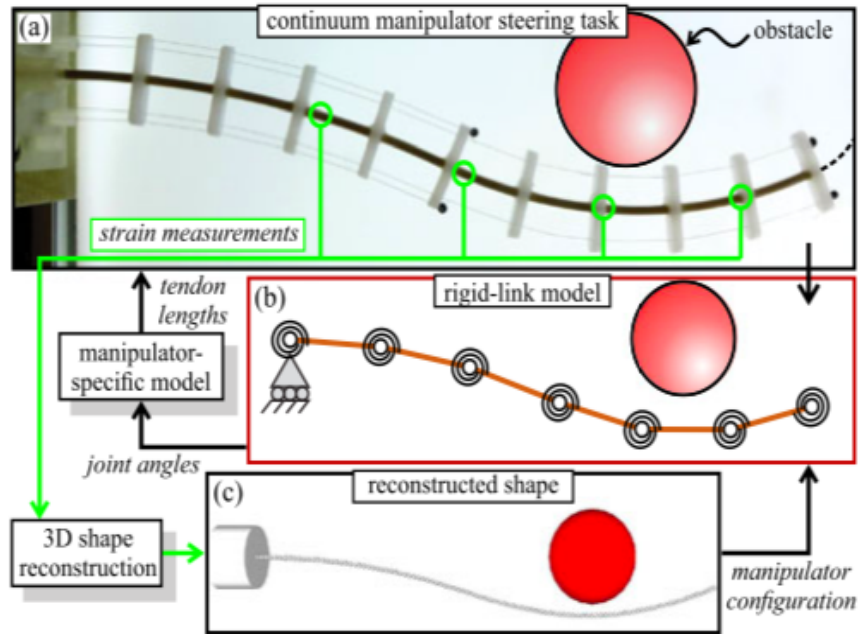
Figure 2.15: (a) Planar continuum manipulator with embedded FBG sensors (b) Rigid-link model of the continuum manipulators (c) Reconstructed shape using FBG sensors [Roesthuis 2016]

[Roesthuis 2016] presents an approach to model the shape of a planar continuum manipulator. The manipulator is assumed to be made up of a series of rigid links connected through flexible rotational joints. The joint angles of the manipulator are calculated using a rigid-link model. Therefore, the shape of the manipulator is estimated by using the formulations from the rigid link manipulators. The approach is tested for the planar continuum manipulator having two bending sections (Fig. 2.15). As shown in Fig. 2.15, FBG sensors are embedded in the manipulator to reconstruct its shape. This sensor-based reconstructed shape is used for the closed-loop control of the manipulator. The steering of the manipulator is tested for the static obstacles and also the straight movement of the manipulator with moving obstacles. Work is done by [Jones 2006] to visualize the soft-continuum manipulators in 3-D using NURBS-based model. This work mainly emphasizes in real-time drawing and display of the continuum manipulators. A circular arc model is used to show each section of the manipulators. Fig. 2.16 shows the model of the trunk displayed using NURBS-based model.
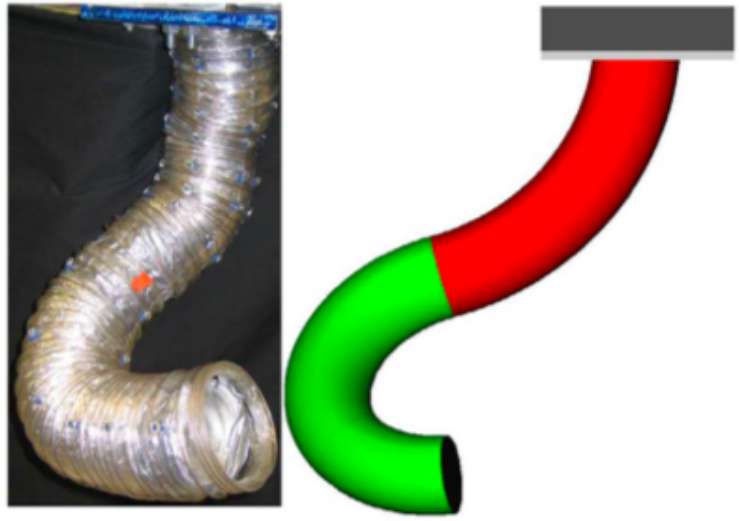
Figure 2.16: Comparison of the Air-Octor continuum trunk with the NURBS-based model [Jones 2006]

2.3.3   Work Contextualization and Contributions

The state of the art to reconstruct the shape of the continuum manipulators was presented in section 2.3. Most of the works use sensors to reconstruct the shape. No doubt we can get better accuracy by using sensors, but they have the following drawbacks:

- In some fields, the continuum manipulators have to work in a confined environment, and there is no place for sensor placement with the manipulator.

- Sometimes there is a low signal to noise ratio in the data from the sensors, and it is difficult to filter.

- The assembly of the sensors is a time-consuming process, and the geometry of the sensors is trial dependent.

There is less work regarding mathematical model-based approaches to estimate the shape of the soft-continuum manipulators.
Figure 2.6 shows the positioning of our work regarding 3-D shape estimation of the soft-continuum manipulators using mathematical model-based approach. We used Pythagorean Hodograph (PH) curves to reconstruct the shape. This work does not require any sensor to reconstruct the optimal shape. The sensors can be used to check the performances and to validate the modeling approach. The shape reconstruction of the soft-continuum manipulators is presented using PH curves-based approach for both freeload as well as under load conditions.

2.4 Kinematic Modeling of Soft-continuum Manipulators

Kinematics of soft-continuum manipulators is extensively explored in the literature using qualitative, quantitative and hybrid approaches. The review on the kinematics of the soft-continuum manipulators is discussed by [Walker 2013], [Webster III 2010], [Chirikjian 2015], [Chawla 2018]. These works discuss the different approaches to model continuum manipulators. In [Godage 2011], the work has been done to model kinematics of multi-section continuum manipulators using mode shape functions. This approach solves the singularity problem associated with the previously available models. In our case, the class of soft-continuum manipulators used for the realization of this thesis is Compact Bionic Handling Assistant (CBHA). The long or extended version of this manipulator is called BHA (Bionic Handling Assistant). The state of the art regarding kinematic models developed for this class of manipulators is as follows:

2.4.1 Qualitative Approaches

Due to the complexity involved in the modeling of soft-continuum manipulators, qualitative approaches, which aim to learn the kinematic problem by using learning algorithms, have a significant role due to their ability to by-pass the modeling task. These approaches are based on the input-output data derived from experimentation and can provide accurate and fast approximations to the kinematic solutions.

[Melingui 2015] proposes the approach which makes use of Multilayer Perceptron (MLP) and Radial Basis Function (RBF) Neural Networks for the approximation of the forward kinematic model (FKM) of CBHA trunk. Qualitative approaches divide the configuration space into several classes according to the operation modes and attempt to determine mathematical relationships between the effects (sensor measurements) and the causes (actuators inputs) using learning techniques. They generally yield accurate models when the database is well built, and the suited technique is chosen. In the case of the inverse kinematics of the CBHA robot, a Distal Supervised Learning (DSL) technique [Jordan 1992] was implemented in [Melingui 2015]. DSL technique proposes learning first the forward kinematic model, and second to exploit the latter to train the inverse kinematics indirectly while keeping fixed the fitted parameters of the forward kinematic model. By doing so, only one of the possibly many solutions is chosen for a given input. However, without additional information (lazy arm movement, minimum end-effector positioning error, etc.) of a particular structure of the input-to-output mapping, there is no way of predicting which of the possibly infinite set of inverse models the procedure will find. Therefore, a minimum norm of the tube lengths was
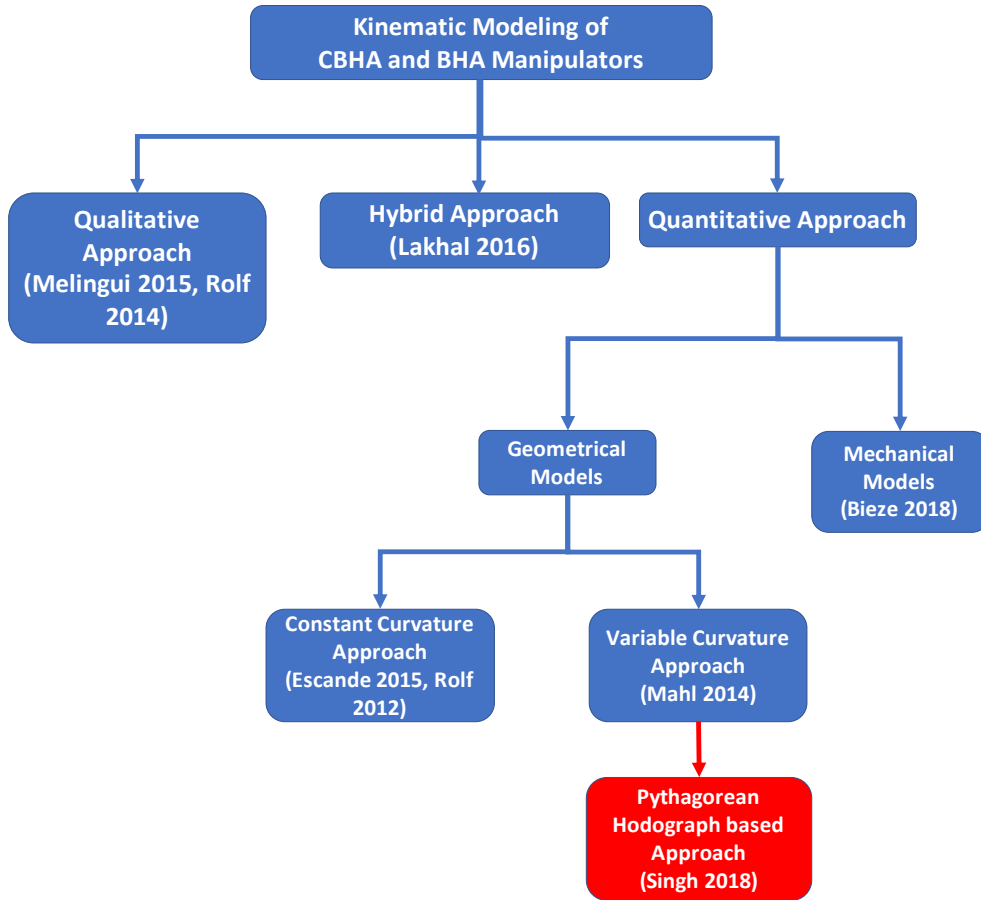
Figure 2.17: Positioning of our work to model kinematics of the soft-continuum manipulators

added as a penalty term into the inverse objective function in [Melingui 2015] to select one particular inverse model from the redundancy manifold.

[Rolf 2014] introduces the inverse kinematics of the BHA manipulator by using a qualitative approach based on online goal babbling. The idea of this model is to learn the inverse model of the BHA manipulator (3 sections), a long version of the CBHA (2 sections), which suggests the joint parameter lengths to reach to the target in the task space.

2.4.2   Quantitative Approaches

Quantitative approaches give the analytical model-based solutions of the kinematics. The FKM of the CBHA manipulator is calculated using a geometric quantitative method [Escande 2015]. Assumptions used in this method are; 1) CBHA's shape is modeled as two cylinders 2) CBHA is considered as a non-extensible arm 3) The curvature of the tubes is assimilated to a perfect

arc of a circle 4) No torsion because tubes are interconnected rigidly at each vertebra. The equations 2.1 are deduced from the geometrical model of CBHA as in fig. 2.18:
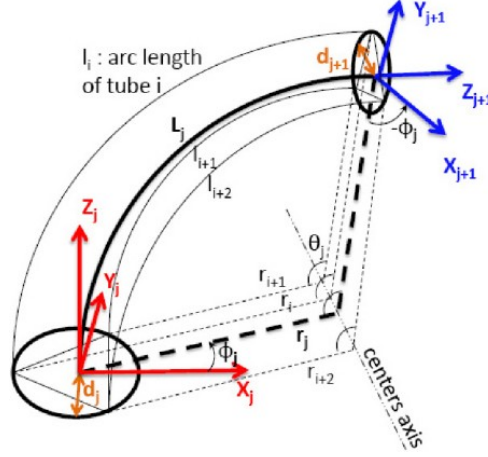
Figure 2.18: Geometrical representation of one section of CBHA [Escande 2015]

$$
\begin{cases}
L_j = \frac{l_i + l_{i+1} + l_{i+2}}{3} \\
\phi_j = \tan^{-1}\left(\frac{\sqrt{3}(l_{i+2} - l_{i+1})}{2l_i - l_{i+1} - l_{i+2}} \right) \\
r_j = \frac{(l_i + l_{i+1} + l_{i+2})}{D_j} d_j \\
\theta_j = \frac{D_j}{3d_j} \\
D_j = 2\sqrt{l_i^2 + l_{i+1}^2 + l_{i+2}^2 - l_i l_{i+1} - l_i l_{i+2} - l_{i+1} l_{i+2}}
\end{cases}
\tag{2.1}
$$

Where, i refers to the number of the tube, j refers to the number of the section, r_j refers to the curvature radius of the j_{th} section, ϕ_j refers to the angle between x-axis and the projection of the j_{th} section, θ_j refers to the curvature angle of the j_{th} section and L_j refers to the length of the j_{th} section. The final position of the manipulator is calculated by using the above equations and transformation matrix.

The transformation matrix for one section of CBHA is eq. 2.2.

$$
{}^{j-1}_{j}T = \begin{bmatrix} R & P \\ 0 & 1 \end{bmatrix}
\tag{2.2}
$$

Here,

$$
P = \begin{bmatrix} r_j c\varphi_j (1 - c\theta_j) \\ r_j s\varphi_j (1 - c\theta_j) \\ r_j s\theta_j \end{bmatrix}
$$

and,

$$R = \begin{bmatrix} c^2\varphi_j c\theta_j + s^2\varphi_j & c\varphi_j s\varphi_j(c\theta_j - 1) & c\varphi_j s\theta_j \\ c\varphi_j s\varphi_j(c\theta_j - 1) & s^2\varphi_j c\theta_j + c^2\varphi_j & s\varphi_j s\theta_j \\ c\varphi_j s\theta_j & -s\varphi_j s\theta_j & c\theta_j \end{bmatrix}$$

Where c and s are cos and sin respectively.

The forward kinematic equations are not easy to invert. Therefore, the Newton Raphson approach is used to approximate the solution [Singh 2017]. The Newton Raphson Method is an iterative method to find the best approximation to the roots of a function. The functions used for the calculation of the inverse kinematic solution of the CBHA, are taken from the forward kinematics of the CBHA [Escande 2015].

Equations 2.3 indicate the x, y and z coordinates of the end point of a two-section CBHA when viewed from the base coordinate frame. These equations are derived from the Forward Kinematic Model of the CBHA Manipulator using transformations from workspace to tube space, through the configuration space.

$$\begin{cases} \begin{aligned} x &= r_1(-C\theta_1 + 1)C\phi_1 + r_2((S\phi_1)^2 + (C\phi_1)^2 C\theta_1) \\ &\quad (-C\theta_2 + 1)C\phi_2 + r_2(C\theta_1 - 1)(-C\theta_2 + 1) \\ &\quad S\phi_1 S\phi_2 C\phi_1 + r_2 S\theta_1 S\theta_2 C\phi_1 \\[6pt] y &= r_1(-C\theta_1 + 1)S\phi_1 + r_2((S\phi_1)^2 C\theta_1 + (C\phi_1)^2) \\ &\quad (-C\theta_2 + 1)S\phi_2 + r_2(C\theta_1 - 1)(-C\theta_2 + 1) \\ &\quad S\phi_1 C\phi_1 C\phi_2 + r_2 S\phi_1 S\theta_1 S\theta_2 \\[6pt] z &= r_1 S\theta_1 - r_2(-C\theta_2 + 1)S\phi_1 S\theta_1 S\phi_2 - r_2 \\ &\quad (-C\theta_2 + 1)S\theta_1 C\phi_1 C\phi_2 + r2 S\theta_2 C\theta_1 \end{aligned} \end{cases} \qquad (2.3)$$

Here C and S represent cos and sin respectively.

The eqs. 2.3, 2.1 are used to approximate the inverse kinematic solution using the Newton Raphson approach.

[Bieze 2018] introduced the FEM-based approach to model soft-continuum manipulators under quasi-static condition. The problem of differential equations with boundary conditions is studied using a FEM approach. Discretization is used to reduce the number of degrees of freedom of continuum manipulators. The methodology explains the models of sensors, actuators, and end-effectors of soft-continuum manipulators. These models are used to solve the kinematics of the CBHA manipulator.

[Rolf 2012] modeled each section of the BHA manipulator as the torus segment as shown in Fig. 2.19. If the segment has the radius b, the deformation of the segment can be represented by r (radius) of the torus deformation, and the angle θ representing which part of the torus represents the segment and

ϕ represents the orientation of the torus in the XY-plane. Using the three lengths of the bellows of the first section of the BHA, geometric parameters r, θ and ϕ can be constructed. The backbone length of the segment is l and is given as:

$$l = \frac{l_1 + l_2 + l_3}{3} \tag{2.4}$$

$$g = sqrt(l_1^2 + l_2^2 + l_3^2 - (l_1 l_2 + l_1 l_3 + l_3 l_2)) \tag{2.5}$$

Then the geometric parameters can be computed as

$$\theta = \frac{2g}{3b} \tag{2.6}$$

$$r = \frac{3lb}{2g} = \frac{l}{\theta} \tag{2.7}$$

$$\phi = tan^{-1}(\frac{\sqrt{3}(l_3 - l_2)}{l_3 + l_2 - 2l_1}) \tag{2.8}$$

These equations are for the first section of the manipulator. Further using coordinate transformations from the end frame to the base frame, FKM of the BHA manipulator is achieved.

[Mahl 2014] presents a methodology to model the continuum manipulators assuming a piecewise constant (variable) curvature of the backbone of the manipulator. At first, the forward and the differential forward kinematics are deduced. This approach defines each section of the manipulator as a series of the finite number of circular arcs. To include the redundancy during the inverse kinematic problem, the solution is provided at the velocity level through the use of a robot's Jacobian matrix which is calculated analytically. This method needs the two following conditions to be satisfied to validate it for a manipulator:

- The manipulator consists of a finite number of serially connected sections.

- Each section has three degrees of freedom, two for spatial bending and one for extension of the manipulator. Torsion is not considered in the model.

This approach is applied to the BHA manipulator and validated experimentally.

2.4.3 Hybrid Approach

The Hybrid Approach uses quantitative (Geometric) as well as qualitative (Neural Network) approaches to solve the inverse kinematics of the CBHA
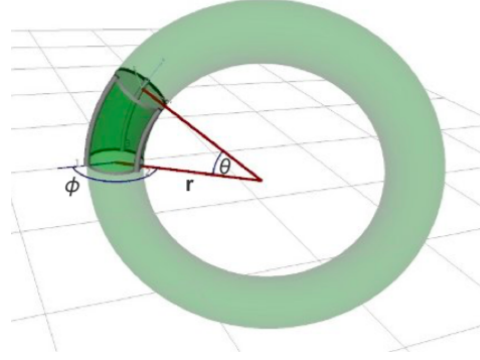
Figure 2.19: Representation of segment of BHA by torus segment [Rolf 2012]

[Lakhal 2016]. CBHA is considered consisting of 17 vertebrae; therefore in this approach, each inter-vertebra is modeled as a parallel robot of type 3UPS-1UP (Universal-Prismatic-Spherical) as shown in Fig. 2.20. Three kinematic serial UPS joints do the control of the position and the orientation of the upper vertebra relative to the lower vertebra, but only the prismatic joints are active. In the case of the CBHA, the translation of the upper vertebrae relative to the lower vertebrae is perpendicular. Moreover, the torsion is not possible. For these constraints, the serial UP is used. The inverse kinematic equations (IKE) of parallel robots are easy to establish with some elementary geometric relationships [Lakhal 2016]. The model of an inter-vertebra, represented by eq. 2.9, is obtained by calculating the joint variable $q_{m,k}$, as shown in the Fig. 2.20, where m=1,...,3 is the prismatic active joint and k=1,...,17 is the vertebra, corresponding to the position Z_k and orientation θ_k (pitch angle) and ψ_k (roll angle) of the upper vertebra relative to the lower vertebra.

$$
\begin{cases}
q_{1k}^2 = Z_k^2 + 2r_k Z_k \ S(\Theta_k) - 2r_k r_{k-1} \ C(\Theta_k) + r_k^2 \\
\qquad + r_{k-1}^2 \\
\\
q_{2k}^2 = Z_k^2 + r_k Z_k \left(\sqrt{3} \ C(\Theta_k) \ S(\Psi_k) - \ S(\Theta_k) \right) \\
\qquad + r_k^2 + r_{k-1}^2 - r_k^2 r_{k-1}^2 \\
\qquad \left(\frac{\sqrt{3}}{2} \ S(\Theta_k) \ S(\Psi_k) + \frac{3}{2} \ C(\Psi_k) + \frac{1}{2} \ C(\Theta_k) \right) \\
\\
q_{3k}^2 = Z_k^2 - r_k Z_k \left(\sqrt{3} \ C(\Theta_k) \ S(\Psi_k) + \ S(\Theta_k) \right) \\
\qquad + r_k^2 + r_{k-1}^2 + r_k^2 r_{k-1}^2 \\
\qquad \left(\frac{\sqrt{3}}{2} \ S(\Theta_k) \ S(\Psi_k) - \frac{3}{2} \ C(\Psi_k) - \frac{1}{2} \ C(\Theta_k) \right)
\end{cases}
\tag{2.9}
$$

Here C, S and r represent *cos*, *sin* and radius of vertebra respectively. Unlike the IKE, the solution of the forward kinematic equation is relatively complex, because eqs. 2.9, are highly nonlinear. Thus, two neural networks are generated to provide the approximated solution of the IKE, allowing

to obtain the position and orientation from the joint variable $q_{m,k}$, as shown in Fig. 2.21. Then, the transformation matrix $^k_{k+1}T$ of the upper vertebra frame relative to the lower vertebra, represented by eq. 2.10, allows estimating cartesian coordinates of the tip arm, from homogeneous transformation matrices. However, CBHA contains only six potentiometers, and a block is added to determine the joint variable from the tube length.

$$
^k_{k+1}T = \begin{bmatrix}
c\theta_k & s\theta_k s\psi_k & s\theta_k c\psi_k & 0 \\
0 & c\psi_k & -s\psi_k & 0 \\
-s\theta_k & s\psi_k c\theta_k & c\theta_k c\psi_k & Z_k \\
0 & 0 & 0 & 1
\end{bmatrix}
\tag{2.10}
$$

Where c and s are cos and sin respectively.
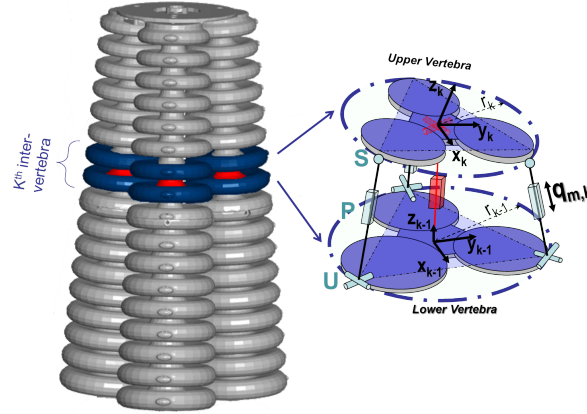
Figure 2.20: Modeling of inter-vertebra

In Fig. 2.22, the algorithm is explained. Four neural networks are used, the first one is used to approximate the position (X_{s1}, Y_{s1}, Z_{s1}) of the first section using the Cartesian coordinates of the tip of the CBHA (X, Y, Z). The other three neural networks are used to approximate the position Z_k, orientation θ_k (pitch angle) and ψ_k (roll angle) of the upper vertebra relative to the lower vertebra. These values are used to compute the lengths of each inter-vertebra using eq. 2.9. Then these lengths are added to compute the overall lengths of the CBHA Manipulator.

2.4.4 Work Contextualization and Contributions

The kinematic models for the class of soft-continuum manipulators, namely CBHA and BHA, are discussed, and the positioning of our work among the discussed works is shown in red color in Fig. 2.17.
Positioning:
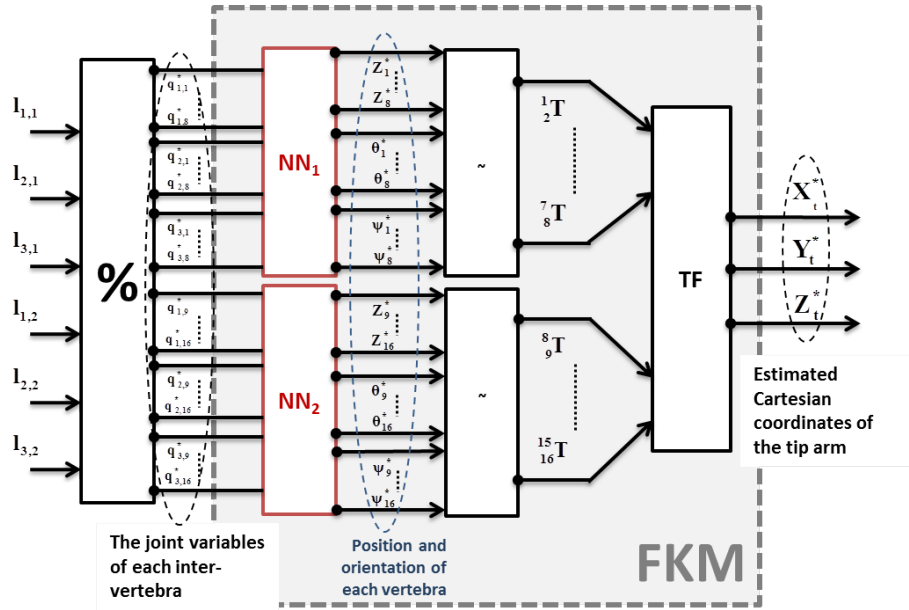
Figure 2.21: Algorithm for Forward Kinematics [Lakhal 2016]

- We used the same shape reconstruction approach based on Pythagorean Hodograph curves to model the kinematics of the soft-continuum manipulators.

- The literature regarding kinematics of the soft-continuum manipulators shows that the methods reviewed are decoupled from the reconstruction of the optimal posture of the manipulators. These methods compute the IKM of the soft-continuum manipulators which do not mean to find the optimal posture. **In this work, we reconstructed the optimal posture of the soft-continuum manipulators using Pythagorean Hodograph curves which leads us to the optimal kinematic solution of the manipulators.**

2.5   Conclusion of the Chapter

This chapter defined the soft-continuum manipulators and reviewed the literature of the soft-continuum manipulators regarding their shape reconstruction. The positioning of the proposed shape reconstruction approach is highlighted among the existing approaches. Further, the proposed approach is used to solve the kinematics of the class of soft-continuum manipulators, named CBHA. Therefore, the literature on the kinematics of the CBHA and BHA manipulators is discussed, and the positioning of our work is highlighted among the existing approaches.
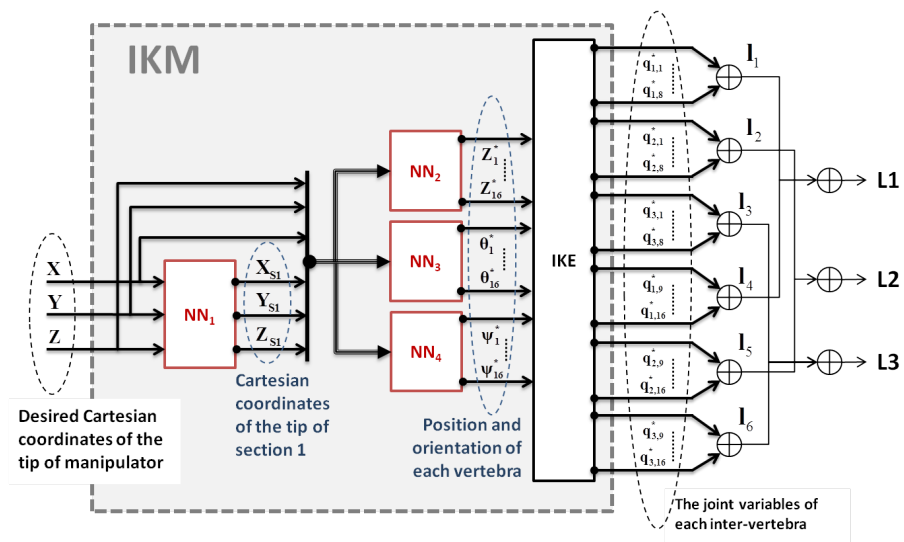
Figure 2.22: Inverse Kinematic modeling algorithm [Lakhal 2016]

Shape Reconstruction of Soft-continuum Manipulators

Contents

3.1   Introduction

Soft-continuum manipulators can curve continuously to provide us the desired motion. It is an imperative task to find an optimal posture of the soft-continuum manipulators for a particular target in their task space. Here, the optimal posture means the actual or real posture of the manipulator for a specific set of input values (for example pressure in the case of pneumatic-based actuation; length in case of cable-based actuation). In this work, we reconstruct the shape of the soft-continuum manipulators using a curve based-approach. Therefore, if we have multiple solutions of reconstructed shapes for a particular set of input values, we choose an optimal posture by using minimum potential energy criteria. This is because we assume that every physical system tends to be in a state of minimum potential energy.

We want to reconstruct the shape of the soft-continuum manipulators with a 3-D curve using four known boundary conditions; the conditions are as follows (Fig. 3.1):

- P_s, initial or starting point position vector of the soft-continuum manipulator located at the base of the manipulator.

- d_s, direction vector at point P_s

- P_f, final or end-point position vector of the soft-continuum manipulator located at the center of the tool of the manipulator.

- d_f, direction vector at point P_f
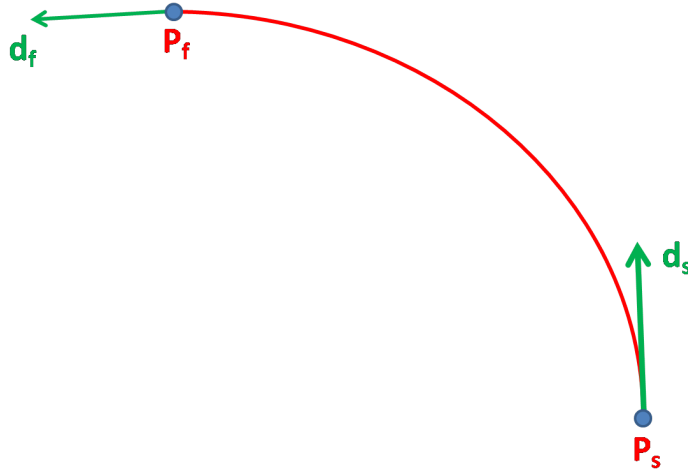
Figure 3.1: Shape of the soft-continuum manipulator represented by a curve

$$P_s(x_s, y_s, z_s), d_s(d_{xs}, d_{ys}, d_{zs}) \xrightarrow{r(h)} P_f(x_f, y_f, z_f), d_f(d_{xf}, d_{yf}, d_{zf}) \qquad (3.1)$$

Here, eq. 3.1 represents the problem statement, where a curve $r(h)$ is constructed to model the shape of the soft-continuum manipulators using the afore mentioned boundary conditions. h represents the curvilinear coordinate along the curve.

Further, in the chapter, the aim is to compare the performances of various approachs in the context of shape reconstruction for the soft-continuum manipulator.

3.2 Geometrical Curves Representation

The classification of different curve representations is presented in fig. 3.2 [Zeid 2004]. As per our requirement, parametric curves are better than non-
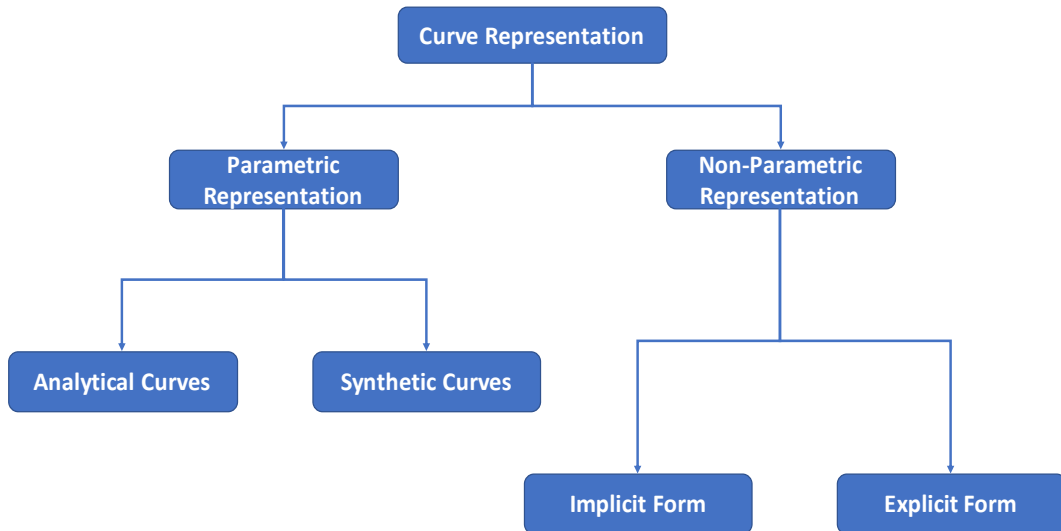
Figure 3.2: Schematic of representation of curves

parametric curves to reconstruct the shape. Besides that, we briefly discussed non-parametric curves to show the reason behind not using them in the following development.

Different methods of curve formulation and representation are discussed as follows:

3.3 Non-Parametric Representation

Non-parametric equations of curves can be expressed in two forms: explicit and implicit.

3.3.1   Explicit Form

This is the form where a dependent variable can be separated in the equation and can be represented in the form of an independent variable. For example, $x + 2y = 0$ is explicit, here the dependent variable y can be separated as $y = \frac{-x}{2}$. A non-parametric explicit form of a point P on a curve is given by:

$$P = [x \quad y \quad z]^T = [x \quad f(x) \quad g(x)]^T \tag{3.2}$$

Where, r is the position vector of a point P represented in cartesian coordinates as shown in Fig. 3.3. In this form, the y and z coordinates of point P are expressed as two different functions of the third coordinate x which acts as an independent variable as shown in eq. 3.2. Following are the examples
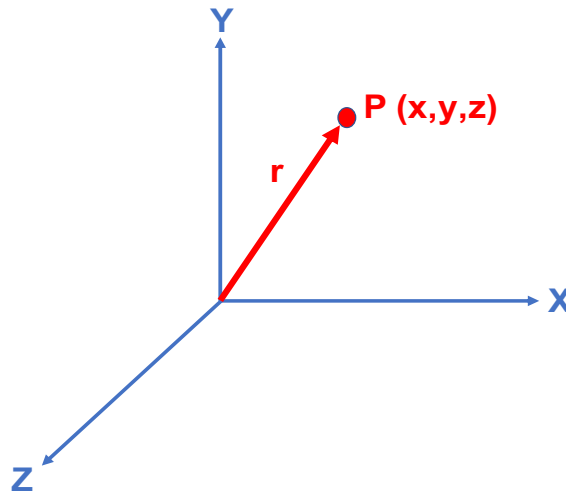
Figure 3.3: Position vector of a point P

of explicit curves:

$$y = mx + c \tag{3.3}$$

$$y = ax^3 + bx^2 + cx + d \tag{3.4}$$

Here, only the value of $x - coordinate$ can define a curve for eqs. 3.3 and 3.4.

3.3.2   Implicit Form

This is the form in which the dependent variable cannot be separated. For example, $x^2 + y^2 + 2xy = 0$ is an implicit form. In implicit form, x, y and z coordinates are related together by two functions as:

$$F(x, y, z) = 0, \quad G(x, y, z) = 0 \tag{3.5}$$

These two functions can be solved simultaneously to obtain all the points on the curve. Following are the examples of the implicit curves:

$$x^2 + y^2 - R^2 = 0 \tag{3.6}$$

$$ax^2 + by^2 + cxy + d = 0 \tag{3.7}$$

3.3.3 Drawbacks of Non-parametric Representation to Model Soft-continuum Manipulators

Representing the curve using non-parametric forms has the following two major drawbacks:

1. If the slope of a curve at a point is vertical or near vertical, it's value becomes very large and approaches infinity. Therefore, this condition is difficult to handle computationally, as well as, in the programming phase. For example; $F(x, y) = 0$ and $G(x, y) = 0$ are two functions in the implicit form. The equation of the tangent line at an regular point (x_0, y_0) is given as:

$$F(x_0, y_0)(x - x_0) + G(x_0, y_0)(y - y_0) = 0 \tag{3.8}$$

   Therefore, the slope of the curve at point (x_0, y_0) is given by:

$$\text{slope} = \frac{-F(x_0, y_0)}{G(x_0, y_0)} \tag{3.9}$$

   If both $F(x, y)$ and $G(x, y)$ are zero at (x_0, y_0), it means the curve is vertical at that point.
   Soft-continuum manipulators can have a straight vertical posture which is difficult to represent using non-parametric curves.

2. The representation of some of the very basic curves like circle and parabola becomes a tedious task while using non-parametric forms (especially explicit form). This limitation can be removed by selection of optimal coordinate system and independent variable. However, the actual shape representation of an object should be intrinsically independent of the selection of the coordinate system.
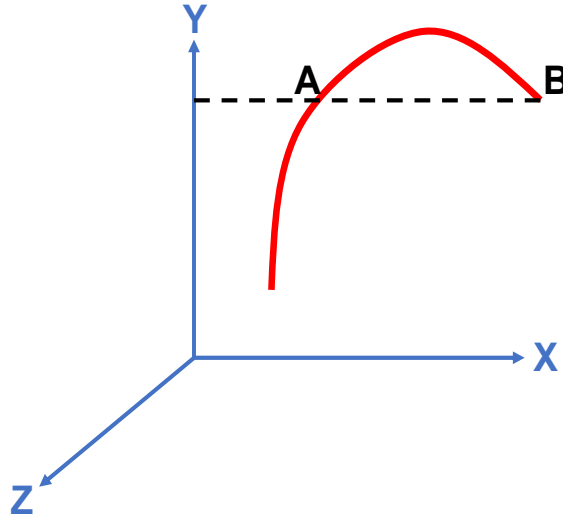
Figure 3.4: A general curve in the Cartesian coordinate space

This can be more clear from Fig. 3.4. Here, we have two values of $x - coordinates$ at points A and B respectively, both having the same value of the $y - coordinate$. This case is not easy to represent with a non-parametric form of equations. **Soft-continuum manipulators can have the shape as represented in fig. 3.4 with a red line. This is the main reason behind not using non-parametric curves to represent the shape of the soft-continuum manipulators.**

3.4   Parametric Representation

The drawbacks of non-parametric representation lead us to study the parametric representation of the curves. In this representation, the coordinates of the points forming the curve are functions of an independent curve parameter, called curvilinear coordinate, represented by h. The curve parameter has varied along the curve from its minimum to maximum value. The parametric representation can be of two categories: analytical and synthetic curves.

3.4.1   Analytical Curves

Parametric analytical curves are those curves which are defined by analytical equations. These curves are such as lines, circles, and conics, etc. The general form of the parametric equations of a curve is as follows:

$$x = x(h), \quad y = y(h), \quad z = z(h) \qquad 0 \le h \le 1 \tag{3.10}$$

Here, h is the curvilinear coordinate along the curve. For example, the parametric equation of a straight line between two points P_1 and P_2 is given by:

$$P_2 = P_1 + h(P_2 - P_1), \qquad 0 \le h \le 1 \tag{3.11}$$

Similarly, points on a circular arc are given by:

$$x = cos(h), \quad y = sin(h) \qquad \frac{-\pi}{4} \le h \le \frac{\pi}{4} \tag{3.12}$$

Likewise, the equations of the other curves (conics, helix, etc.) can be represented as a parametric form. Therefore, these curves can represent the shape of manipulators from the start point to the end point by varying parameter 'h'. These curves did not define any points in between the start and the end-points, known as control points which can be used to control the shape of the curve. **The main drawback of parametric analytical curves lies in the fact that these curves are not sufficient to design the physical systems. This is because it is not possible to control over these curves. Hence, the need arises for synthetic curves.**

3.4.2 Synthetic Curves

Synthetic curves are the ones which can be described by the set of control points. This control makes them appropriate to design ***actual***[1] parts as we have control in our hands to change them as per design requirements. Different synthetic curves are discussed in detail in the next section.

3.5 Synthetic Curves

Multiple synthetic curves exist in the literature. In the following, we consider the main used curves.

3.5.1 Hermite

Cubic Hermite spline is the simplest synthetic curve. The development of cubic splines was in the context of shipbuilding since they can simulate the behavior of wooden splines used to construct ships, see, e.g., [Liming 1944]. Cubic splines are the most famous splines to interpolate a sequence of data points. Cubic splines are studied in depth and used in many applications in Computer Aided Geometric Design (CAGD) [De Boor 1962], [Schoenberg 1969], [Keys 1981], [Gasca 2000]. Hermite splines are used in path planning and tracking of mobile robots in [Wagner 2010], [Lekkas 2014]. These curves are also used for the purpose of trajectory planning [Su 2012].

---

[1]Actual parts means the physical systems.

Now, in our work, we are studying these curves to model the shape of the soft-continuum manipulators.

Definition 3.5.1. Hermite cubic spline can be generated using four known boundary conditions to model the shape of the soft-continuum manipulators. The parametric equation of a cubic spline segment is given as:

$$r(h) = \sum_{i=0}^{3} C_i h^i, \qquad 0 \leq h \leq 1 \tag{3.13}$$

Here, r is the point on the reconstructed shape of the soft-continuum manipulator, h is the curvilinear coordinate and C_i are the polynomial coefficients. The scalar form of eq. 3.13 is written as:

$$
\begin{aligned}
x(h) &= C_{3x}h^3 + C_{2x}h^2 + C_{1x}h + C_{0x} \\
y(h) &= C_{3y}h^3 + C_{2y}h^2 + C_{1y}h + C_{0y} \\
z(h) &= C_{3z}h^3 + C_{2z}h^2 + C_{1z}h + C_{0z}
\end{aligned}
\tag{3.14}
$$

The expanded vector form of eq. 3.13 is as follows:

$$r(h) = C_3 h^3 + C_2 h^2 + C_1 h + C_0 \tag{3.15}$$

The same equation in matrix form becomes:

$$r(h) = H^T C \tag{3.16}$$

Where, $H = [h^3 \quad h^2 \quad h \quad 1]^T$ and $C = [C_3 \quad C_2 \quad C_1 \quad C_0]^T$, C is the coefficient vector.
As we have two direction vectors as input boundary conditions, the tangent vector at any point on the curve is given by:

$$r'(h) = \sum_{i=0}^{3} C_i i h^{i-1}, \qquad 0 \leq h \leq 1 \tag{3.17}$$

Now, we have to relate these parametric equations according to our input boundary conditions to model the shape of the soft-continuum manipulators. Therefore, applying the four known boundary conditions i.e. the end points and tangents at those points (P_s, d_s at h=0 and P_f, d_f at h=1), eqs. 3.13 and 3.17 gives:

$$
\begin{aligned}
P_s &= C_0 \\
d_s &= C_1 \\
P_f &= C_3 + C_2 + C_1 + C_0 \\
d_f &= 3C_3 + 2C_2 + C_1
\end{aligned}
\tag{3.18}
$$

Using the above conditions, the polynomial coefficients can be expressed in terms of the known boundary conditions as:

$$
\begin{aligned}
C_0 &= P_s \\
C_1 &= d_s \\
C_2 &= 3(P_f - P_s) - 2(d_f - d_s) \\
C_3 &= 2(P_s - P_f) + d_s + d_f
\end{aligned}
\tag{3.19}
$$

Substituting eq. 3.19 into eq. 3.15 and rearranging gives;

$$
r(h) = (2h^3 - 3h^2 + 1)P_s + (-2h^3 + 3h^2)P_f + (h^3 - 2h^2 + h)d_s + (h^3 - h^2)d_f,
$$
$$
0 \le h \le 1
\tag{3.20}
$$
$$
r(h) = H^T[M_H]V, \qquad 0 \le h \le 1 \tag{3.21}
$$

Here, $[M_H]$ is the **Hermite matrix**, $H = \begin{bmatrix} 1 & h & h^2 & h^3 \end{bmatrix}$ and V is the boundary condition vector;

$$
[M_H] =
\begin{bmatrix}
2 & -2 & 1 & 1 \\
-3 & 3 & -2 & -1 \\
0 & 0 & 1 & 0 \\
1 & 0 & 0 & 0
\end{bmatrix}
\tag{3.22}
$$

$$
V = \begin{bmatrix} P_s & P_f & d_s & d_f \end{bmatrix}
\tag{3.23}
$$

Figure 3.5 shows a basic schematic of the Hermite curve generated using four known boundary conditions.
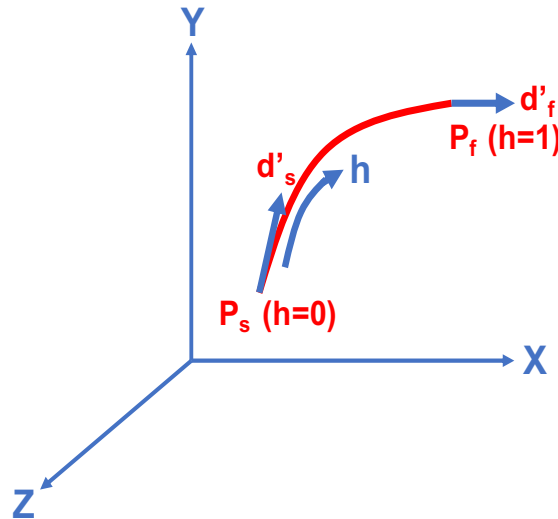
Figure 3.5: Hermite cubic curve

Equation 3.20 defines a Hermite cubic curve which passes through two end points (at h=0 and h=1) and their tangent vectors. The shape of the curve can be changed either by changing the end points or by changing the tangent vectors. The control of Hermit cubic curve is shown in Fig. 3.6.

Change of end points   Change of end tangents
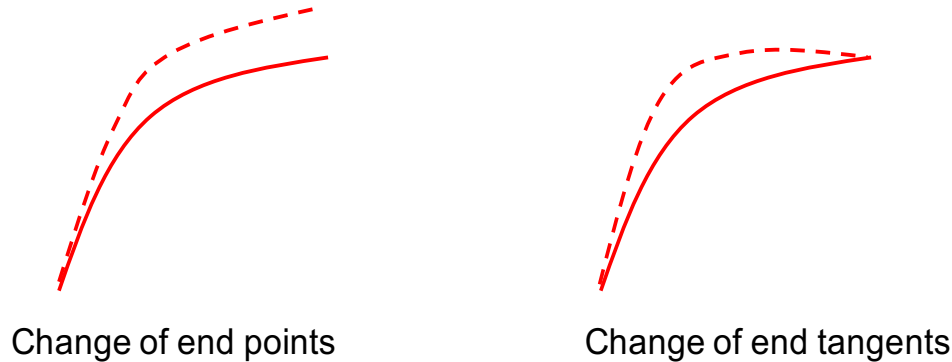
Figure 3.6: Control of Hermite cubic curve

Remark 3.5.1. Cubic Hermite curves are the simplest synthetic curves to model the shape of the soft-continuum manipulators. Therefore, these curves are computationally efficient. But they can be controlled only through their end conditions. They do not have any control points in between to control their shape.

3.5.2   Bezier

A new class of parametric synthetic curves named Bezier curves were introduced in the mid of 1950's by Pierre Bézier and Paul de Casteljau in the French automotive industry [Farin 2002]. These curves has been applied in many applications in computer aided geometric design, e.g. [Gordon 1974], [Böhm 1984], [Farin 2000]. In the robotics field, Bezier curves are used to plan trajectories, collision and obstacle avoidance for mobile robots [Jolly 2009], [Škrjanc 2010], [Yang 2013]. Further, shape estimation of a wire-driven flexible robot with multiple bending sections is done using Bezier curves [Song 2015b]. This work uses electromagnetic sensors to sense the position and orientation of the end points of each section of the soft-continuum manipulators. We are exploring Bezier curves to reconstruct the shape of the soft-continuum manipulators as per our known boundary conditions without using any external sensor data.

Definition 3.5.2. Bezier curve is a parametric curve which uses Bernstein polynomials as the basis functions. The Bezier curve r with degree n is represented by:

$$r(h) = \sum_{i=0}^{n} P_i B_{i,n}(h), \qquad 0 \le h \le 1 \qquad (3.24)$$

Here, $r(h)$ is the point on the reconstructed shape of the soft-continuum manipulator and the coefficients P_i are the control points of the Bezier curve. $B_{i,n}(h)$ are the Bernstein basis functions. Control points together with the basis functions define the shape of the curve. The lines joining the consecutive control points define the control polygon of the Bezier curve. The Bernstein polynomial is given by;

$$B_{i,n}(h) = C(n,i)h^i(1-h)^{n-i}, \qquad 0 \le h \le 1 \qquad (3.25)$$

Here $C(n,i)$ is the binomial coefficient

$$C(n,i) = \frac{n!}{i!(n-i)!} \qquad (3.26)$$

$$C(n,0) = C(n,n) = 1 \qquad (3.27)$$

Combining eqs. 3.25 and 3.27, eq. 3.24 becomes;

$$r(h) = P_0(1-h)^n + P_1 C(n,1)h(1-h)^{n-1} + P_2 C(n,2)h^2(1-h)^{n-2} +$$
$$---- + P_{n-1}C(n,n-1)h^{n-1}(1-h) + P_n h^n, \qquad 0 \le h \le 1 \qquad (3.28)$$

In case of Bezier curve, we can generate a cubic Bezier curve from our four known boundary conditions. Figure 3.7 shows a cubic Bezier curve along with its control polygon. Here, $P_0 = P_s$ is the starting point of the manipulator and $P_3 = P_f$ is the end point of the manipulator.
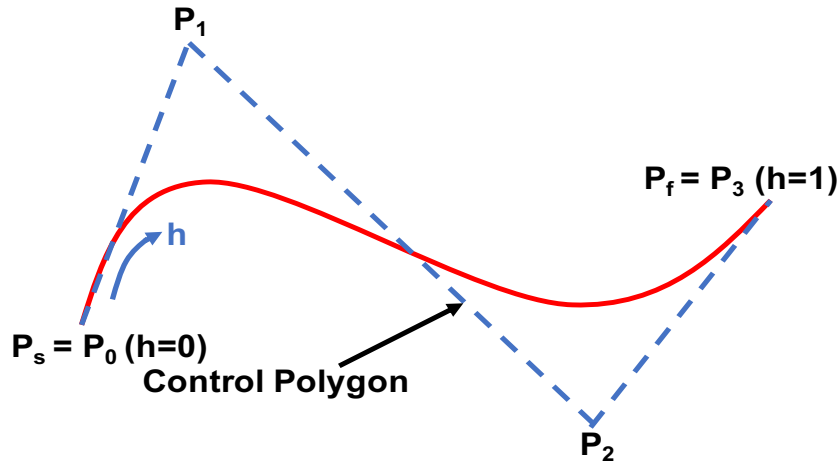
Figure 3.7: A cubic Bezier curve

Properties: The main properties of the Bezier curves are:

1. The first and the last control points are the end points of the Bezier curve. It means it passes through P_0 and P_n if we substitute $h = 0 \quad and \quad h = 1$ in eq. 3.28.

2. The curve is always tangent to the control polygon at the end segments. Using eqs. 3.24 and 3.25, the first order derivatives at the end points are given by:

$$r'(0) = \frac{n!}{(n-s)!} \sum_{i=0}^{s} (-1)^{s-i} C(s,i) P_i \qquad (3.29)$$

$$r'(1) = \frac{n!}{(n-s)!} \sum_{i=0}^{s} (-1)^{i} C(s,i) P_{n-i} \qquad (3.30)$$

Therefore, at the end points, the first derivatives are given as:

$$r(0) = n(P_1 - P_0) \qquad (3.31)$$

$$r(1) = n(P_n - P_{n-1}) \qquad (3.32)$$

It shows that the curve is tangent to the first and the last segment of the control polygon.

3. There is global control in Bezier curves, it means the change in even one control point will affect the whole curve.

4. With n conditions or n number of control points, we can always generate a $n - 1$ degree curve.

Remark 3.5.2. A cubic Bezier curve can be used to model the shape of the soft-continuum manipulator, as n boundary conditions can produce an $n - 1$ degree curve. Bernstein basis functions used for Bezier curves are easy to solve, and they have an analytical solution. Cubic Bezier curves have two control points in addition to the endpoints. There is global control in case of Bezier curves, where the change of one control point will change the overall shape of the curve.

3.5.3   B-Splines and NURBS

B-splines are used to represent free shapes in computer aided geometric applications as in [Farin 1987], [Unser 1993]. These are also used for trajectory planning and obstacle avoidance purposes for mobile robots [Komoriya 1989], [Berglund 2010], [Elbanhawi 2015]. Bezier curves are very convenient for less number of control points, but for conditions with a large number of control points, the global control of points over the curve and fixed order of curve emerge as a drawback. Basis functions chosen for B-splines have the additional degree of freedom which does not exist in case of Bernstein polynomials.

Therefore, B-splines have flexibility in the degree which Bezier curves do not have.

Properties 1: B-splines give more flexibility than Bezier curves because of these two advantages:

1. B-splines provide the local control of the shape of the curve by using blending functions which have the local influence.

2. For B-splines, the degree of the curve is independent of the number of the control points. A B-spline made using n control points can have an order lower than $n-1$. For example, with four control points, the B-spline can be of degree cubic, quadratic or linear.

In our work, B-splines are studied to represent them as the shape of the soft-continuum manipulators.

Definition 3.5.3. Same as Bezier curves, the B-spline curve defined by $n+1$ control points P_i, is given as:

$$r(h) = \sum_{i=0}^{n+1} P_i N_{i,k}(h), \qquad 0 \le h \le h_{max} \tag{3.33}$$

$N_{i,k}(h)$ are the B-spline basis functions. The control points P_i are also called deBoor points. These control points form the vertices of the control or deBoor polygon.

Positioning: The major differences in the eqs. 3.24 and 3.33 are:

1. In B-splines, the parameter k controls the degree $k-1$ of the curve which is independent of the number of control points.

2. The maximum limit of the curvilinear coordinate h is no longer limited to 1 as it is chosen for the Bezier curve.

Properties 2: The B-spline basis functions have the following properties:

1. Partition of unity: $\sum_{i=0}^{n} N_{i,k}(h) = 1$
   The first property describes that the relationship between the control points of the curve and the curve itself is invariant under affine transformations.

2. Positivity: $N_{i,k}(h) > 0$
   The second property ensures that the curve lies completely within the convex hull of control points P_i.

3. Local support: $N_{i,k}(h) = 0 \quad if \quad h\varepsilon\,[h_i, h_{i+k+1}]$
   The third property explains that every single segment of the curve is influenced by only k control points.

4. Continuity: $N_{i,k}(h)$ is $(k-2)$ times continuously differentiable.

From these properties, it can be noticed that Bernstein polynomial, $B_{i,n}(h)$, has the same first two properties like B-spline basis functions.
The basis functions of B-spline also have the property of recursion which is described as follows:

$$N_{i,k}(h) = (h - h_i)\frac{N_{i,k-1}(h)}{h_{i+k-1} - h_i} + (h_{i+k} - h)\frac{N_{i+1,k-1}(h)}{h_{i+k} - h_{i+1}} \tag{3.34}$$
$$for \quad k > 1 \quad and \quad i = 0, 1, 2, ..., n$$

and,

$$N_{i,1} = \begin{cases} 1, & h_i \leq h \leq h_{i+1} \\ 0, & otherwise \end{cases} \quad for \quad k = 1 \tag{3.35}$$

$N_{i,1}$ is constant for the value of $k = 1$ (eq. 3.35). General value of k generates a polynomial in h which leads to the formulation of a curve having order k and degree $k - 1$ (eq. 3.34). The h_i are known as parametric knots or knot values. For an open curve;

$$h_i = \begin{cases} 0, & j < k \\ j - k + 1 & k \leq j \leq n \\ n - k + 2 & j > n \end{cases} \tag{3.36}$$

Where,

$$0 \leq j \leq n + k \tag{3.37}$$

and the range of h is:

$$0 \leq h \leq n - k + 2 \tag{3.38}$$

Therefore, eq. 3.37 makes it clear that $(n + k + 1)$ knots are required to make a $(k - 1)$ degree curve defined by $(n + 1)$ control points.

$$n - k + 2 > 0 \tag{3.39}$$

The above expression shows that at least two, three, and four control points are needed to define a linear, quadratic, and cubic B-spline curve respectively. The summary of the characteristics of B-spline curves is as follows:

1. Local control of the curve can be achieved by changing the position of the control points. Figure 3.8 shows the local control of a cubic B-spline by moving P_3 to P_3^* and P_3^{**}.
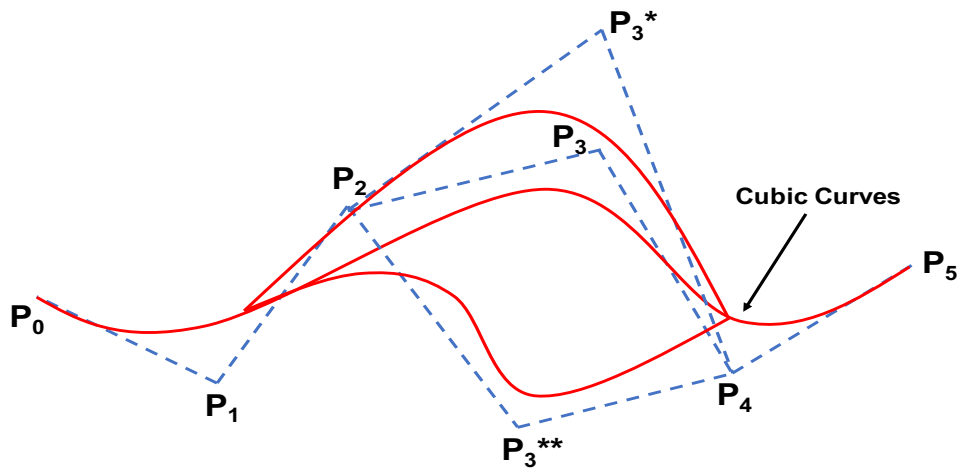
Figure 3.8: Local control of B-spline curves

2. Like Bezier curve, B-splines also passes through the first and last point and is tangent to the first and last segments of the control polygon.

3. For the same number of control points, the increase in the degree of the B-spline curve tighten the curve (Fig. 3.9).
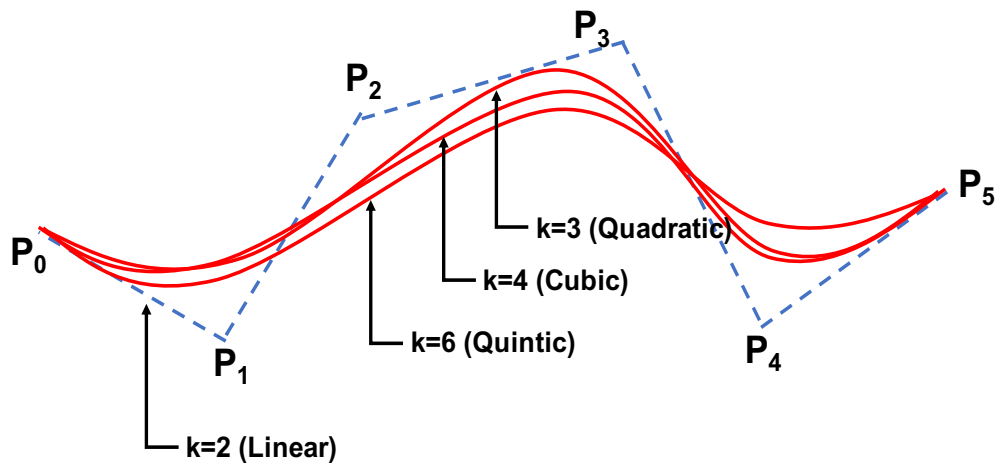
Figure 3.9: Effect of the degree of B-spline curve

4. If k = the number of control points $(n+1)$, the resulting B-spline becomes the bezier curve. Also, in this case, h varies in the range of 0 to 1 (eq. 3.38), same as bezier curves.

In the case of B-splines, the increment in the knot values defined in eq. 3.36 is

always uniform, and the incremental value is 1. A B-spline based on these uniform knots is called a uniform B-spline. During the modification in the shape of the curve, the addition or the deletion of the knot values usually happens, which produces the non-uniform gaps between the knots. Also, it creates Non-Uniform Rational B-Splines (NURBS). NURBS are used in trajectory planning for mobile robots in [Aleotti 2005], [Jalel 2015], [Hashemian 2017]. NURBS have the following form:

$$r(h) = \frac{\sum_{i=0}^{n+1} N_{i,k}(h)w_i P_i}{\sum_{i=0}^{n+1} N_{i,k}(h)w_i} \tag{3.40}$$

Here, $N_{i,k}$ is the basis function, n is the number of control points P_i and w_i are the corresponding weights. Therefore, the only difference from B-splines is the weights provided to the control points.

Remark 3.5.3. For the given four boundary conditions, either cubic, or quadratic, or linear B-spline can be generated to reconstruct the shape of the soft-continuum manipulators. The advantage in this case is the local control of the curve. But the basis functions used for B-splines are not easy to solve, and they have an iterative solution. Also, it is given that as per our known four boundary conditions, the cubic B-spline will be the same as the cubic Bezier [Zeid 2004]. **B-spline is not a single continuous function from start (P_s) to the endpoint (P_f) of the manipulator. It is a sequence of different polynomials joined at the knot vectors. Therefore, they are complicated for the control of posture of the soft-continuum manipulator, and the complexity will not allow us to further exploit these curves for either kinematic or dynamic model of the soft-continuum manipulators.** Therefore, besides certain advantages of B-splines, they are complex to use for the reconstruction of the shape of the soft-continuum manipulators.

3.5.4   Pythagorean Hodograph

PH curves are the synthetic parametric curves. These curves were introduced by Farouki and Sakkalis [Farouki 1990] in 1990. **These curves were added to overcome the drawbacks of the previously used curves, e.g., Bezier, B-splines, NURBS, etc. The most notable properties of these curves are, their arc-length has closed form solution, and they possess rational offset curves which are not possible with the Hermite, Bezier, B-splines, and NURBS.** Since then, PH curves are used in many fields. 3D path planning and obstacle avoidance of Unmanned Aerial Vehicles (UAVs) is done using PH curves [Shanmugavel 2007], [Shah 2010]. In [Bruyninckx 1997], PH curves are used for path planning of mobile robots and also the concept of modeling the shape of the planar hyper-redundant

manipulator is introduced. In this work, we are exploiting PH curves to model the shape of the spatial soft-continuum manipulators. PH curves are the special case of normal polynomial parametric curves having additional properties. These curves are explained using ordinary polynomial parametric curves as follows [Farouki 2008]:

Definition 3.5.4. Let $r(h)$ be the polynomial curve characterizing the shape of the soft-continuum manipulator.

$$r(h) = (x(h), y(h), z(h)); \qquad 0 \leq h \leq 1 \tag{3.41}$$

Where, h is the normalized curvilinear coordinate of the curve. Therefore,

$$\begin{aligned} P_s &= r(0) = (x(0), y(0), z(0)) \\ P_f &= r(1) = (x(1), y(1), z(1)) \end{aligned} \tag{3.42}$$

Definition 3.5.5. The Hodograph $r'(h)$ is defined as the first derivative of the curve. It is parallel to the tangent to the curve. The hodograph of the curve r is given by:

$$r'(h) = (x'(h), y'(h), z'(h)) \tag{3.43}$$

$x'(h), y'(h), z'(h)$ are the first derivative components of the position vector.

Definition 3.5.6. Let $L(h)$ represents the length of the soft-continuum manipulator reconstructed using the curve $r(h)$:

$$L(h) = \int_0^1 |r'(h)| \, \mathrm{d}h = \int_0^1 \sqrt{x'(h)^2 + y'(h)^2 + z'(h)^2} \, \mathrm{d}h \tag{3.44}$$

Equation 3.44 can compute the length of the soft-continuum manipulator but the closed form solution is not possible, due to the presence of the square root inside the integral. Therefore, a numerical quadrature is required to obtain a numerical approximation of the true solution. To resolve this situation, the square root sign can be eliminated from eq. 3.44, if:

$$x'(h)^2 + y'(h)^2 + z'(h)^2 = \sigma(h)^2 \tag{3.45}$$

Equation 3.45 is called Pythagorean law or condition in three-dimensions. Hence,

Definition 3.5.7. The first derivatives (hodographs) of parametric polynomials, which satisfy the Pythagorean condition, are known as Pythagorean Hodographs.

Therefore, eq. 3.44 can be written as:

$$L(h) = \int_0^1 |\sigma(h)| \, \mathrm{d}h \tag{3.46}$$

Equation 3.46 shows that the Pythagorean hodographs can yield a closed form solution to determine the length of the soft-continuum manipulator.

A sufficient and necessary condition to satisfy eq. 3.45 is identified in [Dietz 1993], i.e. the hodograph components are expressed in function of four polynomials $u(h)$, $v(h)$, $p(h)$ and $q(h)$, as:

$$x'(h) = [u^2(h) + v^2(h) - p^2(h) - q^2(h)] \tag{3.47}$$

$$y'(h) = 2[u(h)q(h) + v(h)p(h)] \tag{3.48}$$

$$z'(h) = 2[v(h)q(h) - u(h)p(h)] \tag{3.49}$$

$u(h)$, $v(h)$, $p(h)$ and $q(h)$ polynomials are chosen so that $\sigma(h)$ is:

$$\sigma(h) = u^2(h) + v^2(h) + p^2(h) + q^2(h) \tag{3.50}$$

In general, from eqs. 3.47-3.49, it is clear that a PH curve is of degree $2n + 1$, when n is the degree of polynomials $u(h)$, $v(h)$, $p(h)$, $q(h)$. Therefore, the lowest degree of a PH-curve is cubic, while polynomials $u(h)$, $v(h)$, $p(h)$ and $q(h)$ are linear. Quintic PH curves are produced using quadratic polynomials.

3.5.4.1   Cubic PH Curve

In order to derive an expression for a spatial cubic PH curve, linear polynomials $u(h)$, $v(h)$, $p(h)$ and $q(h)$ are chosen in the Bernstein form as follows:

$$u(h) = u_0(1 - h) + u_1 h \tag{3.51}$$

$$v(h) = v_0(1 - h) + v_1 h \tag{3.52}$$

$$p(h) = p_0(1 - h) + p_1 h \tag{3.53}$$

$$q(h) = q_0(1 - h) + q_1 h \tag{3.54}$$

Such that the pythagorean condition

$$\sigma(h) = u^2(h) + v^2(h) + p^2(h) + q^2(h) \tag{3.55}$$

is satisfied. Substituting these values in equations 3.47, 3.48 and 3.49, and integrating from both sides, gives:

$$x(h) = \int [[u_0^2 + v_0^2 - p_0^2 - q_0^2](1 - h)^2 + 2[u_0 u_1 + v_0 v_1 - p_0 p_1 \\ - q_0 q_1](1 - h)h + [u_1^2 + v_1^2 - p_1^2 - q_1^2]h^2]dh \tag{3.56}$$

$$y(h) = \int [[u_0 q_0 + v_0 p_0](1-h)^2 + 2[u_1 q_0 + u_0 q_1 + v_1 p_0$$
$$- v_0 p_1](1-h)h + [u_1 q_1 + v_1 p_1]dh \tag{3.57}$$

$$z(h) = \int [[v_0 q_0 + u_0 p_0](1-h)^2 + 2[v_1 q_0 + v_0 q_1 - u_1 p_0$$
$$- u_0 p_1](1-h)h + [v_1 q_1 - u_1 p_1]dh \tag{3.58}$$

The indefinite integrals of Bernstein is given as in [Farouki 1990], [Farouki 1995];

$$\int \left[\binom{n-1}{k} (1-h)^{n-1-k} h^k \right] dt = \frac{1}{n} \sum_{j=k+1}^{n} \binom{n}{j} (1-h)^{n-j} h^j$$
$$= \frac{1}{n} \sum_{j=k+1}^{n} \binom{n}{j} (1-h)^{n-(k+1)} h^{k+1} \tag{3.59}$$

Where, n = degree of the curve, $k = 0, 1, ...n - 1, j = k+1, \binom{n}{j} = \frac{n!}{(n-j)!j!}$ and $h \in [0 \quad 1]$. Therefore, for the cubic (n = 3) curve, eqs. 3.56, 3.57, 3.58 implies,

$$x(h) = \sum_{k=0}^{3} x_k \binom{3}{k} (1-h)^{3-k} h^k \tag{3.60}$$

$$y(h) = \sum_{k=0}^{3} y_k \binom{3}{k} (1-h)^{3-k} h^k \tag{3.61}$$

$$z(h) = \sum_{k=0}^{3} z_k \binom{3}{k} (1-h)^{3-k} h^k \tag{3.62}$$

Using these equations, the general equation of a spatial cubic PH curve $r(h)$ with control points P_k is written as:

$$r(h) = \begin{bmatrix} x(h) \\ y(h) \\ z(h) \end{bmatrix} = \sum_{k=0}^{3} P_k \binom{3}{k} (1-h)^{3-k} h^k \tag{3.63}$$

Therefore,

$$r(h) = P_0(1-h)^3 + 3P_1(1-h)^2 h + 3P_2(1-h)h^2 + P_3 h^3 \tag{3.64}$$

It is similar to the Bezier curve equation, as we used Bernstein polynomials to formulate this equation. Therefore, it is called PH-Bezier equation. Further, control points of this equation have to be calculated using Pythagorean

Condition. The equation can be written in the matrix form as:

$$r(h) = \begin{bmatrix} 1 \\ h \\ h^2 \\ h^3 \end{bmatrix}^T \begin{bmatrix} 1 & 0 & 0 & 0 \\ -3 & 3 & 0 & 0 \\ 3 & -6 & 3 & 0 \\ -1 & 3 & -3 & 1 \end{bmatrix} \begin{bmatrix} P_0 \\ P_1 \\ P_2 \\ P_3 \end{bmatrix} \tag{3.65}$$

Calculation of the Control Points

A cubic PH curve has four control points (P_0, P_1, P_2, P_3). We want to reconstruct the shape of the soft-continuum manipulators using PH curve construction from the base (P_s) to the tip (P_f) of the manipulator. As shown
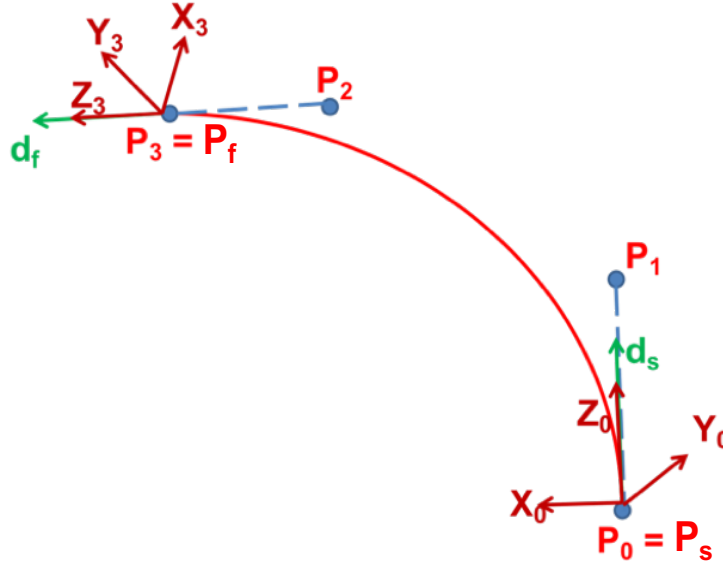
Figure 3.10: Basic schematic of a cubic PH curve

in Fig. 3.10, the first and the last control points are given as;

$$P_0 = P_s$$
$$P_3 = P_f$$

The remaining two control points P_1 and P_2 are computed using the given four conditions. Derivative of eq. 3.64 gives:

$$r'(h) = 3(P_1 - P_0)(1 - h)^2 + 3(P_2 - P_1)(1 - h)h + 3(P_3 - P_2)h^2 \tag{3.66}$$

At the base of the manipulator (h=0);

$$r(0) = P_0, \qquad r'(0) = 3(P_1 - P_0) \tag{3.67}$$

At the tip of the manipulator (h=1);

$$r(1) = P_3, \qquad r'(1) = 3(P_3 - P_2) \qquad (3.68)$$

Since the initial and final points and the derivatives at these points are known;

$$r(0) = P_0 = (x_s, y_s, z_s) \qquad (3.69)$$

$$r'(0) = 3(P_1 - P_0) = (dx_s, dy_s, dz_s) \qquad (3.70)$$

$$r(1) = P_3 = (x_f, y_f, z_f) \qquad (3.71)$$

$$r'(1) = 3(P_3 - P_2) = (dx_f, dy_f, dz_f) \qquad (3.72)$$

Rearranging 3.70 and 3.72 gives;

$$P_1 = P_0 + \frac{1}{3}(dx_s, dy_s, dz_s) \qquad (3.73)$$

$$P_2 = P_3 - \frac{1}{3}(dx_f, dy_f, dz_f) \qquad (3.74)$$

Therefore, using these four control points, a cubic PH curve representing the shape of the backbone of the soft-continuum manipulator is generated using eq. 3.65.

As all of the control points are fixed in the formulation of cubic PH curve, there are no free control points.

3.5.4.2 Quintic PH Curve

The derivation of the expression for the quintic PH curve chooses the four quadratic polynomials $u(h)$, $v(h)$, $p(h)$, $q(h)$ in Bernstein form [Farouki 2002, Farouki 2008] as follows:

$$
\begin{aligned}
u(h) &= u_0(1-h)^2 + u_1 2(1-h)h + u_2 h^2 \\
v(h) &= v_0(1-h)^2 + v_1 2(1-h)h + v_2 h^2 \\
p(h) &= p_0(1-h)^2 + p_1 2(1-h)h + p_2 h^2 \\
q(h) &= q_0(1-h)^2 + q_1 2(1-h)h + q_2 h^2
\end{aligned}
\qquad (3.75)
$$

u_m, v_m, p_m, q_m are called Bernstein coefficients with $m = 0,1,2$. Inserting eqs. 3.75 in eqs. 3.47, 3.48, 3.49, and integrating from both sides yields:

$$
\begin{aligned}
x(h) = \int (&[u_0^2 + v_0^2 - p_0^2 - q_0^2](1-h)^4 + 4[u_0 u_1 + v_0 v_1 - p_0 p_1 \\
&- q_0 q_1](1-h)^3 h + 2[u_1^2 + u_0 u_2 + v_1^2 + v_0 v_2 - p_1^2 - p_0 p_2 \\
&- q_1^2 - q_0 q_2](1-h)^2 h^2 + 4[u_1 u_2 + v_1 v_2 - p_1 p_2 - q_1 q_2] \\
&(1-h)h^3 + [u_2^2 + v_2^2 - p_2^2 - q_2^2]h^4)dh
\end{aligned}
\qquad (3.76)
$$

$$
\begin{aligned}
y(h) = \int \big(& 2[u_0 q_0 + v_0 p_0](1-h)^4 + 4[u_0 q_1 + u_1 q_0 + v_0 p_1 \\
& + v_1 p_0](1-h)^3 h + 2[u_0 q_2 + 4u_1 q_1 + u_2 q_0 + v_0 p_2 + 4v_1 p_1 \\
& + v_2 p_0](1-h)^2 h^2 + 4[u_1 q_2 + u_2 q_1 + v_1 p_2 + v_2 p_1] \\
& (1-h)h^3 + 2[u_2 q_2 + v_2 p_2]h^4 \big) dh
\end{aligned}
\tag{3.77}
$$

$$
\begin{aligned}
z(h) = \int \big(& 2[v_0 q_0 - u_0 p_0](1-h)^4 + 4[v_0 q_1 + v_1 q_0 - u_0 p_1 \\
& - u_1 p_0](1-h)^3 h + 2[v_0 q_2 + 4v_1 q_1 + v_2 q_0 - u_0 p_2 - 4u_1 p_1 \\
& - u_2 p_0](1-h)^2 h^2 + 4[v_1 q_2 + v_2 q_1 - u_1 p_2 - u_2 p_1] \\
& (1-h)h^3 + 2[v_2 q_2 - u_2 p_2]h^4 \big) dh
\end{aligned}
\tag{3.78}
$$

Since the indefinite integral of the Bernstein polynomial is given by [Farouki 1990], [Farouki 1995]:

$$
\begin{aligned}
\int \left[\binom{n-1}{k} (1-h)^{n-1-k} h^k \right] dt &= \frac{1}{n} \sum_{j=k+1}^{n} \binom{n}{j} (1-h)^{n-j} h^j \\
&= \frac{1}{n} \sum_{j=k+1}^{n} \binom{n}{j} (1-h)^{n-(k+1)} h^{k+1}
\end{aligned}
\tag{3.79}
$$

Where, n = degree of the curve, $k = 0, 1, ... n-1$, $j = k+1$, $\binom{n}{j} = \frac{n!}{(n-j)!j!}$ and $h \in [0 \quad 1]$. Therefore, for the quintic ($n = 5$) curve, eqs. 3.76, 3.77, 3.78 implies,

$$
x(h) = \sum_{k=0}^{5} x_k \binom{5}{k} (1-h)^{5-k} h^k
\tag{3.80}
$$

$$
y(h) = \sum_{k=0}^{5} y_k \binom{5}{k} (1-h)^{5-k} h^k
\tag{3.81}
$$

$$
z(h) = \sum_{k=0}^{5} z_k \binom{5}{k} (1-h)^{5-k} h^k
\tag{3.82}
$$

Where x_k, y_k, z_k are in terms of coefficients u_m, v_m, p_m, and q_m. From eqs. 3.80, 3.81, 3.82, the general equation of quintic PH curve $r(h)$ with control points $P_k = (x_k, y_k, z_k)$ can be written as:

$$
r(h) = \begin{bmatrix} x(h) \\ y(h) \\ z(h) \end{bmatrix} = \sum_{k=0}^{5} P_k \binom{5}{k} (1-h)^{5-k} h^k
\tag{3.83}
$$

This is Bernstein-Bezier form. The matrix form of the curve $r(h)$ is given by:

$$r(h) = \begin{bmatrix} 1 \\ h \\ h^2 \\ h^3 \\ h^4 \\ h^5 \end{bmatrix}^T \begin{bmatrix} 1 & 0 & 0 & 0 & 0 & 0 \\ -5 & 5 & 0 & 0 & 0 & 0 \\ 10 & -20 & 10 & 0 & 0 & 0 \\ -10 & 30 & -30 & 10 & 0 & 0 \\ 5 & -20 & 30 & -20 & 5 & 0 \\ -1 & 5 & -10 & 10 & -5 & 1 \end{bmatrix} \begin{bmatrix} P_0 \\ P_1 \\ P_2 \\ P_3 \\ P_4 \\ P_5 \end{bmatrix} \tag{3.84}$$

The objective is to find the optimal non-linear quadratic polynomials $u(h)$, $v(h)$, $p(h)$, and $q(h)$ to compute the control points $P_0, ...P_5$. Fig. 3.11 shows
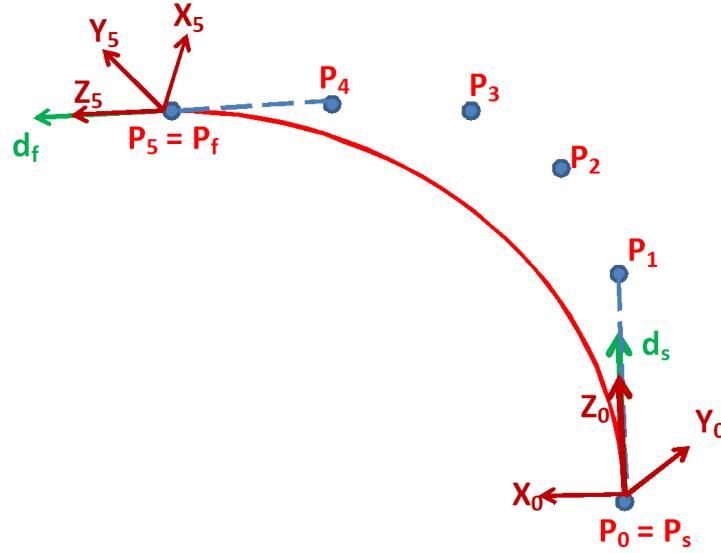
Figure 3.11: Basic Schematic of a quintic PH curve

the basic schematic of a PH curve used to reconstruct the shape of the soft-continuum manipulator. $\vec{d_s}$ and $\vec{d_f}$ are the direction vectors at starting (base) and final point (center of tool) of soft-continuum manipulator respectively. P_0 to P_5 are the control points of quintic PH-curve. To simplify the computation of these control points, a quaternion formulation (appendix A) is used. Using eqs. 3.47, 3.48 and 3.49, the hodograph of the spatial PH becomes:

$$\vec{r}'(h) = [u^2(h) + v^2(h) - p^2(h) - q^2(h)]\vec{i} + 2[u(h)q(h) - \\ v(h)p(h)]\vec{j} + 2[v(h)q(h) - u(h)p(h)]\vec{k} \tag{3.85}$$

Where $\vec{i}, \vec{j}, \vec{k}$ are unit vectors. Equation 3.85 can be expressed in the quaternion form, in terms of $A(h)$ [Choi 2002] as follows:

$$\vec{r}'(h) = A(h)\vec{i}A^*(h) \tag{3.86}$$

$A(h)$ is the polynomial in quaternion form in terms of $u(h), v(h), p(h), q(h)$. $A^*(h)$ is the conjugate of $A(h)$. Left hand side of eq. 3.86 is always a pure vector (appendix A).

Quadratic polynomials $(u(h), v(h), p(h), q(h))$ are required to generate a quintic PH curve. Therefore, in quaternion form, the quadratic polynomial $A(h)$ is assumed in Bernstein form [Farouki 2002, Farouki 2008] as:

$$A(h) = A_0(1-h)^2 + A_1(1-h)2h + A_2h^2 \tag{3.87}$$

This quadratic polynomial has quaternion coefficients as:

$$A_m = u_m + v_m\vec{i} + p_m\vec{j} + q_m\vec{k} \tag{3.88}$$

$$\text{with m} = 0,1,2.$$

The control points of quintic curve (eq. 3.84) are given in quaternion form [Farouki 2002]:

$$\vec{P_1} = \vec{P_0} + \frac{1}{5}A_0\vec{i}A_0^* \tag{3.89}$$

$$\vec{P_2} = \vec{P_1} + \frac{1}{10}(A_0\vec{i}A_1^* + A_1\vec{i}A_0^*) \tag{3.90}$$

$$\vec{P_3} = \vec{P_2} + \frac{1}{30}(A_0\vec{i}A_2^* + 4A_1\vec{i}A_1^* + A_2\vec{i}A_0^*) \tag{3.91}$$

$$\vec{P_4} = \vec{P_3} + \frac{1}{10}(A_1\vec{i}A_2^* + A_2^*\vec{i}A_0^*) \tag{3.92}$$

$$\vec{P_5} = \vec{P_4} + \frac{1}{5}A_2\vec{i}A_2^* \tag{3.93}$$

The known data in the pure vector quaternion form is as follows:

$$\vec{P_s} = x_s\vec{i} + y_s\vec{j} + z_s\vec{k}, \ \vec{d_s} = d_{sx}\vec{i} + d_{sy}\vec{j} + d_{sz}\vec{k}$$
$$\vec{P_f} = x_f\vec{i} + y_f\vec{j} + z_f\vec{k}, \ \vec{d_f} = d_{fx}\vec{i} + d_{fy}\vec{j} + d_{fz}\vec{k}$$

As mentioned above, we have four conditions, similar to those required for Hermite interpolation problem. Therefore using these conditions, the Hermite interpolation problem is solved to compute the coefficients A_0, A_1, A_2. Using eq. 3.86, interpolation at the end points yields the following equations:

$$\begin{aligned} A_0\vec{i}A_0^* = \vec{r'}(0) = \vec{d_s} \\ A_2\vec{i}A_2^* = \vec{r'}(1) = \vec{d_f} \end{aligned} \tag{3.94}$$

Since eqs. 3.94 are of the type A.12, they can be solved as mentioned in appendix A to give A_0 and A_2 as:

$$A_0 = \sqrt{\frac{1}{2}(1+\lambda_s)|\vec{d_i}|}(-\sin\phi_0 + \cos\phi_0\vec{i} +$$
$$\frac{\mu_s\cos\phi_0 + \nu_s\sin\phi_0}{1+\lambda_s}\vec{j} + \frac{\nu_s\cos\phi_0 - \mu_s\sin\phi_0}{1+\lambda_s}\vec{k}) \tag{3.95}$$

$$A_2 = \sqrt{\frac{1}{2}(1+\lambda_f)|\vec{d_f}|}(-\sin\phi_2 + \cos\phi_2\vec{i}+$$
$$\frac{\mu_f\cos\phi_2 + \nu_f\sin\phi_2}{1+\lambda_f}\vec{j} + \frac{\nu_f\cos\phi_2 - \mu_f\sin\phi_2}{1+\lambda_f}\vec{k}) \tag{3.96}$$

Where $(\lambda_s, \mu_s, \nu_s)$ and $(\lambda_f, \mu_f, \nu_f)$ are the direction cosines of $\vec{d_s}$ and $\vec{d_f}$ respectively. ϕ_0 and ϕ_2 are free angular variables.

To determine A_1, position vector $(\vec{P_f} - \vec{P_i})$ can be calculated as the summation of the vectors connecting initial and final points through lines as [Farouki 2002]:

$$\int_0^1 A(h)\vec{i}A^*(h)dh = \vec{P_f} - \vec{P_i}$$
$$= \frac{1}{5}A_0\vec{i}A_1^* + \frac{1}{10}(A_0\vec{i}A_1^* + A_1\vec{i}A_0^*)$$
$$+ \frac{1}{30}(A_0\vec{i}A_2^* + 4A_1\vec{i}A_1^* + A_2\vec{i}A_0^*) \tag{3.97}$$
$$+ \frac{1}{10}(A_1\vec{i}A_2^* + A_2\vec{i}A_1^*) + \frac{1}{5}(A_2\vec{i}A_2^*)$$

$$\implies \vec{P_f} - \vec{P_i} = \frac{1}{120}(24A_0\vec{i}A_0^* + 12(A_0\vec{i}A_1^* + A_1\vec{i}A_0^*)+$$
$$4(A_0\vec{i}A_2^* + 4A_1\vec{i}A_1^* + A_2\vec{i}A_0^*) + 12(A_1\vec{i}A_2^* + A_2\vec{i}A_1^*)+ \tag{3.98}$$
$$24A_2\vec{i}A_2^*)$$

$$120(\vec{P_f} - \vec{P_i}) = 24A_0\vec{i}A_0^* + 12(A_0\vec{i}A_1^* + A_1\vec{i}A_0^*) + 4(A_0\vec{i}A_2^*+$$
$$4A_1\vec{i}A_1^* + A_2\vec{i}A_0^*) + 12(A_1\vec{i}A_2^* + A_2\vec{i}A_1^*) + 24A_2\vec{i}A_2^* \tag{3.99}$$

Subtracting $15(A_0\vec{i}A_0^* + A_2\vec{i}A_2^*)$ from both sides of eq. 3.99;

$$120(\vec{P_f} - \vec{P_i}) - 15(A_0\vec{i}A_0^* + A_2\vec{i}A_2^*) = 9A_0\vec{i}A_0^* + 12(A_0\vec{i}A_1^* + A_1\vec{i}A_0^*)+$$
$$4(A_0\vec{i}A_2^* + 4A_1\vec{i}A_1^* + A_2\vec{i}A_0^*) + 12(A_1\vec{i}A_2^* + A_2\vec{i}A_1^*) + 9A_2\vec{i}A_2^* \tag{3.100}$$

Adding $5(A_0\vec{i}A_2^* + A_2\vec{i}A_0^*)$ to the both sides of eq. 3.100;

$$120(\vec{P_f} - \vec{P_i}) - 15(A_0\vec{i}A_0^* + A_2\vec{i}A_2^*) + 5(A_0\vec{i}A_2^* + A_2\vec{i}A_0^*) = 9A_0\vec{i}A_0^*+$$
$$12(A_0\vec{i}A_1^* + A_1\vec{i}A_0^*) + 4(A_0\vec{i}A_2^* + 4A_1\vec{i}A_1^* + A_2\vec{i}A_0^*)+$$
$$12(A_1\vec{i}A_2^* + A_2\vec{i}A_1^*) + 9A_2\vec{i}A_2^* + 5(A_0\vec{i}A_2^* + A_2\vec{i}A_0^*) \tag{3.101}$$

Simplification of eq. 3.101 gives;

$$120(\vec{P_f} - \vec{P_i}) - 15(\vec{dp}_{si} + \vec{dp}_{fi}) + 5(A_0\vec{i}A_2^* + A_2\vec{i}A_0^*) =$$
$$(3A_0 + 4A_1 + 3A_2)\vec{i}(3A_0 + 4A_1 + 3A_2)^* \tag{3.102}$$

Equation 3.102 has the form $A\vec{i}A^*$ if $A = (3A_0 + 4A_1 + 3A_2)$ and $(3A_0 + 4A_1 + 3A_2)\vec{i}(3A_0 + 4A_1 + 3A_2)^* = c_x\vec{i} + c_y\vec{j} + c_z\vec{k}$. Therefore, from Appendix A, the solution becomes;

$$
\begin{aligned}
(3A_0 + 4A_1 + 3A_2) = \sqrt{\frac{1}{2}(1 + \lambda)|\vec{c}|}(-\sin\phi_1 + \cos\phi_1\vec{i} + \\
\frac{\mu\cos\phi_1 + \nu\sin\phi_1}{1 + \lambda}\vec{j} + \frac{\nu\cos\phi_1 - \mu\sin\phi_1}{1 + \lambda}\vec{k})
\end{aligned}
\tag{3.103}
$$

Using eq. 3.103 as well as known values of A_0 and A_2, value of A_1 is computed as:

$$
\begin{aligned}
A_1 = -\frac{3}{4}(A_0 + A_2) + \frac{1}{4}\sqrt{\frac{1}{2}(1 + \lambda)|\vec{c}|}(-\sin\phi_1 + \cos\phi_1\vec{i} + \\
\frac{\mu\cos\phi_1 + \nu\sin\phi_1}{1 + \lambda}\vec{j} + \frac{\nu\cos\phi_1 - \mu\sin\phi_1}{1 + \lambda}\vec{k})
\end{aligned}
\tag{3.104}
$$

and,

$$
\begin{aligned}
\vec{c} = 120(\vec{P_f} + \vec{P_s}) - 15(\vec{d_f} + \vec{d_s}) \\
+ 5(A_0\vec{i}A_2^* + A_2\vec{i}A_0^*)
\end{aligned}
\tag{3.105}
$$

Here, (λ, μ, ν) are the direction cosines of $\vec{c}$. ϕ_1 is an another free angular variable, it depends on ϕ_0 and ϕ_2.

Control points are computed using eqs. 3.89-3.93. From eqs. 3.89 and 3.93, P_1 and P_4 are fixed due to the input direction vectors at the end points. But the presence of free angular variables makes P_2 and P_3 as free control points. Different PH curves can be generated using different combinations of the free angular variables ϕ_0 and ϕ_2, as shown in Fig. 3.12. In this figure, P_s and P_f are chosen randomly, to show the effect of free variable angles on the shape of the curve. Therefore, we need to choose one optimized curve for the shape reconstruction of soft-continuum manipulators.

Minimizing Potential Energy

The curvature of the curve differs from one combination of free angular variables to the other. A physical system always tends to move from one point to the other with minimum potential energy, which is the combination of bending and twisting energy for the case of soft-continuum manipulators. Therefore, a curve with minimum potential energy can approximate the real shape, and expressed as follows:

$$
Min(E = \int \omega^2(L)dL)
\tag{3.106}
$$

$$
\text{subject to} \qquad L_{min} \leq L \leq L_{max}
\tag{3.107}
$$
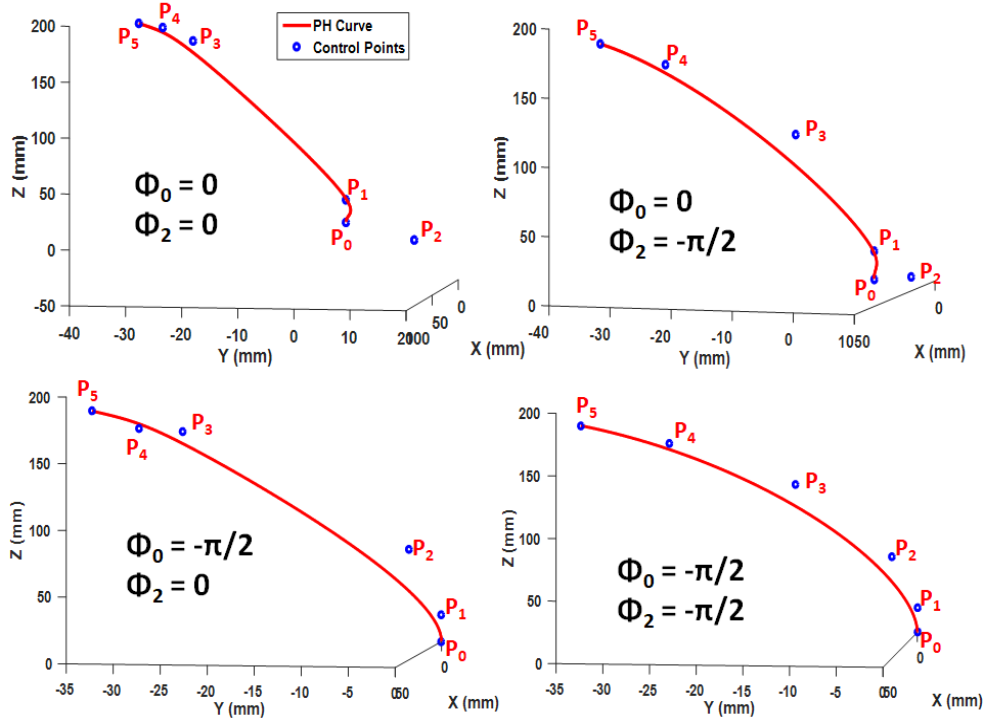
Figure 3.12: Variation of control points P_2, P_3 w.r.t. ϕ_0, ϕ_2

$$where \qquad E = \int \omega^2(L)\frac{dL}{dh}dh = \int \omega^2(h)\sigma(h)dh \qquad (3.108)$$

Where ω is the total bending of the curve as a function of h. In [Farouki 1996], it is also concluded that the constraint of lower energy is most appropriate for application of PH in context of modeling the actual parts [Farouki 2002]. Total bending ω is given by :

$$\omega = \sqrt{\kappa^2 + \tau^2} \qquad (3.109)$$

where κ is the curvature and τ is the torsion of the curve, as:

$$with \qquad \kappa = \frac{|\vec{r}' \times \vec{r}''|}{|\vec{r}'|^3} \qquad and \qquad \tau = \frac{(\vec{r}' \times \vec{r}'').\vec{r}'''}{|\vec{r}' \times \vec{r}''|^2} \qquad (3.110)$$

If the torsion is restricted in the structure of the soft-continuum manipulator, the value of τ can be assumed as zero ($\tau = 0$). The first, second and third derivatives of the vector curve $\vec{r}$ are represented in quaternion representation as:

$$\vec{r}' = A\vec{i}A^*$$
$$\vec{r}'' = A'\vec{i}A^* + A\vec{i}A'^*$$
$$\vec{r}''' = A''\vec{i}A^* + 2A'\vec{i}A'^* + A\vec{i}A''^*$$

It is empirically proved [Farouki 2008] that a PH curve will have minimum bending energy if $\phi_0 = \phi_2 = \frac{-\pi}{2}$. Therefore, in our case, ϕ_0 and ϕ_2 are varied in the range of $[-\pi \quad \pi]$. Potential energy is calculated for all of the PH curves generated with ϕ_0, $\phi_2 \in [-\pi \quad \pi]$ in order to select a PH curve with minimum potential energy.

3.5.4.3   Generalized PH Curve

Formulation of cubic and quintic PH curves can be extended to the generalized form of the PH curve. As mentioned earlier, a PH curve of degree $2n + 1$ can be formulated while n degree polynomials $u(h)$, $v(h)$, $p(h)$, $q(h)$ are used. For generalized PH curve formulation, the four n^{th} degree polynomials $u(h)$, $v(h)$, $p(h)$, $q(h)$ in Bernstein form are as follows:

$$
\begin{aligned}
u(h) &= \sum_{k=0}^{n} u_k B_{k,n}(h) \\
v(h) &= \sum_{k=0}^{n} v_k B_{k,n}(h) \\
p(h) &= \sum_{k=0}^{n} p_k B_{k,n}(h) \\
q(h) &= \sum_{k=0}^{n} q_k B_{k,n}(h)
\end{aligned}
\tag{3.111}
$$

Here, $B_{k,n}(h)$ is the Bernstein polynomial and is given by:

$$
B_{k,n}(h) = \frac{n!}{k!(n-k)!}(1-h)^{n-k}h^k
\tag{3.112}
$$

Use of these polynomials leads to a generalized PH curve of degree $2n + 1$ same as in the case of cubic and quintic PH curves. The generalized equation of PH is as follows:

$$
r(h) = \sum_{k=0}^{2n+1} P_k \binom{2n+1}{k}(1-h)^{2n+1-k}h^k
\tag{3.113}
$$

Therefore, the use of linear, quadratic, cubic,... degree $u(h)$, $v(h)$, $p(h)$, $q(h)$ polynomials produces cubic, quintic, seven degree,...PH curve respectively.

Remark 3.5.4. For the given four boundary conditions, cubic and quintic PH curves are developed. The higher degree means these curves can generate more flexible shapes. **The PH curves possess significant computational advantages over polynomial curves in general.** Also, for given points and tangents, PH curves can exhibit better profiles due to their advantages in arc length calculation and their rational offset property.

Table 3.1: Comparison of different synthetic curves to reconstruct the shape of the soft-continuum manipulators for four known boundary conditions

	Hermite	Bezier	B-spline & NURBS	Cubic PH	Quintic PH
Degree	Always cubic	Cubic	Cubic, quadratic or linear	Cubic	Quintic
Basis functions	No basis functions are used	Bernstein	B-spline	Bernstein	Bernstein
Solution of basis functions	N.A.	Analytical	Iterative	Analytical	Analytical
Solution to the curve	Unique	Unique	Unique	Unique	Multiple
Optimization	Not required	Not required	Not required	Not required	Minimum potential energy
Calculation of the length	Not closed form	Not closed form	Not closed form	Closed form	Closed form
Curvilinear Coordinate 'h'	$0 \leq h \leq 1$	$0 \leq h \leq 1$	$0 \leq h \leq h_{max}$	$0 \leq h \leq 1$	$0 \leq h \leq 1$

3.6   Synthetic Curves v/s Soft-continuum Manipulators

It is clear from the previous development that synthetic curves are more suitable to reconstruct the shape of the soft-continuum manipulators because they provide the advantage to control the shape through control points. Therefore, table 3.1 shows the comparison of different synthetic curves based on their formulation for the known boundary conditions. This theoretical comparison of Hermite, Bezier, B-spline & NURBS, cubic PH and quintic PH curves to reconstruct the shape of the soft-continuum manipulators leads us to the following conclusions:

1. The flexibility in the shape of the soft-continuum manipulators depends on the degree of the curves used to reconstruct it. **The highest degree possible with Hermite, Bezier, and B-spline curves is cubic only**. But in the case of PH curves, even quintic PH curves can be generated. Therefore, it is a positive point, and we are free to use cubic or quintic degree curve according to the needed flexibility behavior of the continuum manipulator. Going for high degrees, PH-curve induces the problem of "Over-fitting" (Runge's phenomenon) [Dahlquist 2008].

2. Bernstein basis function is used in case of Bezier and PH curves, and B-spline basis functions are used for B-spline & NURBS. The solution of Bernstein basis functions is analytical, but the solution to the B-spline basis functions are iterative which concludes that Bernstein basis functions are computationally effective. This point is positive for Bezier and PH curves.

3. There are no free control points in the formulation of Hermite, Bezier, B-spline, NURBS and cubic PH-curves. Therefore, in these cases, the solution to the shape of the soft-continuum manipulators (curve) is unique. Quintic PH-curve has six control points, and four of them are fixed with the four known boundary conditions, while two free control points can be used to reconstruct the redundant shape (multiple solutions) of the continuum manipulator. The optimal shape is chosen by using the criteria of minimum potential (bending and twisting) energy.

4. The calculation of the length of the curve does not have the closed form solution in case of Hermite, Bezier, B-spline, and NURBS. Therefore, numerical methods are needed to approximate the solution of their length. But in the case of PH-curves, the calculation of the length has a closed form solution. Therefore, it is a positive point for PH-curves to use them for reconstructing the shape of the soft-continuum manipulators.

This theoretical comparison concludes that PH curves are more beneficial to model the shape of the soft-continuum manipulators. In the next section,

experimental validation is done to check the real-time performances for shape reconstruction, using these curve-based approaches. In [Song 2015a], it is stated that for known endpoints and direction vectors at those points, Bezier curves are better than B-splines to reconstruct the shape of the soft-continuum manipulators. This is because of the absence of the information in between the endpoints. Therefore, we are going to check Hermite, Bezier and PH curves only, for experimental validation.

3.7 Shape Reconstruction of Soft-continuum Manipulators Based on Curves

The above-discussed curve-based approaches are applied on a class of continuum manipulators, named Compact Bionic Handling Assistant (CBHA). The description of the manipulator, the experimental setup, and the application of the curve-based approaches to the CBHA manipulator are discussed in this section.

3.7.1 Compact Bionic Handling Assistant Manipulator

The Compact Bionic Handling Assistant (CBHA) manipulator of Fig. 3.13 is designed by Festo [fes 2018]. The CBHA manipulator, also called elephant
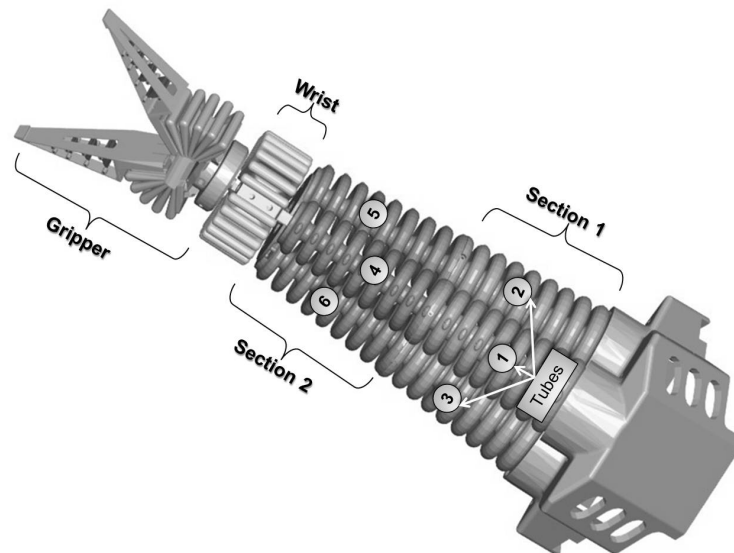
Figure 3.13: CBHA manipulator description

trunk manipulator, is made up of a soft elastic polyamide material, where it is divided into two sections, a rotating wrist and a compliant gripper (Fig.

3.13). Each section is composed of three tubes, connected each other through a backbone, and actuated by electro-pneumatic actuators. Pressure change inside the tubes leads to change in their respective lengths, inducing the change in the position and orientation of the tip of the manipulator.

Equal pressures in all three tubes maintain the robot in straight line longitudinal posture. An inextensible cable placed at the backbone of the manipulator limits the maximum extension. To create bending, differential pressures can be applied inside the tubes. The elongation of each tube is measured with a wire-potentiometer. There are six wire-potentiometers, three of them measure the tube lengths of the first section, and the three others measure the total tube lengths. The CBHA is not able to make a torsion movement around its longitudinal axis. Thus, no twisting behavior can be generated during its displacement.

The CBHA manipulator can be attached to an omni-directional mobile base, called Robotino. Combination of the mobile base with the bionic manipulator is called RobotinoXT (Fig. 3.14). Fig. 3.14 shows the coordinate frame attached to at the endpoint (P_f) of the manipulator. The CBHA manipulator
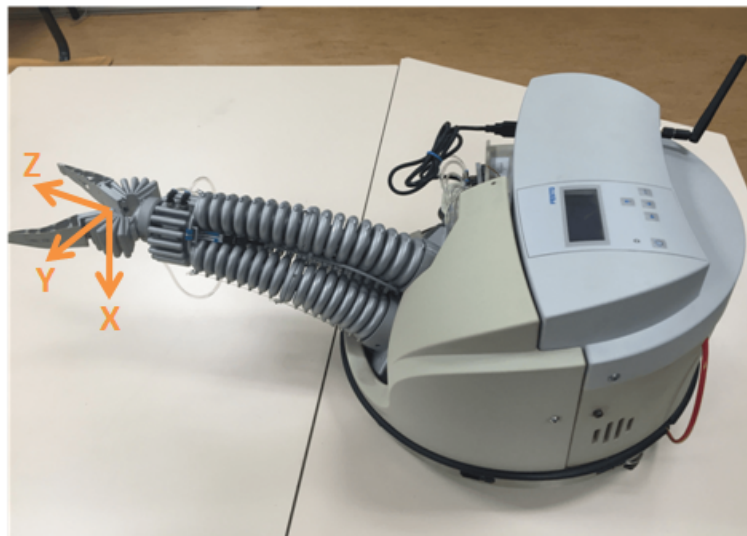
Figure 3.14: RobotinoXT

is made up of polyamide (PA 12) material [Grzesiak 2011]. The mechanical properties of this material are tabulated in Table 3.2.

Table 3.2: Mechanical properties of material PA 12

	Minimum Value	Maximum Value	Unit
Bending Strength	70	85	MPa
Density	1010	1020	kg/m^3
Friction Coefficient	0.3	0.4	
Impact Strength	0.5	2	J/cm
Shear Modulus	300	500	MPa
Tensile Strength	35	55	MPa
Young's Modulus	1270	2600	MPa
Elongation	120	300	%

3.7.2 Experimental Setup

In the following development, it is supposed that the two bending sections (Fig. 3.13) of the CBHA are fused to one entire continuum section, without any shape disconnection. An OptiTrack vision system (Fig. 3.15) is used for all of the experimental validations. This system tracks the position of the reflective markers. Four Prime13 cameras are used for tracking, each of them having specifications as follows:

- Resolution: 1.3 MP (1280×1024)

- Frame rate: 240 FPS

- Filter Switcher: Included

- Interface: GigE/PoE

- No. of LEDs: 62

- Latency: 4.2 ms

Motive 2.0 software is used for this OptiTrack vision system.
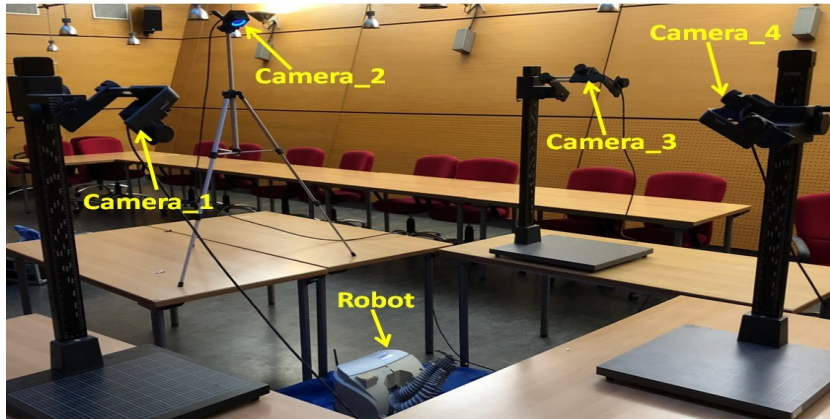
Figure 3.15: Experimental set-up

The purpose is to model the backbone of the CBHA manipulator using different curve-based approaches. To perform the experimental validation, five markers are attached to each tube of the CBHA arm (at corresponding levels) (Fig. 3.17), i.e., at the starting point, ending point, junction point, and two intermediate points. Virtual rigid bodies are created using corresponding markers of each tube to calculate the position and orientation at the corresponding backbone point (Fig. 3.18). Inputs are given to the CBHA arm to create a random posture. Using the vision system, the poses of the backbone of the CBHA are tracked. Four inputs to construct a curve for the CBHA arm are starting point, direction vector at the starting point, ending point and direction vector at the ending point. Therefore, using these inputs, Hermite, Bezier, cubic PH, and quintic PH curves are constructed representing the shape of the CBHA arm. **It is experimentally noticed that the CBHA manipulator can have maximum two inflection points in its shape (Fig. 3.16) and quintic PH curves are sufficient to model shapes with two inflection points as they have two free control points. Therefore, the higher order PH (Beyond quintic) curves are not applied to the CBHA manipulator.** The junction point and the other two intermediate points are tracked to verify the reconstructed shape with the actual shape.

Figure 3.18 shows the tracking of the backbone of the CBHA manipulator using Motive 2.0.

Assumptions: The experimentation has been done under the following assumptions:

- The manipulator is considered under free load condition.

- In our case, the torsion is restricted in the structure of the CBHA manipulator. Therefore, the value of τ is assumed as zero ($\tau = 0$).

- The weight of the markers attached to the manipulator is negligible.
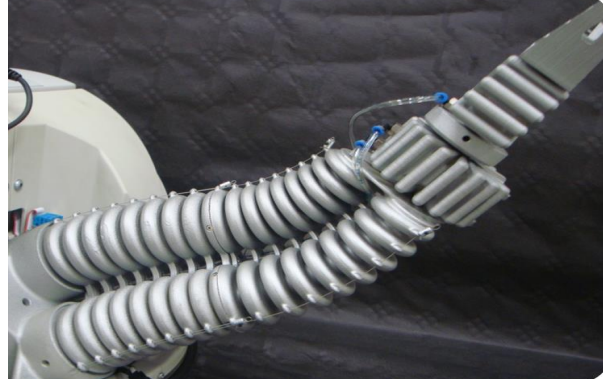
Figure 3.16: CBHA manipulator with two inflection points
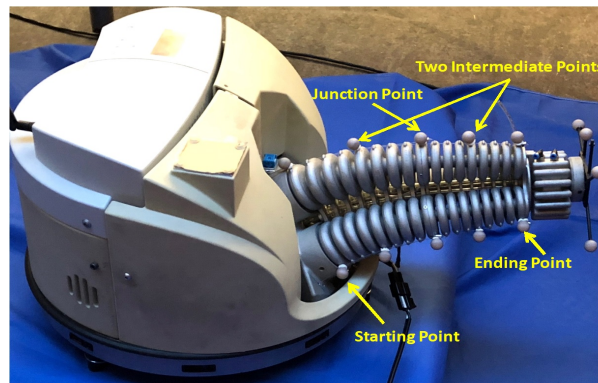
Figure 3.17: Shape tracking of CBHA arm

3.7.3 Results and Discussions

The results and discussions from the chapter are presented as follows:
Random pressure inputs are injected into the CBHA manipulator to create a random posture to test our curve-based approaches. The four boundary conditions for this posture are tracked using the vision system as follows:

1. $P_s = (0, \quad 0, \quad 0)$

2. $d_s = (0, \quad 0, \quad 1)$

3. $P_f = (47.8369, \quad -28.0541, \quad 183.1658)$

4. $d_f = (0.3190, \quad -0.4684, \quad 0.8239)$

All dimensions are in mm.

These boundary conditions are used to reconstruct the posture of the CBHA manipulator using Hermite, Bezier, cubic PH, and quintic PH curves (Fig. 3.19). The four boundary conditions can produce cubic degree Hermite and
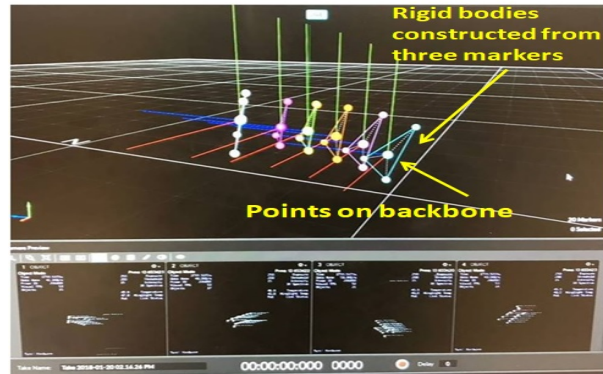
Figure 3.18: Shape tracking of backbone of the CBHA arm

Bezier curves. It is noticed from the results that Hermite and Bezier give the same resulting curve. It means for the known boundary conditions there is no difference in the resulting cubic Hermite and Bezier curves. Fig. 3.19 experimentally confirmed it.
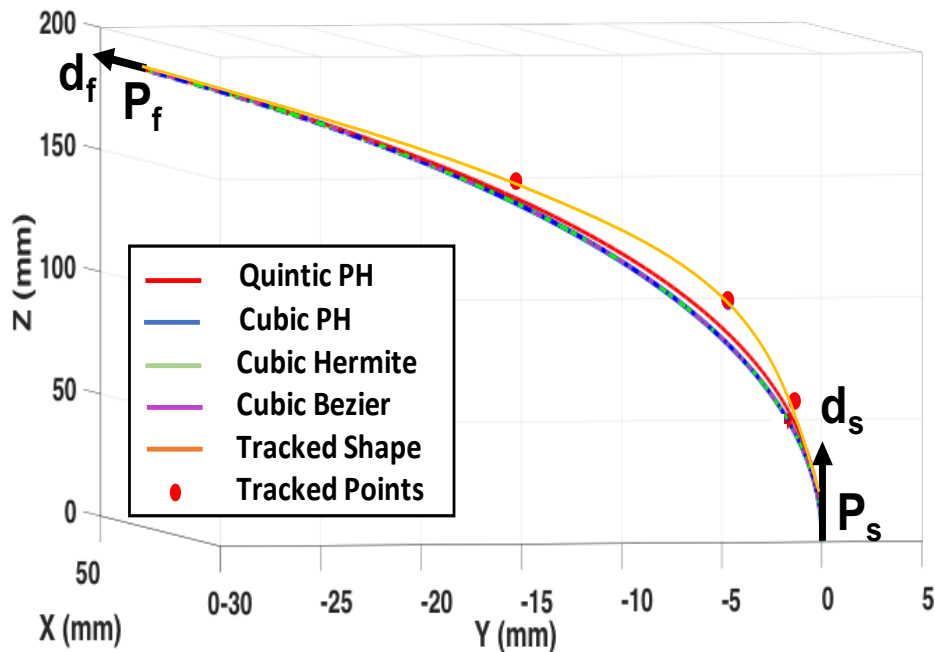
Figure 3.19: Comparison of different curve-based approaches to reconstruct the shape of the backbone of the CBHA manipulator

The average distances of the constructed shapes (different curves) are recorded from the actual shape of the CBHA manipulator. The Hermite

and Bezier have the average distance of 2.1363 mm. Cubic PH and quintic
PH have the distances of 1.9149 and 1.6005 mm respectively. It shows that
the quintic PH curve gives the best approximation to the shape of the CBHA
manipulator. It is not easy to conclude on the performance from the results
for only one posture. Therefore, a trajectory with more tracked postures is
needed.

A trajectory (Fig. 3.21) with 102 points is recorded using the vision system
from the workspace of the CBHA manipulator (Fig. 3.20). The base of the
CBHA manipulator is fixed, so, the starting point, as well as the orientation
at this point, remain fixed. The ending point, as well as its orientation, are
taken from the tracked trajectory (Fig. 3.21). Figs. 3.22 to 3.25 show the
Hermite, Bezier, cubic PH and quintic PH curves to reconstruct the shape of
the backbone of the CBHA arm for the whole trajectory (102 postures).
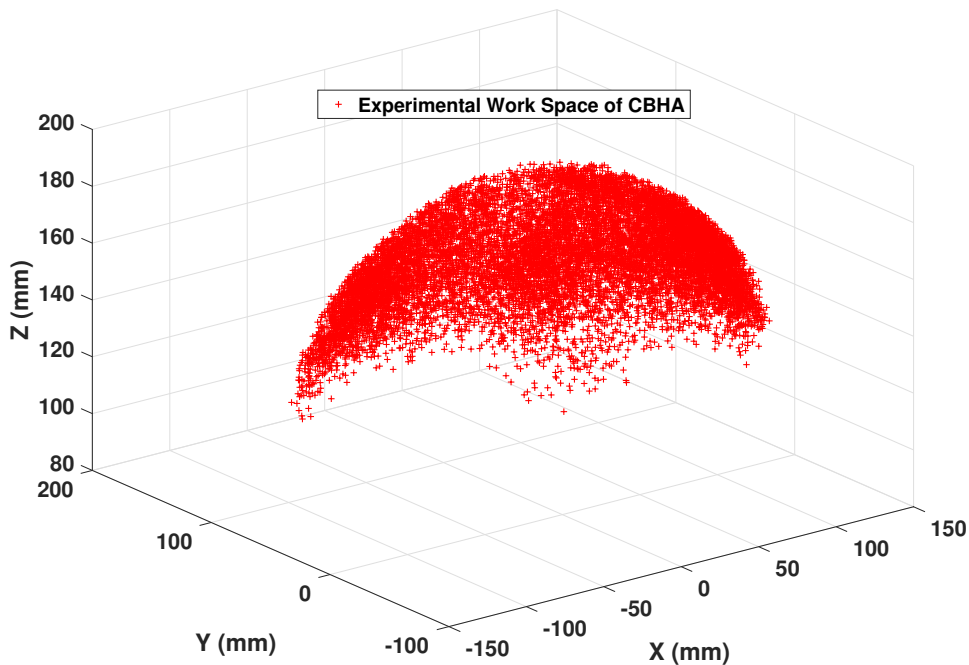
Figure 3.20: Work space of the CBHA manipulator
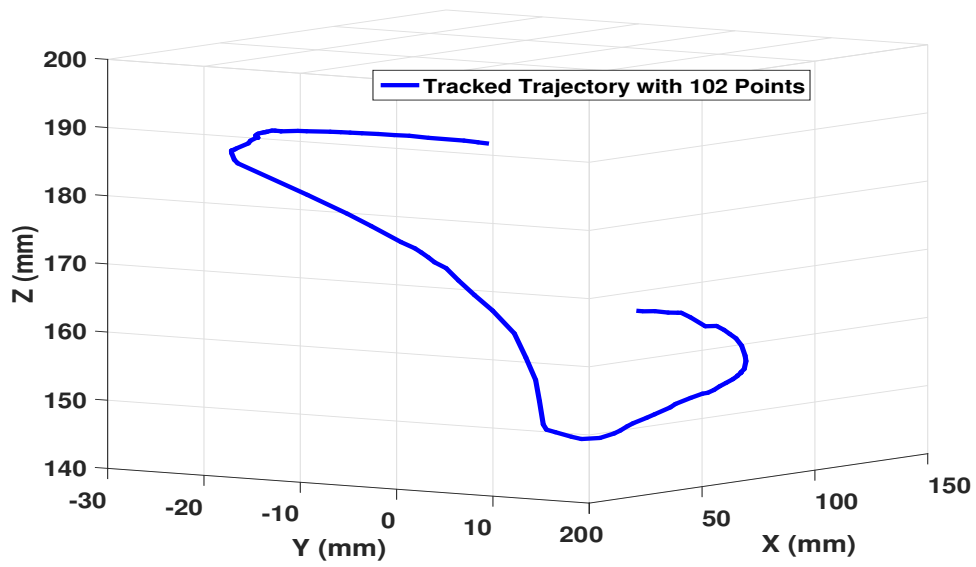
Figure 3.21: Trajectory tracked using vision system
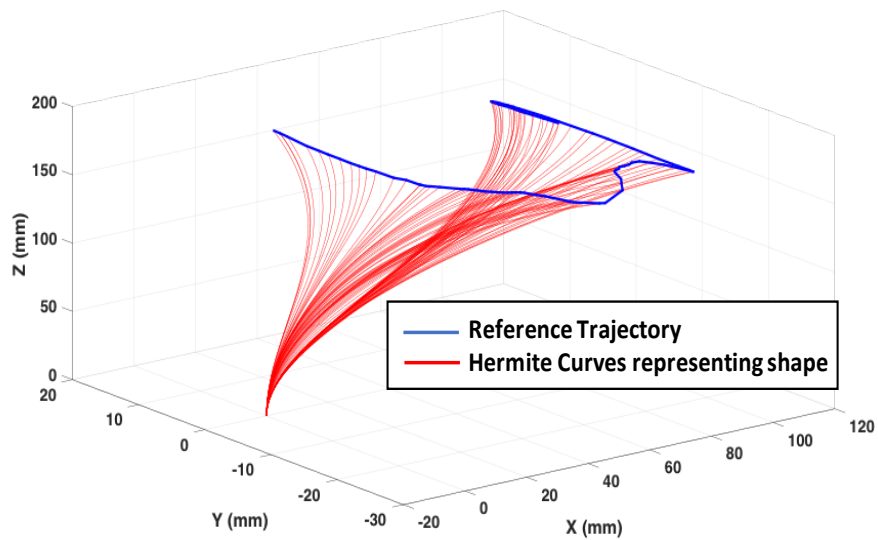
Figure 3.22: Shape reconstruction of the backbone of the CBHA manipulator using Hermite curves for a reference trajectory
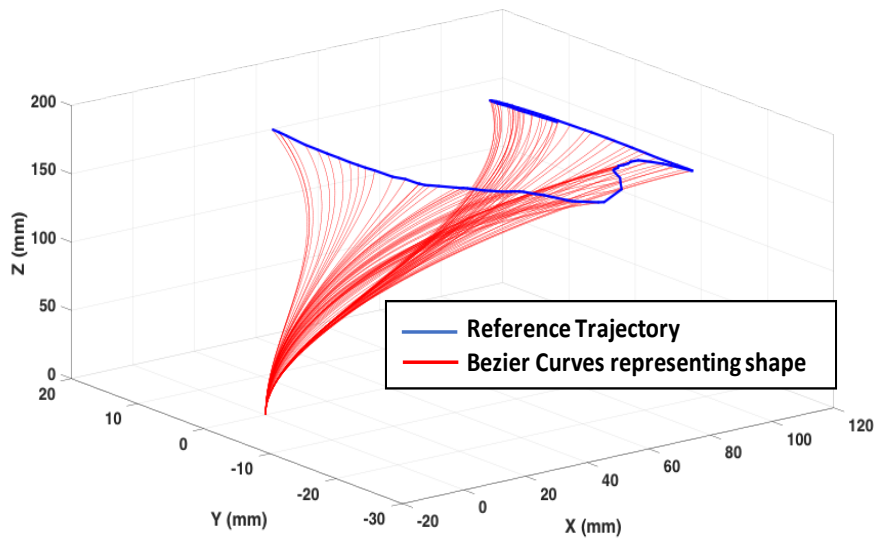
Figure 3.23: Shape reconstruction of the backbone of the CBHA manipulator using Bezier curves for a reference trajectory
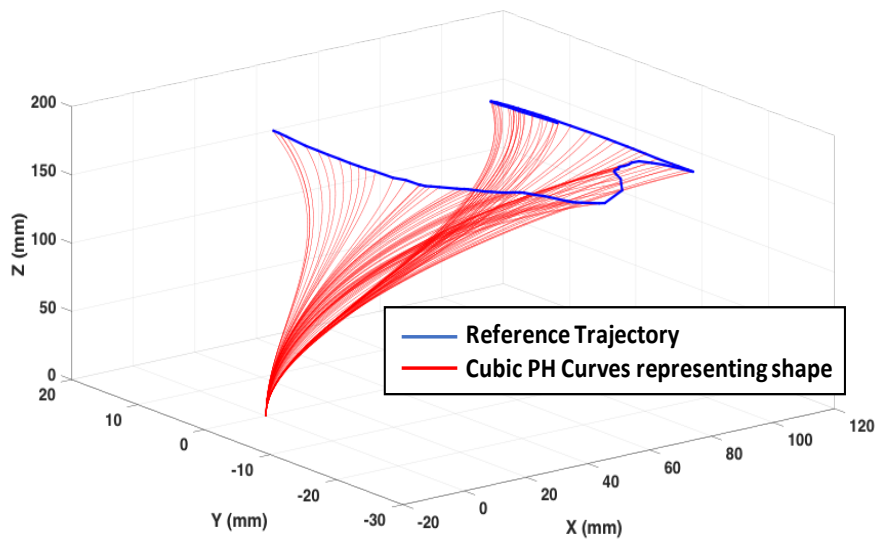
Figure 3.24: Shape reconstruction of the backbone of the CBHA manipulator using cubic PH curves for a reference trajectory
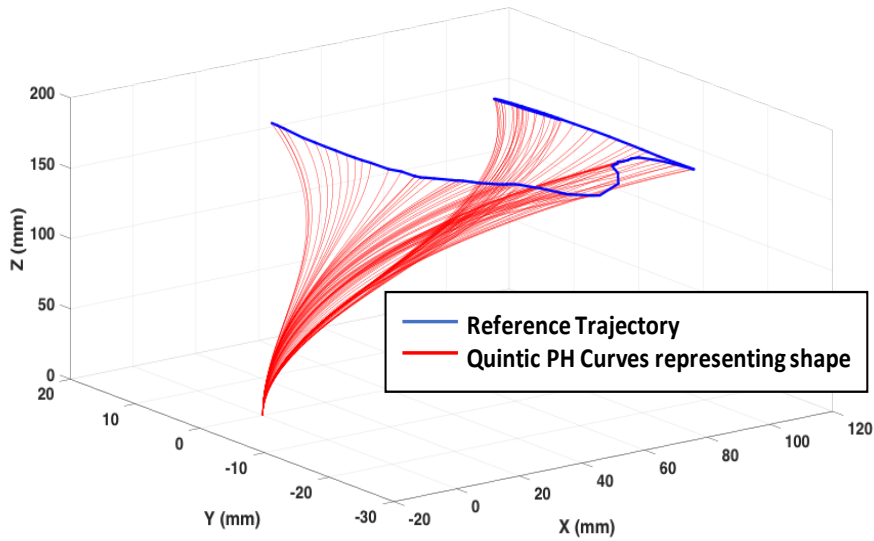
Figure 3.25: Shape reconstruction of the backbone of the CBHA manipulator using quintic PH curves for a reference trajectory
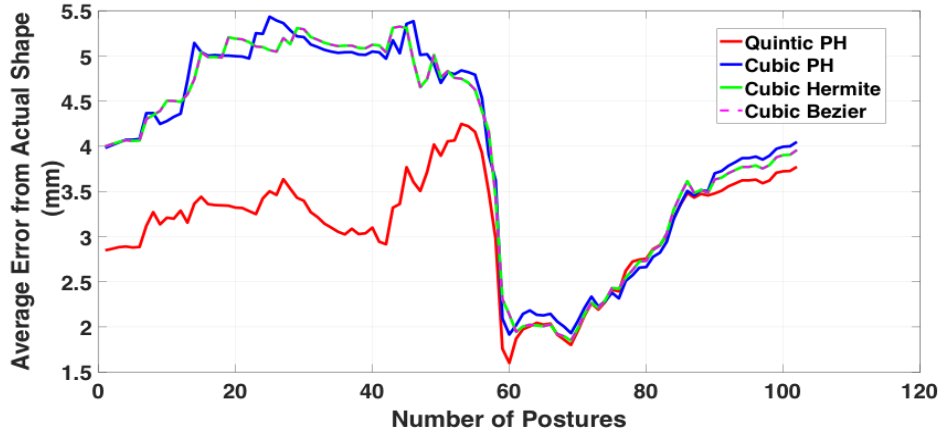
Figure 3.26: Error of reconstructed shapes from the actual shape

Errors are computed for curve-based reconstructed shapes from the actual tracked shape. Figure 3.26 shows the average distance between the reconstructed shapes and the actual shape for the 102 postures along the trajectory. The results show that most of the times quintic PH curve can better approximate the shape of the manipulator. The analysis of 102 postures to check the best approximation to the actual posture is represented by:

1. Quintic PH based reconstructed shape gives the best approximation for

89 postures (87.25 %).

2. Cubic PH based reconstructed shape gives the best approximation for ten postures (9.80 %).

3. Hermite, Bezier based reconstructed shapes give the best approximation for three postures (2.90 %).

Table 3.3, represents the minimum, maximum as well as average distances of the reconstructed shapes from the actual shapes.

Table 3.3: Average distances (in mm) of reconstructed shapes from the actual shape for whole trajectory

Shape Reconstruction	Min. dis. (mm)	Max. dis. (mm)	Average dis. (mm)
Hermite	1.8473	5.3252	4.1524
Bezier	1.8473	5.3252	4.1524
Cubic PH	1.9149	5.4345	4.0021
Quintic PH	1.6005	4.2470	3.1203

The reason behind the best shape representation using quintic PH is:

1. PH condition enable us to generate higher degree curves for the same input conditions.

2. There is no free control point in the cubic Hermite, Bezier, and cubic PH representations. But in the case of quintic PH curves, there are two free control points which lead to multiple solutions and the minimum bending energy optimization is used to choose one optimal solution to the shape.

Table 3.4 shows the time cost of reconstructing a single posture of the continuum manipulators using different curves. It means all of the curves have less time cost.

Table 3.4: Time cost to compute one posture (in sec)

	Time (sec)
Hermite	0.00017
Bezier	0.00021
Cubic PH	0.00023
Quintic PH	0.00025

The results show that the quintic PH-curves are better for the tracked trajectory. The trajectory is tracked randomly from a region in the workspace. Therefore, it is necessary to verify the shape reconstruction for the whole region of the workspace. Further, we tracked the data for the whole workspace

of the CBHA manipulator. Fig. 3.28 shows the workspaces of the tracked
marker positions on the backbone of the CBHA manipulator. Hermite, Bezier,
cubic PH, and quintic PH-based shapes are used for the whole workspace to
reconstruct the shape of the backbone of the CBHA manipulator to compare
them with the actual shape. The analysis of 668 postures to check the best
approximation to the actual posture is represented by:

1. Quintic PH based reconstructed shape gives the best approximation for
   511 postures (76.50 %).

2. Cubic PH based reconstructed shape gives the best approximation for
   104 postures (15.57 %).

3. Hermite, Bezier based reconstructed shapes give the best approximation
   for 53 postures (7.93 %).
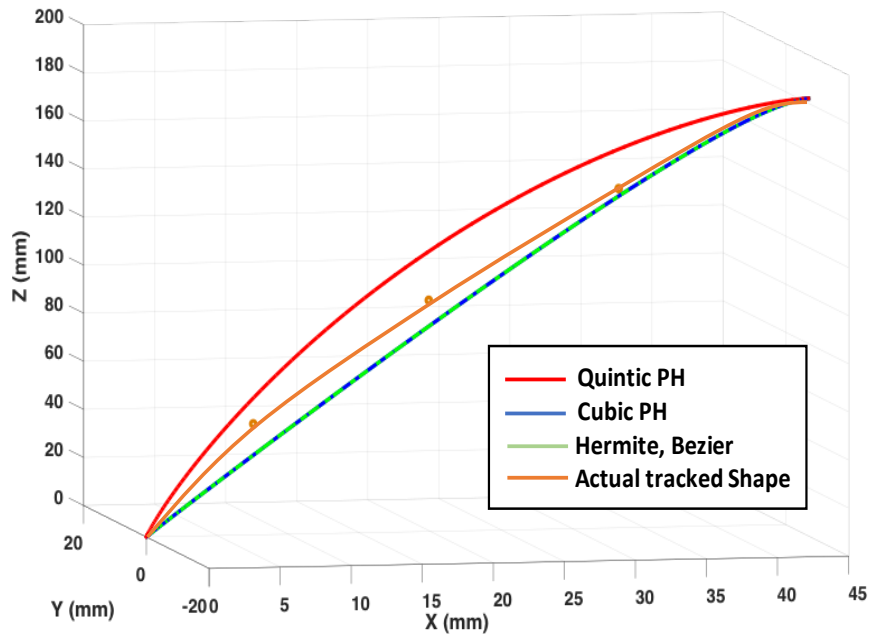
Figure 3.27: Case with better shape reconstruction using cubic PH and Hermite

This analysis shows that even for the case of whole task space of the
CBHA, quintic PH curves are better to reconstruct its shape in most of the
cases. There are approximately 20% cases where the Hermite and cubic PH
curves give the best estimation to the shape. To analyze, one of the cases
is plotted as in Fig. 3.27 in which cubic PH and Hermite curves can better
estimate the shape than quintic PH curves. It is noticed that cubic PH and

Hermite more accurately estimate the postures which are near to the straight configuration. The reason behind this is the higher degree of quintic PH curves, which is more flexible to model the shape of the CBHA manipulator with straight configurations.
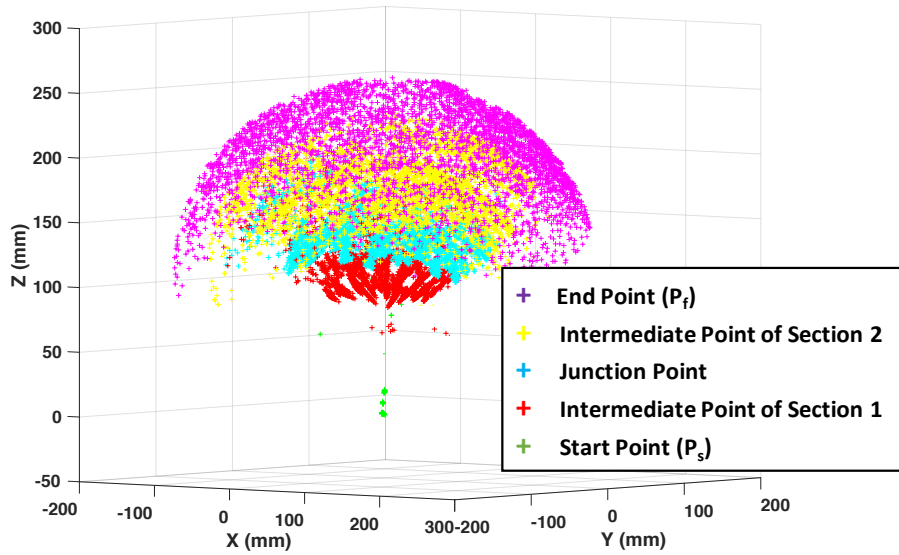
Figure 3.28: Experimental tracked positions of markers on the backbone of CBHA

3.8 Modified PH-Curves for Reconstructed Shape

The modeling of the shape for the CBHA case is made of the quintic PH-curve. The formulation of quintic PH-curve involves two free control points, and the optimal points are chosen by minimizing the bending of the resulting PH-curve. Even this geometrical reconstruction is close to the real postures, the minimization of the errors, originally from the selection of optimal control points for the soft-continuum manipulator can be improved using specific calibration of the model using external tracking vision system. Therefore, this section explains how the accuracy of the quintic PH curves can be further enhanced.

3.8.1 Calibration of the Shape

When the quintic PH-based reconstructed shape and the actual shape are superposed, a slight deviation is observed. So quintic PH-curves based approach can construct the nearest possible shape of the CBHA manipulator. The presence of small errors can be explained as follows:

- There is non-uniformity in the structure of the tubes. As, in the case of the CBHA manipulator, each tube is made up of the concatenation of 16 vertebrae. Also, the diameter of each tube decreases continuously from its base to the top.

- The material has highly non-linear elastic behavior.

Therefore, the minimum energy calculation of the PH curve does not fully adhere to such uncertainties. The reconstructed shape based on quintic PH-curve needs to be calibrated for better accuracy.
During the shape reconstruction of the CBHA manipulator, it is supposed that the two bending sections (Fig. 3.13) are fused into one total continuum section. It is observed that the reconstructed shape does not pass through the junction point of the two CBHA sections. The junction point should lie on the curve defining the shape of the CBHA manipulator. Therefore, a calibrated curve is generated, which not only closely resembles the quintic PH-curve but is also made to pass through the junction point.
Formulation of quintic PH-curves consists of six control points ($P_0 = P_s$, P_1, P_2, P_3, P_4, $P_5 = P_f$). Out of these six control points, P_0 and P_5 are the input points, and the formulation of the curve fixes P_1 and P_4 according to the input direction vectors at the end points. Therefore, the two free control points, namely P_2 and P_3 can be calibrated to pass the reconstructed curve from the junction point of the real manipulator.
The construction of quintic PH-based shape uses Bezier interpolation as shown in eq. 3.83. Therefore, it can also be called a Bezier curve satisfying the PH condition. So, the properties of the bezier polynomial are exploited to calibrate the free control points of quintic PH-based reconstructed shape, to generate the calibrated curve. Hence, the calibrated shape should also be a Bezier curve of the same order. **Knowing that the resulting calibrated curve will be a modified PH-curve as the shifting of the control points does not include the PH condition**. It is achieved as follows:

1. **Selection of h corresponding to the tracked junction point:** The junction point of the CBHA manipulator is tracked using an external tracking vision system. Now, the value of the curvilinear coordinate h is needed at which the calibrated curve should pass through the tracked junction point. As the quintic PH-curve gives very close initial results, it is assumed that the quintic PH and the calibrated curves will be approximately similar in shape. Therefore, we take the value of the curvilinear coordinate h from the already constructed quintic PH-curve. Thus, the value of curvilinear coordinate h of the point closest to the tracked junction point in the quintic PH is selected as the value of the curvilinear coordinate h at the junction point in the calibrated shape.

As shown in Fig. 3.29, if A is the nearest point on the quintic PH curve from the tracked junction point, then the value of h is taken from the point A. This value is used for the calibrated curve to pass it through the tracked junction point at this chosen h value.
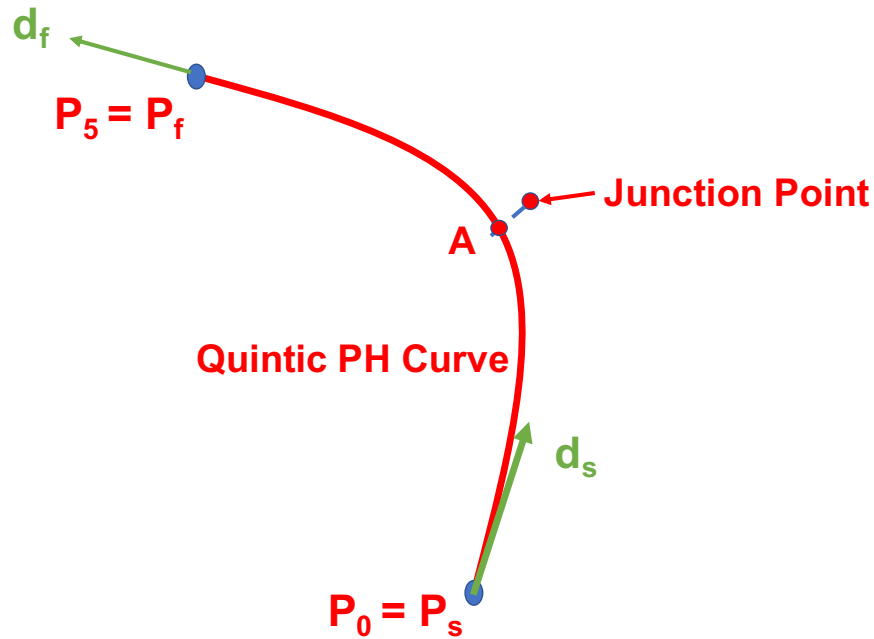
Figure 3.29: Selection of h value corresponding to the tracked junction point

2. To calibrate the shape with minimum effort and minimum deviation from quintic PH, in this method, only one of the free control points is altered at a time to shift the curve to pass it through the junction point.
   In a bezier curve, the control points have global influence, but the weight of each control point at a particular value of curvilinear coordinate h is given by the variation in Bernstein coefficients (Fig. 3.30). To have a minimum deviation from the initial quintic PH, only the control point which has the maximum influence at the selected curvilinear coordinate h, is shifted.

3. The quintic PH-bezier curve eq. 3.83 is exploited to find the formulation of the desired calibrated control point when the value of the curvilinear coordinate h and the tracked junction point is known. In case, junction point is represented by P_{mid} and $h \leq 0.5$ at the junction point, P_2 has

to be modified. Thus, using eq. 3.83, the junction point is,

$$P_{mid} = \sum_{k \neq 2, k=0}^{5} \binom{5}{k}(1-h)^{5-k}h^k P_k + \binom{5}{2}(1-h)^{5-2}h^2 P_2 \qquad (3.114)$$

Therefore,

$$P_2 = \frac{P_{mid} - \sum_{k \neq 2, k=0}^{5} \binom{5}{k}(1-h)^{5-k}h^k P_k}{\binom{5}{2}(1-h)^{5-2}h^2} \qquad (3.115)$$

In case, $h > 0.5$ at the junction point, P_3 has to be modified. Therefore using eq. 3.83, the junction point is,

$$P_{mid} = \sum_{k \neq 3, k=0}^{5} \binom{5}{k}(1-h)^{5-k}h^k P_k + \binom{5}{3}(1-h)^{5-3}h^3 P_3 \qquad (3.116)$$

Therefore,

$$P_3 = \frac{P_{mid} - \sum_{k \neq 3, k=0}^{5} \binom{5}{k}(1-h)^{5-k}h^k P_k}{\binom{5}{3}(1-h)^{5-3}h^3} \qquad (3.117)$$

As, we are modifying P_2 or P_3 at a time, the general form to compute the control point is given by P_c as;

$$P_c = \frac{P_{mid} - \sum_{k \neq c, k=0}^{5} \binom{5}{k}(1-h)^{5-k}h^k P_k}{\binom{5}{c}(1-h)^{5-c}h^c} \qquad (3.118)$$

Here, P_c is the corrected or modified control point, either of the free control points P_2 or P_3, in case of the CBHA, P_{mid} is the desired tracked junction point from experimental data, and h is the desired value of the curvilinear coordinate at the junction point, P_k are the rest of the control points except the point which has to be corrected.

In general, the concerned control point by the calibration can be selected by noticing the most influential control point from Fig. 3.30. For example, at $h \leq 0.5$, P_2 is more influential to the shape, otherwise it is P_3.

3.8.2   Relationship between Quintic PH and Calibrated Curve

New control points are computed to calibrate the quintic PH-curve. Now, it is advantageous to develop a relationship between the old conditions (old control point, h corresponding to the junction point) and the new control points. It is not easy to develop this relationship quantitatively, it is for that a qualitative Neural Networks (NN) approach is proposed. Markers are attached on the CBHA manipulator as shown in Fig. 3.17. Data for all of the workspace (4096 samples) of the CBHA manipulator is tracked using the
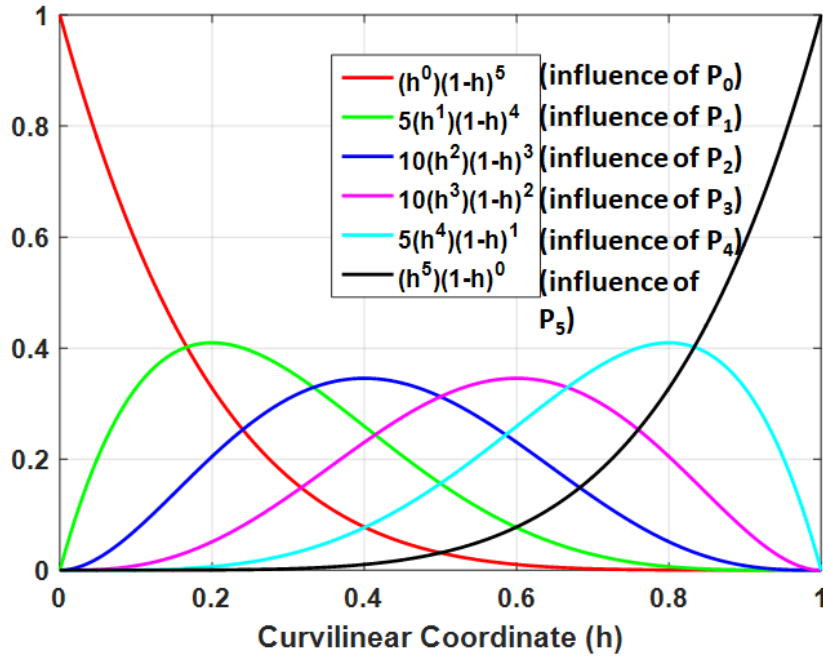
Figure 3.30: Variation of Bernstein coefficients with curvilinear coordinate for quintic bezier curve

external tracking vision system. This data is used to compute the shapes of the backbone of the CBHA manipulator for all of the workspace using quintic PH-curves based approach. The control points are recorded for all of the quintic PH-curves. Then the new calibrated control points (P_2 and P_3) are computed using the shape calibration method as discussed above. As shown in Fig. 3.31, the inputs for NN are the old control point and the h value at the tracked junction point which gives the new calibrated control point as an output.

In our case either control point P_2 or P_3 is changed depending upon the value of the curvilinear coordinate h at the junction point. This property was exploited to split the input data to train two different NN as shown in Fig. 3.31. The database is divided as, 70% data is utilized for training, 30% for validation and 30% for test sets. The Levenberg-Marquardt method in MATLAB is used to train both of the feed-forward neural networks each containing ten neurons in a single hidden layer. In NN_1, the Mean Square Errors (MSEs) of 2.21783×10^{-5}, 3.89162×10^{-5} and 3.60386×10^{-5} are achieved for training, validation and test sets respectively. In NN_2, the MSEs of 2.37198×10^{-5}, 1.42342×10^{-5} and 4.302266×10^{-5} are achieved for training, validation and test sets respectively.

Fig. 3.31 presents a block representation of the discussed method used to
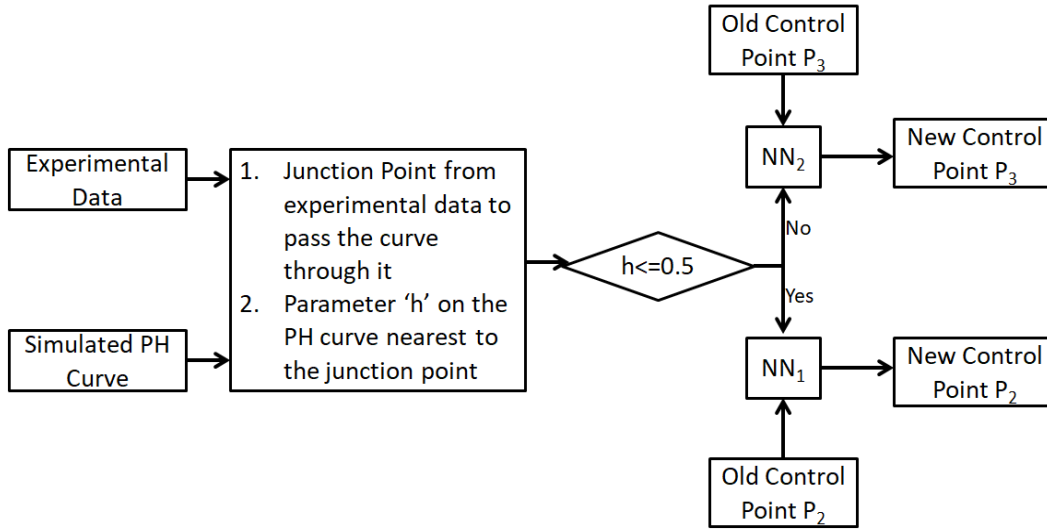
Figure 3.31: Block representation of calibration method

find the new control points for the calibrated shape of the CBHA manipulator.

3.8.3   Results and Discussions

To validate the calibration method, random pressures are injected in the CBHA, then the posture of the CBHA is estimated using quintic PH-curve. Afterward, the corrected shape is deduced by calculating the new control points. Fig. 3.32 presents the comparison of actual shape, PH-based shape construction and the calibrated shape using the proposed methodology. Here, the three intermediate tracked marker points are at distances 1.7132 mm, 0 mm, and 2.5424 mm respectively from the calibrated shape. These distances are less than the distances of quintic PH-based shape (1.6135 mm, 4.2048 mm, and 3.8339 mm). Therefore, an overall improvement in the accuracy of the shape of the CBHA manipulator is validated. Furthermore, a trajectory (Fig. 3.33) with 50 points is recorded using the vision system. End-point, as well as its orientation, is taken from the tracked trajectory (Fig. 3.33). The PH-curves methodology is used to reconstruct the shape of the backbone of the CBHA arm for the whole trajectory. Some random postures reconstructed using PH-curves are shown in Fig. 3.34. The improved shapes are also constructed using the calibration method (Fig. 3.34). In Fig. 3.34, the control points of the curves are not shown to avoid the confusion with the tracked marker points. To compare the PH-based and the calibrated shape with the experimental data, the distances of the junction point and two intermediate points from both of the shapes are tracked over the trajectory. The average errors for the whole trajectory (50 postures) are tabulated in Table 3.5.
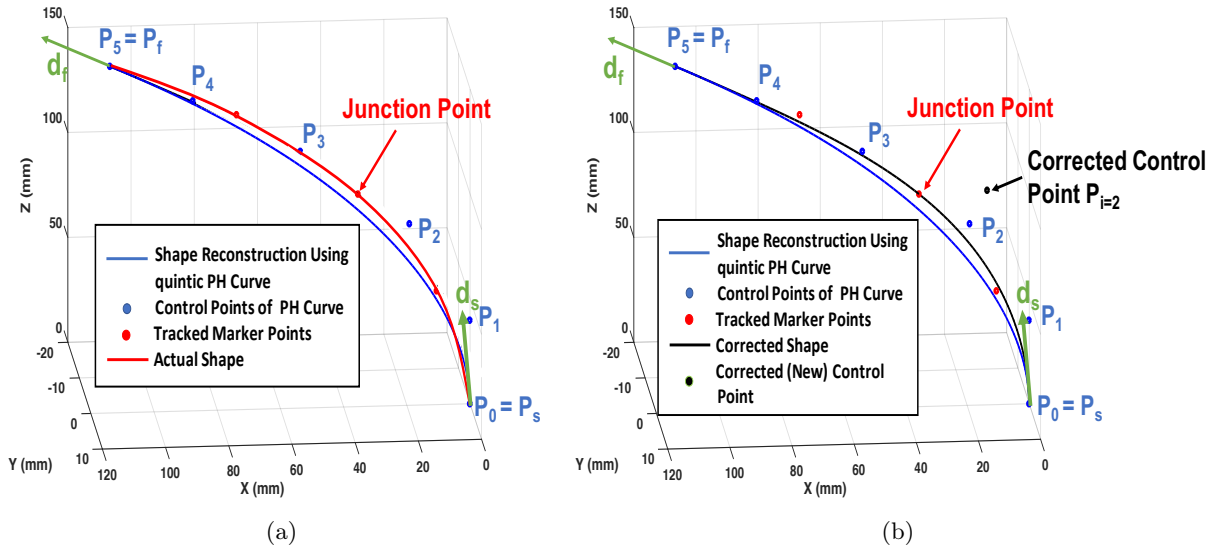
Figure 3.32: (a) Actual shape v/s quintic PH based reconstructed shape (b) Quintic PH based reconstructed shape v/s calibrated shape
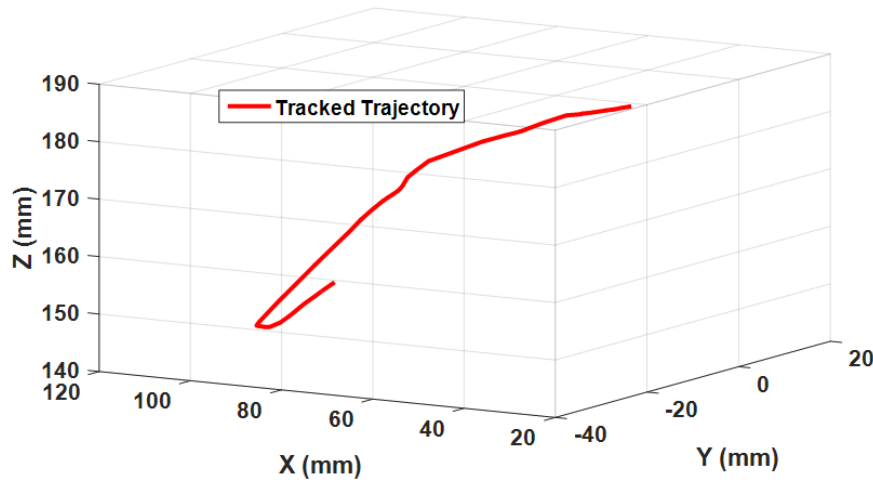
Figure 3.33: Trajectory tracked using vision system

Table 3.5: Average errors for whole trajectory (50 postures) in mm

Distance	PH based shape	Corrected Shape
Intermediate Marker of Section 1	1.3331	1.2088
junction point	3.6660	0.0000
Intermediate Marker of Section 2	4.2215	2.9104
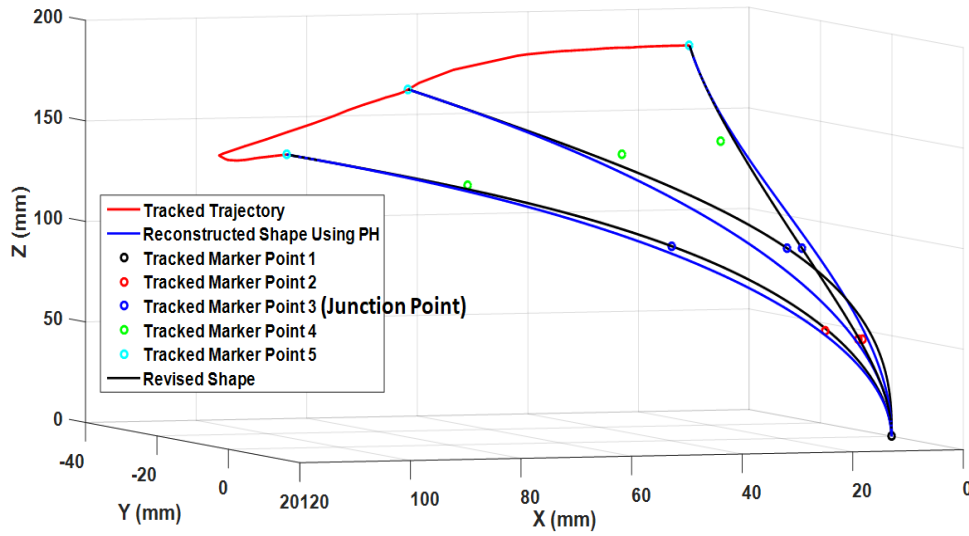
Figure 3.34: Random postures reconstructed using PH curves as well as the calibration method along the trajectory

From table 3.5, it is clear that these errors are reduced by using the calibration method to correct the quintic PH-based shape. As we tried to improve the overall errors in the shape only by changing one of the existing control points of the PH based curve, this can be the reason for the remaining errors.

3.9   Conclusion of the Chapter

This chapter discusses the different types of geometrical curves. The synthetic curves are found more suitable for reconstructing the shape of the soft-continuum manipulators due to the ability to control them. Furthermore, different synthetic curves are discussed and compared theoretically. Theoretical comparison concludes that Pythagorean Hodograph (PH) curves are better than the other synthetic curves because they can produce higher order curves using four boundary conditions. They have closed-form solution to compute the length of the curve; also, quintic PH curves have free control points to choose an optimal shape according to geometrical requirement.
The next step involves the experimental comparison of the discussed synthetic curves with their application to the CBHA manipulator. This comparison validates that quintic PH curves are better to model the shape of the soft-continuum manipulators in 76.50 % of the cases. Rest of the 23.50 % cases are in favor of cubic PH and Hermite curves, and these cases include the shape reconstruction of straight configurations of the CBHA manipulator. Therefore, this chapter concludes that quintic PH curves can be used to reconstruct

the optimal shapes of the soft-continuum manipulators as they are accurate in most of the cases.

In [Song 2010], a comparative study is done for the path planning of a mobile robot using Hermit, Bezier, and B-splines. This paper concludes that out of these three curves, Bezier curves are the best ones, as, they can produce a smoother and shorter path. Also, [Song 2015a] stated that Bezier curves are better to represent the shape of the continuum manipulators than the B-splines. Bezier-curves and PH-curves use Bernstein basis functions. Therefore, PH-curves have the advantages of Bezier-curves along with their benefits. Consequently, we obtain better results with PH-curves to reconstruct the shape of the soft-continuum manipulators.

Two free control points in the formulation of the quintic PH-curves are chosen by minimizing the bending energy of the resulting curve. But due to some uncertainties in the structure of the CBHA manipulator, the minimizing bending energy criteria does not correctly adhere to our case. Therefore, a calibration method to improve the accuracy of the quintic PH-based reconstructed shape using the experimental data is discussed and validated for the CBHA manipulator. It is a generalized method, and can be applied to any soft-continuum manipulator to calibrate its quintic PH-based approximated shape.

Observation of the benefits of the quintic PH-curves for the shape reconstruction of the soft-continuum manipulators makes us curious to further explore these curves. The optimal shape reconstruction should lead us to the inverse kinematic solution of the manipulators. Therefore, the next chapter deals with the use of PH-curves to model the kinematics of the soft-continuum manipulators.

Kinematics of Soft-continuum Manipulators using PH-Curves

Contents

4.1 Introduction

The first objective of this thesis to model the shape of the soft-continuum manipulators is dissertated in the previous chapter which concludes that the quintic PH curves can better approximate the shape. Control of the soft-continuum manipulators in their task space demands an optimal inverse kinematic model. Therefore, the following objective is to extend the PH-based shape reconstruction approach to solve the kinematics of the soft-continuum manipulators. This chapter discusses the inverse, as well as, forward kinematics of the continuum manipulators using PH-curves. Inverse kinematics solution of the soft-continuum manipulators is to find their joint parameters, described in our case study on the backbone lengths for a particular target position in their task space. Therefore, the solution to the backbone lengths of

the soft-continuum manipulators can be deduced from the formulation of the PH curves used to model the shape profile. Forward kinematics of the soft-continuum manipulators imposes a specific posture to the manipulator with the known joint parameters to calculate the end effector position in the task space. The inverse kinematic equation of the soft-continuum manipulators deduced from quintic PH curves is used to formulate the FKM equation of the soft-continuum manipulators. These kinematic models have been validated on the CBHA manipulator and also compared with the existing kinematic modeling approaches. These kinematic models have been developed for free load manipulation. Unlike rigid manipulators, the soft-continuum manipulators can not manipulate loads without making changes to their structure due to their inherent soft material. Therefore, the robustness of PH-curves based approach is tested for the variable load manipulation by computing the change in the end pose of the manipulator for load handled, using the NN-based learning approach.

4.2 Inverse Kinematics of Soft-continuum Manipulators from PH-curves

In the literature, the study of the Inverse Kinematic Model (IKM) of the soft-continuum robots is often decoupled from the reconstruction of the shape. Due to the soft behavior of these robots, a redundancy in their posture exists. Finding an accurate inverse kinematic model of a hyper-redundant manipulator does not mean finding the optimal shape. In this thesis work, we first reconstructed an optimal shape from an approach based on the modeling of curves, allowing us to deduce the inverse model for an optimal posture of the soft-continuum manipulators. Therefore, this section deals with the IKM of the soft-continuum manipulators, its application to the CBHA manipulator and the comparison with the existing IKMs for the same manipulator.

4.2.1 Shape Reconstruction towards Inverse Kinematic Model

PH-curves are used to model the shape of the soft-continuum manipulators with four input conditions $(P_s,\ d_s,\ P_f,\ d_f)$. Now, the task is to use the same PH-curve based formulation to compute the inverse kinematics of the soft-continuum manipulators. This means computing their length for a particular tip position of the manipulator. In our case, the tip position of the manipulator is represented by P_f. Therefore, the inverse kinematics of the soft-continuum manipulators should be the relationship of their backbone length with the tip position (P_f) as:

$$L(h) = f(P_f) \tag{4.1}$$

The length of the PH-curve which represents as the backbone length of the soft-continuum manipulators is represented as in eq. 3.44. Also, the derivative $r'(h)$ of the generalized equation of the PH-curve $r(h)$ is given by:

$$r'(h) = \begin{bmatrix} x'(h) \\ y'(h) \\ z'(h) \end{bmatrix} = \sum_{k=0}^{2n+1} P_k \binom{2n+1}{k} (2n+1-k)(1-h)^{2n-k}kh^{k-1} \quad (4.2)$$

This $(2n+1)^{th}$ degree PH-curve is formulated when n^{th} degree polynomials $u(h)$, $v(h)$, $p(h)$, $q(h)$ (eq. 3.111) are used in Bernstein form. In eq. 4.2, P_k represents the control points of the PH-curve. The nth degree PH-curve contains $(n+1)$ control points. A PH-curve formulated using start (P_s, d_s) and end (P_f, d_f) conditions of the soft-continuum manipulator always passes through P_s and P_f. Also, P_s and P_f represent the first and the last control points of the PH-curve respectively. Therefore the last control point of the PH-curve always coincides with the end position (P_f) of the soft-continuum manipulator. It means using eq. 4.2 in 3.44, relates the length of the soft-continuum manipulator with the tip position of the manipulator, which illustrates the inverse kinematics of the soft-continuum manipulators as follows.

$$\begin{aligned} L(h) = \int_0^1 |&((C_{1s}h + C_{2s}h^2 + ... + C_{2ns}h^{2n})\vec{P_s} \\ &+ ((C_{1k}h + C_{2k}h^2 + ... + C_{2nk}h^{2n})\vec{P_k} \\ &+ ((C_{1l}h + C_{2l}h^2 + ... + C_{2nl}h^{2n})\vec{P_l} \\ &+ .... \\ &+ ((C_{1m}h + C_{2m}h^2 + ... + C_{2nm}h^{2n})\vec{P_m} \\ &+ ((C_{1f}h + C_{2f}h^2 + ... + C_{2nf}h^{2n})\vec{P_f})|dh \end{aligned} \quad (4.3)$$

Here, $P_s, P_k, P_l, ..., P_m, P_f$ represent the $(2n+2)$ control points of the $(2n+1)^{th}$ degree PH-curve. The set of C_i describes the n degree polynomial coefficients. The infinite solutions of the inverse kinematics are illustrated by the free control points in case of PH formulation. For PH-curves, this problem is handled by choosing an optimal solution of the free control points as discussed in the previous chapter.

4.2.2 Application of IKM to the CBHA Manipulator

It is discovered that the quintic PH-curves are the best representatives of the shape of the soft-continuum manipulators with their application to the CBHA manipulator, due to it's two inflection points. Therefore, to formulate

the inverse kinematic equation for the quintic PH-curves in case of the CBHA, the derivative of the equation of quintic PH-curve is used:

$$r'(h) = \begin{bmatrix} x'(h) \\ y'(h) \\ z'(h) \end{bmatrix} = \sum_{k=0}^{5} P_k \binom{5}{k} (5-k)(1-h)^{4-k} k h^{k-1} \tag{4.4}$$

Using eq. (4.4) in eq. (3.44), it gives:

$$
\begin{aligned}
L(h) = \int_0^1 |((-5 + 20h - 30h^2 + 20h^3 - 5h^4)\vec{P_0} \\
+ (5 - 40h + 90h^2 - 80h^3 + 25h^4)\vec{P_1} \\
+ (20h - 90h^2 + 120h^3 - 50h^4)\vec{P_2} \\
+ (30h^2 - 80h^3 + 50h^4)\vec{P_3} + (20h^3 - 25h^4)\vec{P_4} \\
+ (5h^4)\vec{P_5})|dh
\end{aligned}
\tag{4.5}
$$

Here, $P_0, P_1, P_2, P_3, P_4, P_5$ represent the six control points of the quintic PH-curve.

$$
\begin{aligned}
P_0 = P_s \\
P_5 = P_f
\end{aligned}
\tag{4.6}
$$

Therefore, eq. 4.5 is the relation between the length and the tip position (P_f) of the soft-continuum manipulator. This equation represents the inverse kinematics of a soft-continuum manipulator modeled using quintic PH-curve. Quintic PH-curve has two free control points and the optimal selection of these two points gives us the optimal inverse kinematic solution of the CBHA manipulator. Therefore, by solving eq. 4.5, the length of the soft-continuum manipulator can be computed. The formulation of the control points of the quintic PH (eqs. 3.89-3.93) illustrates that the point $P_f = P_5$ can be represented in terms of the other control points. Also, eqs. 3.94 and 3.93 show the involvement of the direction vector of the endpoint in the inverse kinematic equation. Therefore, eq. 4.5 uses the given tip position, as well as, its orientation in the task space to calculate the optimal length.

The structure of the CBHA manipulator includes three tubes attached to its backbone as shown in Fig. 4.1. Therefore, the joint parameters for the CBHA manipulator are the lengths L_1, L_2 and L_3. The change in these lengths allows the CBHA manipulator to reach a specific position in the task space. IKM of CBHA manipulator needs to solve the optimal lengths L_1, L_2 and L_3 for a target position in the task space.

The end-point P_f of the backbone has to follow a desired trajectory. The desired target includes the position as well as orientation of endpoint $P_f(x_f, y_f, z_f)$. The PH-curve is generated from P_s to P_f. As there is no torsion in the structure of CBHA, only bending energy is minimized to select an
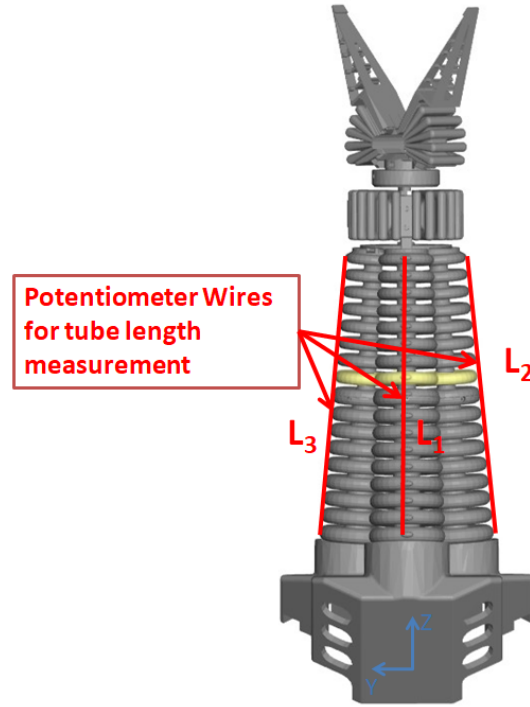
Figure 4.1: Three measurable total tube lengths of the CBHA

optimal curve. Inverse Kinematic eq. 4.5 is used to calculate the backbone length L of the CBHA manipulator. The tubes are attached to the backbone of the CBHA manipulator. Therefore, the lengths L_1, L_2 and L_3 are computed using the backbone curve according to the following steps:

- The three potentiometer wires, that can measure the total tube lengths L_1, L_2 and L_3 are attached from one side to points A_1, A_2 and A_3 of the lower vertebrae of the CBHA and from the other side to points B_1, B_2 and B_3 of the upper vertebrae (Fig. 4.2). The backbone of the manipulator starts at P_s and ends at P_f. Both of these points are known geometrically. R_1 and R_2 represent the radius of lower as well as upper vertebrae respectively.

- In Fig. 4.2, the geometry of the triangle $A_1 A_2 A_3$ and the radius R_1 are used to compute the coordinates of points A_1, A_2 and A_3. The tubes are attached to the backbone through a rigid link. Therefore, the same orientation is imposed on these points as the center point of the triangle, i.e., the point on the backbone PH curve.

- Likewise, assuming the linear variation of the radius from R_1 to R_2, the
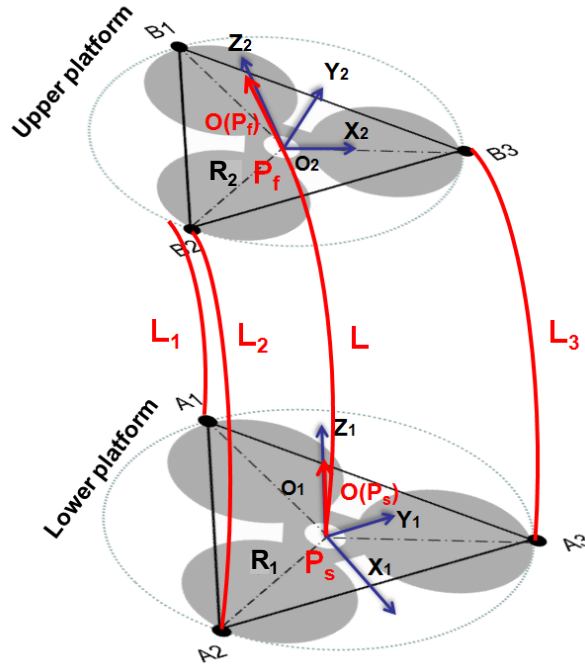
Figure 4.2: Boundary conditions for PH curves

three triangular vertices are determined along the entire backbone length
of the CBHA manipulator.

- Fig. 4.3 shows the lengths L_1, L_2, L_3, generated using the backbone PH-
curve.

4.2.3 Experimental Validation

Experimental validation of the PH-based IKM of the CBHA is realized with
the OptiTrack vision system. To validate the proposed methodology, a refer-
ence trajectory with 6314 points is tracked (Fig. 4.4). Markers are used for
the detection of the tip point of the CBHA manipulator. During the real-time
movement of the manipulator, the three full-lengths L_1, L_2 and L_3 are recorded
from the data of three potentiometer wires, which are mounted from the base
to the end of the manipulator. The lengths are calculated for all of the tra-
jectory points using the quintic PH-based approach. Fig. 4.5 represents two
random postures of the CBHA manipulator, computed using PH-based IKM
while following the desired trajectory of Fig. 4.4. An optimal posture should
have lengths close to the actual lengths of the CBHA. Therefore, estimated
lengths are compared with the measured lengths for the validation of the
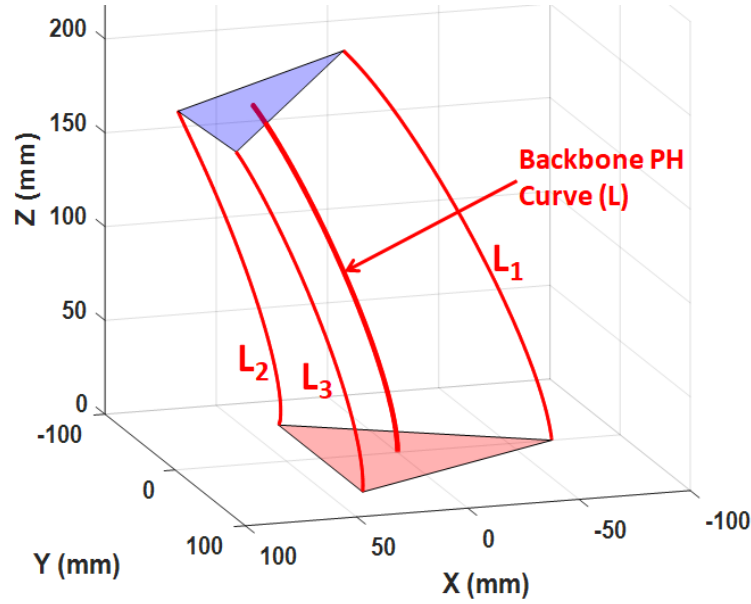
Figure 4.3: Shape reconstruction of the CBHA manipulator in case of free load manipulation

proposed inverse kinematic model. For the same trajectory, other previously developed IKMs for CBHA: 1) Hybrid Approach [Lakhal 2016], 2) Newton Raphson Approach [Singh 2017], 3) Computational Mechanics [Bieze 2018] are used for comparison.

The Hybrid approach modeled the CBHA manipulator as a series of parallel robots. As CBHA manipulator consists of 17 vertebrae, it is modeled as 16 serial-parallel robots. The Newton Raphson approach is used to directly invert the forward kinematic equations of the CBHA manipulator developed using the Arc Geometry approach [Escande 2015]. Finally, the Computational Mechanics [Bieze 2018] approach, a Finite Element Method (FEM-based) modeling applied to the CBHA manipulator in quasi-static behavior.

Assumptions: The experimentation has been done under the following assumptions:

- The manipulator is considered under free load condition.

- The torsion is restricted in the structure of the CBHA manipulator. Thus, the value of τ is assumed null ($\tau = 0$).

4.2.4   Results and Discussions

The lengths are calculated, based on IKM and corresponding to each point of trajectory, using PH-curves, Computational Mechanics, Hybrid and Newton
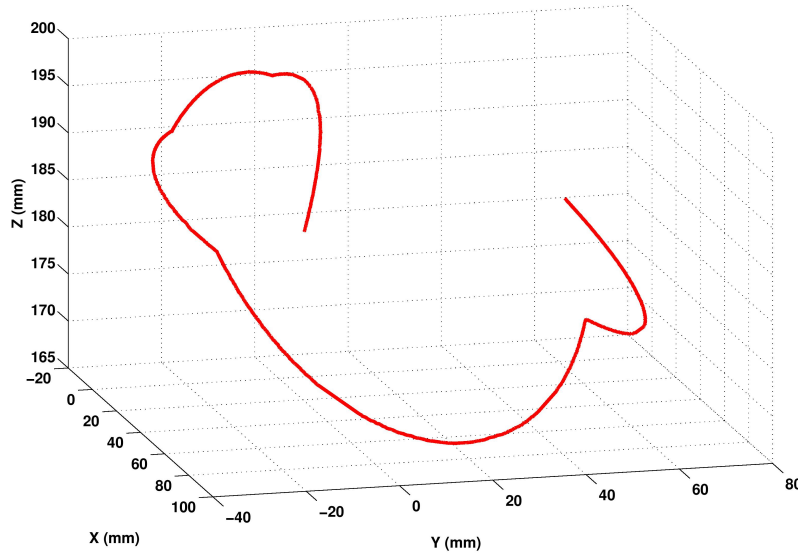
Figure 4.4: Desired trajectory of the tip of the manipulator

Raphson approaches respectively. Figs. 4.7, 4.8-4.9 represent the comparison of lengths L_1, L_2 and L_3 respectively, when the tip of CBHA is realizing the spatial trajectory of Fig. 4.4. The comparison shows that the lengths from all of the approaches approximately follows the same trend as reference lengths. Absolute extremum and average errors from the actual data are tabulated in the table 4.1, for different IKMs. PH-IKM is more accurate than other methods. When compared to Newton Raphson approach [Singh 2017], PH-based IKM approach assumes variable curvature of the manipulator. The former approach is directly developed from FKM with the assumption of constant curvature. To verify, Fig. 4.6 shows the variation of the curvature of a quintic PH-curve along its backbone length for a random posture. The Hybrid approach [Lakhal 2016] used geometrical representation to generate inverse kinematic equations of the inter-vertebraes, and then these equations are approximated using a learning approach based on Neural Networks. [Bieze 2018] modeled the CBHA manipulator using computational mechanics, where the length errors for the same trajectory (Fig. 4.4) are less than the Hybrid, and Newton Raphson approaches but bigger than of PH-based IKM approach. All of the approaches are compared on the same CBHA manipulator realizing the same trajectory. For PH-based IKM, the average errors in all calculated lengths are in the range of 1-2 mm in the case of the free load. PH-based IKM is a geometrical approach which considers the **variable curvature** of the CBHA manipulator and the **optimal shape after bending energy minimization**. The latter can justify the optimal estimation of the lengths, where
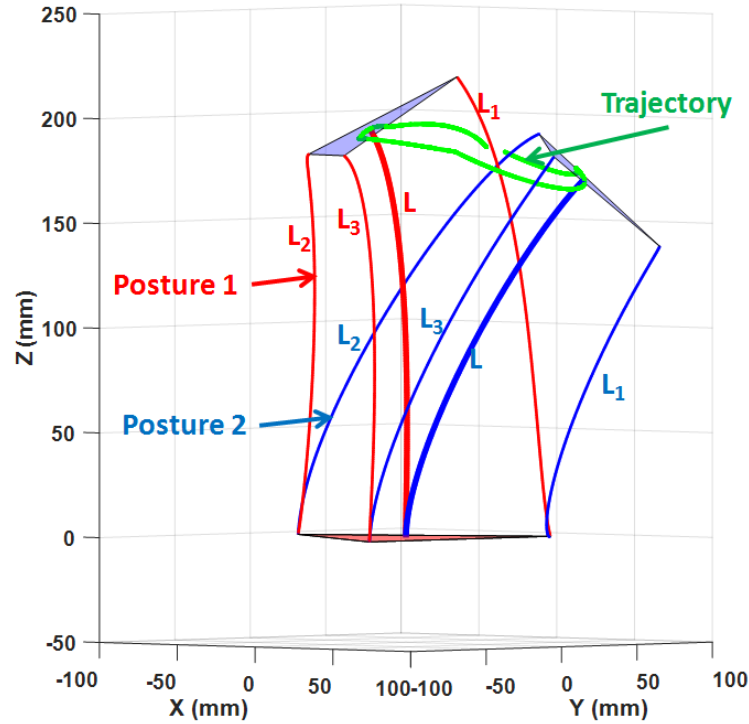
Figure 4.5: Two random postures while following the required trajectory in case of free load manipulation

the reconstructed posture is close to the real CBHA's posture.

Table 4.2 shows the time cost to calculate the IKM of the CBHA for one trajectory point (one posture), using the four approaches. PH-based IKM takes minimum time followed by Hybrid, FEM-based and Newton Raphson approaches. The Newton Raphson approach [Singh 2017] is an iterative approach. Therefore it takes more time. The Hybrid approach [Lakhal 2016] takes less time than the Newton Raphson approach, but it needs more time to handle high size matrices, as four neural networks are trained. Also, the FEM approach has more computational cost.
Therefore, results conclude that the PH-based IKM approach gives better performances in terms of accuracy as well as the time cost in free-load configuration.

Table 4.1: Absolute errors in lengths for full trajectory

	Min Err in L1 (mm)	Max Err in L1 (mm)	Avg Err in L1 (mm)
Pythagorean Hodograph Curves Approach	0.0024	4.4020	1.9904
Newton Raphson Approach	0.0004	13.2310	6.1716
Hybrid Approach	0.0002	3.9830	1.3250
FEM Based Approach	0.0052	8.2240	3.6400

	Min Err in L2 (mm)	Max Err in L2 (mm)	Avg Err in L2 (mm)
Pythagorean Hodograph Curves Approach	0.0001	5.2327	1.9227
Newton Raphson Approach	0.0009	29.4663	9.4906
Hybrid Approach	0.0013	27.4152	9.6253
FEM Based Approach	0.0042	5.6530	3.0150

	Min Err in L3 (mm)	Max Err in L3 (mm)	Avg Err in L3 (mm)
Pythagorean Hodograph Curves Approach	0.0002	8.3140	1.9893
Newton Raphson Approach	0.0008	14.3226	5.7737
Hybrid Approach	0.0074	11.5314	4.9394
FEM Based Approach	0.00460	6.4230	3.7750
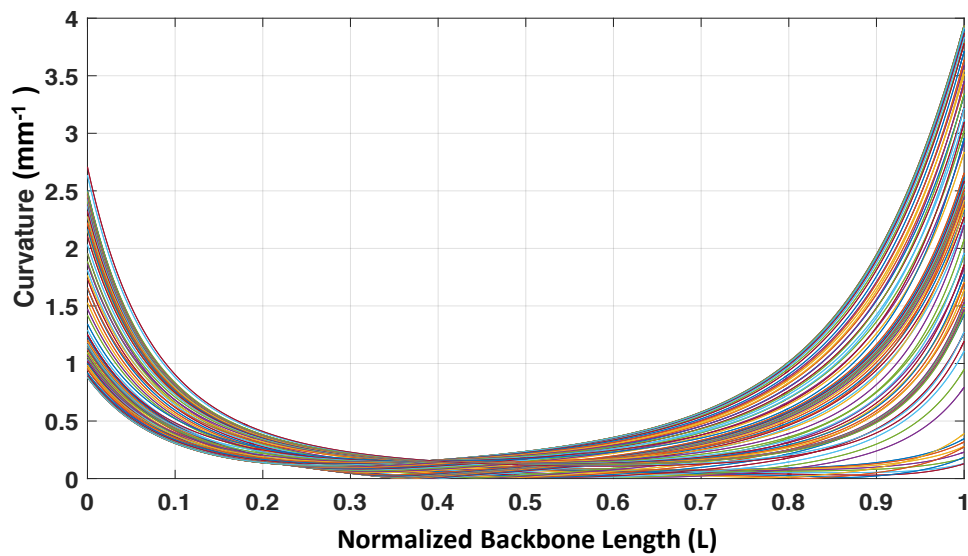
Figure 4.6: Variation of curvature of the quintic PH-curve along its backbone length
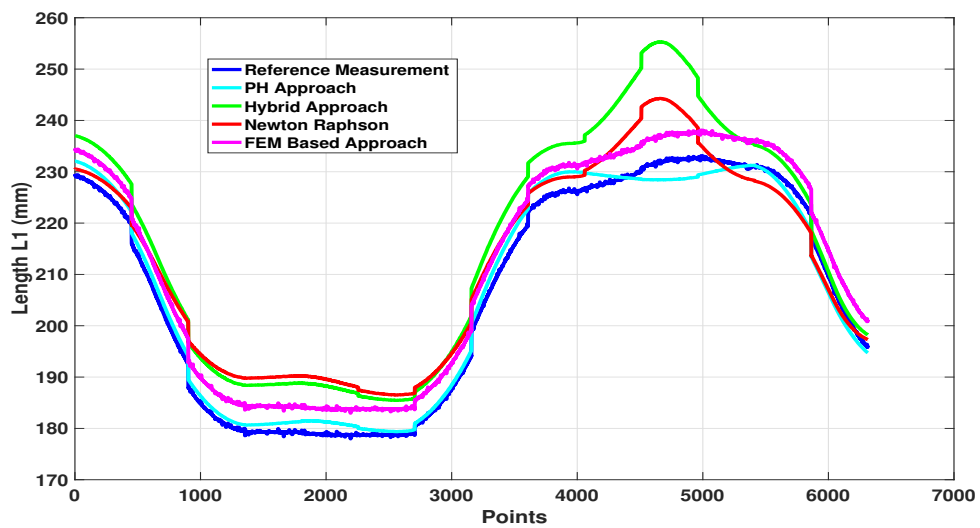
Figure 4.7: Comparison of length L1
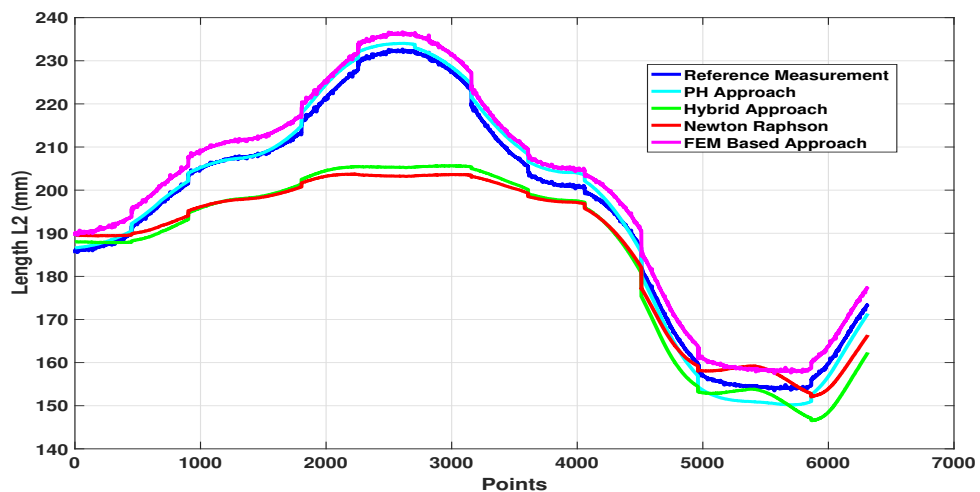
Table 4.2: Time cost for one sample

	Time Cost (sec)
Pythagorean Hodograph Curves Approach	0.00027
Newton Raphson Approach	0.23351
Hybrid Approach	0.01208
FEM Based Approach	0.05000
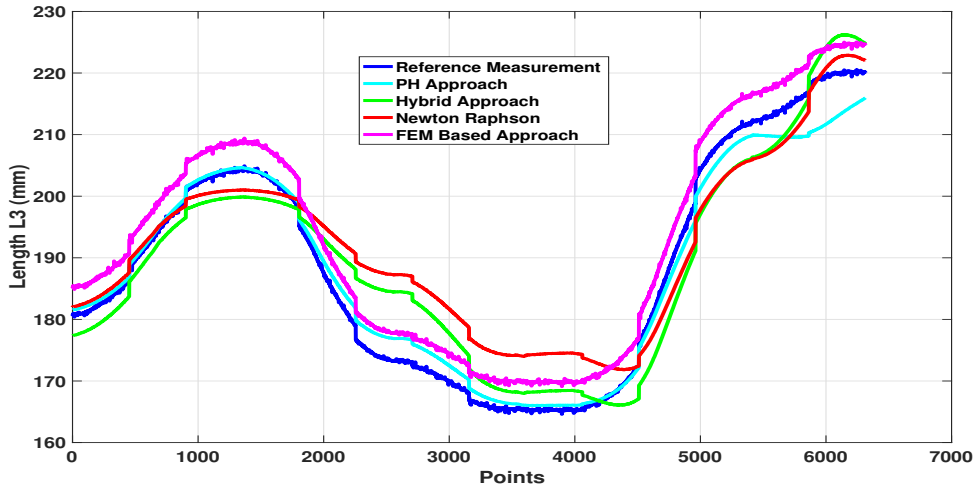
Figure 4.9: Comparison of length L3

4.3 Performances Robustness of PH-curves

Until now, the shape reconstruction of the considered soft-continuum CBHA manipulator was conducted in the case of the free-load manipulation. **However, unlike the rigid manipulators that are dimensioned in part according to their lifted loads, the soft-continuum manipulators can change their kinematic behavior in function of the lifted loads.** This is due to the flexible-made structure of the soft-continuum manipulators, where their bending is sensitive to the grasped loads. A kinematic model which can adapt to the variation of the load is therefore necessary. Shape reconstruction of soft-continuum manipulators using PH-curves is a geometrical model. Consequently, it can not accommodate the changes due to the dynamic parameters, namely: loads' mass and flexibility of the structure. These changes affect the performance of the curve-based reconstruction. To answer this problem in the context of the thesis, a qualitative learning-based approach with Neural Network (NN) is used to predict the effect of the loads on the positioning of the tip of the soft-continuum manipulator.

Let us assume that the end-point of the manipulator and the direction vector at that point, in case of free-load manipulation is given as:

$$P_{fl} = (x_{fl}, y_{fl}, z_{fl})$$
$$d_{fl} = (dx_{fl}, dy_{fl}, dz_{fl})$$

(4.7)

As shown in Fig. 4.10, the NN uses the position vector $P_{fl}(x_{fl}, y_{fl}, z_{fl})$, the direction vector d_{fl} $(dx_{fl}, dy_{fl}, dz_{fl})$ as well as the mass m as inputs. Then, the NN gives as an output an approximation of the final pose $P_f(x_f, y_f, z_f)$, d_f (dx_f, dy_f, dz_f) according to the mass handled by soft-continuum manipulator. P_s is fixed at the base of the manipulator and P_f is approximated using NN approach according to the handled mass. Furthermore, the PH shape reconstruction is used to estimate the shape of manipulator under the mass variation of the manipulated load.
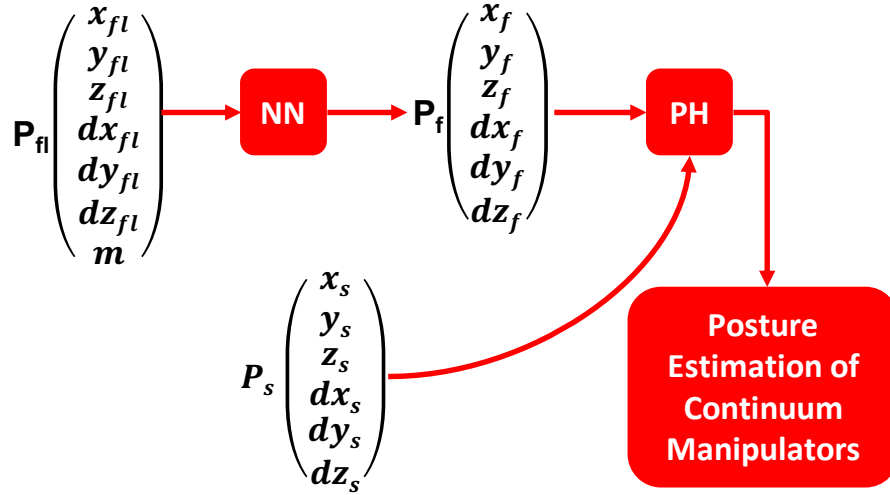
Figure 4.10: Robustness of PH curves in case of variable load manipulation

4.3.1 NN-based Approach for End-point Approximation

Using a tracking vision system, it is noticed that the end-position of the CBHA manipulator changes with the variation of mass (Fig. 4.11), which leads to the change in the shape of the manipulator. Fig. 4.11 shows the reconstructed shape by using PH-curve of the backbone of the CBHA manipulator for different masses. Fig. 4.12 shows that the manipulator does not have the same workspace in case it handles different masses. Workspace with 305 g of mass has more voids than the one with 105 g. Also, when both of the workspaces are plotted together, they did not overlap. It means with the effect of load, the end-position of the manipulator changes. The CBHA can operate as a manipulator if its kinematic (i.e., bending) doesn't change with the variation

of its admissible payload. In this case, it is essential to predict what should be the real pose in the presence of admissible payload, before starting piloting the manipulator. Therefore, an NN based approach is used to predict the variation of the end position of the CBHA manipulator in the presence of the load. Multilayer Feed-forward Networks (MFNN) are considered to approximate the pose of the CBHA. They are capable of approximating a measurable non-linear function, provided sufficiently enough hidden units [Hornik 1989]. However, finding the best MFNN structure is a difficult and unsolved problem [Spooner 2002]. Therefore, in this work, an MFNN with two hidden layers and random initial parameters is first considered, and based on the performance achieved on the test set, the parameters of MFNN are determined.

The MFNN is used to predict the influence of the mass on the
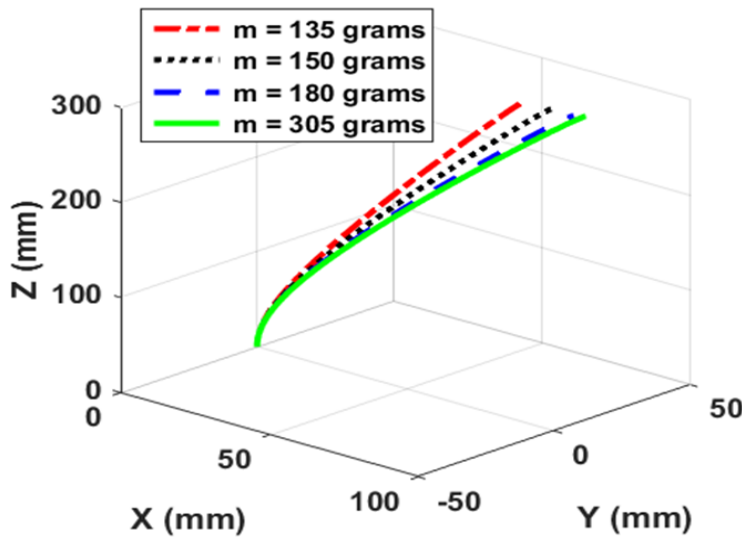
Figure 4.11: Effect of mass on the shape of CBHA manipulator

CBHA's pose. The CBHA pose $P_{fl}(x_{fl}, y_{fl}, z_{fl})$, d_{fl} $(dx_{fl}, dy_{fl}, dz_{fl})$ **with the free-load and the mass** m **are taken as inputs of NN, where the novel CBHA's pose** $P_f(x_f, y_f, z_f)$, d_f (dx_f, dy_f, dz_f) **in presence of the load is approximated as output of the NN (Fig.** 4.10)**. The latter will be used for the shape reconstruction in the presence of the handled load.**

The learning database is built using the tracking vision system. As the CBHA manipulator has pneumatic actuations, the position, with and without the mass at the end-effector is varied proportionally with the actuated pressures. These pressures have been varied in the range of [0; 1.5] bar. Thus, using a step size of 0.5, each tube has been controlled by one of these values (0; 0.5; 1; 1.5). With six controlled inputs, we get a learning database of $4^6 = 4096$

samples, for each mass. The samples are collected for a mass varying from 0 to 350 g with a step size of 15 g. In all, we obtain a learning database of 98304 samples. The learning base is divided into three subsets whose 70% is used in the training set, 15% in the validation set, and 15% in the test set.

The training set is used during the learning phase, and the test set is only used to evaluate the performance of the neuronal models. For a good generalization and to avoid over-fitting, the validation set is used during the training phase, and the early-stopping method is applied for training. The early-stopping method is required to stop the iterations after a period of training (called an epoch) using the training set and the fixed weight matrices of the MFNN. The process is reiterated until the Mean Square Error (MSE) on the validation set reaches its minimum value.

Among existing NN training algorithms (Gradient descent, Newton's method, Conjugate gradient, Quasi-Newton method, the Levenberg-Marquardt algorithm, etc.), the Gradient descent is the one requiring less memory. For instance, compared to Newton's method where the Hessian matrix (size $n \times n$) has to be stored, only the gradient vector (size n) is stored in the Gradient descent method. In the case study, the choice of Gradient descent is motivated mainly, due to the size of our training database. The training speed is improved by adding a momentum term.

The Gradient descent algorithm requires information from the gradient vector. It starts at an initial weight matrix w_0 and moves from w_i to w_{i+1} in the opposite direction of the gradient until a stopping criterion is satisfied. Therefore, the weight matrix iterates in the following way:

$$w_{i+1} = w_i - g_i \eta_i, \qquad i = 0, 1, ... \tag{4.8}$$

Where g_i is the gradient vector and η_i the training rate. The latter can either set to a fixed value or found by the optimization algorithm along the training direction at each step. In the CBHA case, the momentum term has been added to the Gradient descent algorithm to increase the rate of convergence. The eq. (4.8) becomes,

$$w_{i+1} = w_i - g_i \eta_i + p w_{i-1}, \qquad i = 0, 1, ... \tag{4.9}$$

In the training phase, the weight matrices were randomly initialized, the training rate was fixed at 0.01, and an MSE of 10^{-5} was used as a stopping criterion. To select the best MFNN model, the values of the neurons in each hidden layer were varied from 4 up to 20 neurons (with a step of 1 neuron), and the number of epochs was fixed at 20000. The optimal MFNN architecture with 11 neurons in each hidden layer was obtained after 9440 epochs. The MSE of 4.23×10^{-4} is obtained on the test set.
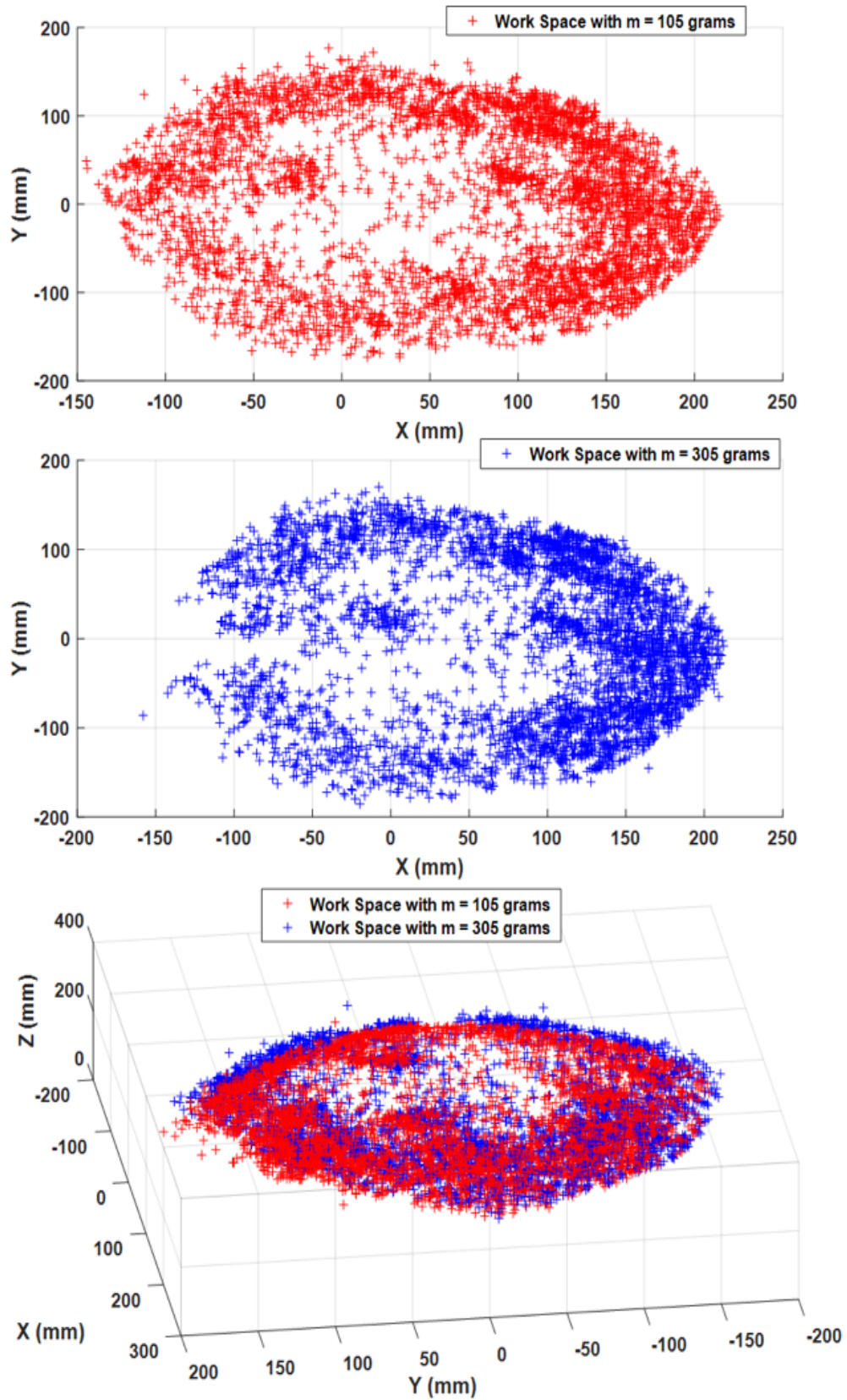
Figure 4.12: Effect of mass change on work space of the CBHA

Finally, the end-positions (P_f) of the CBHA manipulator are noted using the vision system in case the CBHA handles the masses: 135, 150, 180 and 305 g. For the same mass, end-positions are also computed using the NN algorithm. Then as shown in Fig. 4.13, the shapes of the CBHA manipulator are reconstructed using PH-curve. It is shown that the shape from the NN algorithm is approximately the same as the actual shape.
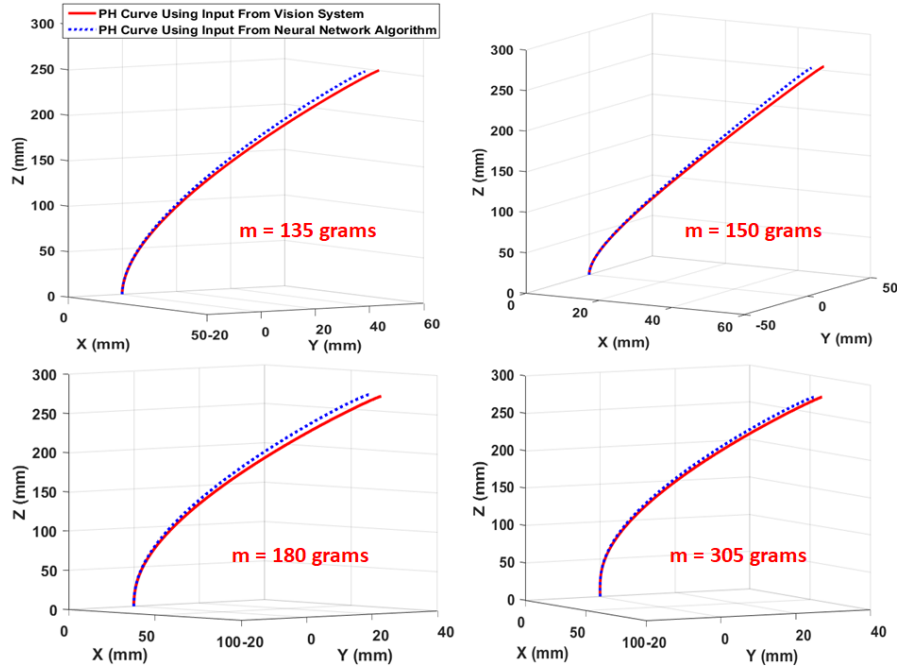
Figure 4.13: Difference b/w shape of the CBHA manipulator generated using input from NN with the one created using input from the vision system

4.4 Forward Kinematics of Continuum Manipulators from PH-curves

In terms of PH-based approach, the FKM of the continuum manipulators should define the relationship between the end-point and the backbone length of the manipulator as:

$$P_f = f(L) \tag{4.10}$$

In the following section, the FKM of the continuum manipulators is developed from PH-IKM. Then, experimental validation of the model to CBHA manipulator and its comparison with the other existing FKM approaches for the CBHA, are discussed as follows:

4.4.1   Inverse Kinematic Model towards Forward Kinematics

FKM is developed using the PH-IKM Equation of the continuum manipulators. The general form of $2n + 1^{th}$ degree PH curve of eq. 4.3 contains the following control points:

$$\vec{P_1} = \vec{P_0} + \frac{1}{2n} A_0 \vec{i} A_0^* \tag{4.11}$$

$$\vec{P_2} = \vec{P_1} + \frac{1}{4n}(A_0 \vec{i} A_1^* + A_1 \vec{i} A_0^*) \tag{4.12}$$

$$\vdots$$

$$\vec{P}_{2n-1} = \vec{P}_{2n-2} + \frac{1}{4n}(A_{2n-4} \vec{i} A_{2n-3}^* + A_{2n-3} \vec{i} A_{2n-4}^*) \tag{4.13}$$

$$\vec{P}_{2n} = \vec{P}_{2n-1} + \frac{1}{2n} A_{2n-3} \vec{i} A_{2n-3}^* \tag{4.14}$$

Therefore using these control points in the solution of eq. 4.3, the FKM of the soft-continuum manipulators can be achieved.

4.4.2   Application of FKM to the CBHA Manipulator

IKM of the CBHA manipulator is calculated using quintic PH-curves based approach. Likewise, FKM of the CBHA manipulator uses the IKM equation developed for the manipulator. The IKM equation of the CBHA manipulator is given as:

$$
\begin{aligned}
L(h) = \int_0^1 |((&-5 + 20h - 30h^2 + 20h^3 - 5h^4)\vec{P_0} \\
+ &(5 - 40h + 90h^2 - 80h^3 + 25h^4)\vec{P_1} \\
+ &(20h - 90h^2 + 120h^3 - 50h^4)\vec{P_2} \\
+ &(30h^2 - 80h^3 + 50h^4)\vec{P_3} + (20h^3 - 25h^4)\vec{P_4} \\
+ &(5h^4)\vec{P_5})|dh
\end{aligned}
\tag{4.15}
$$

Differentiating eq. 4.15 w.r.t. h from both sides;

$$
\begin{aligned}
\frac{dL(h)}{dh} = |(&-5 + 20h - 30h^2 + 20h^3 - 5h^4)\vec{P_0} \\
+ &(5 - 40h + 90h^2 - 80h^3 + 25h^4)\vec{P_1} \\
+ &(20h - 90h^2 + 120h^3 - 50h^4)\vec{P_2} \\
+ &(30h^2 - 80h^3 + 50h^4)\vec{P_3} + (20h^3 - 25h^4)\vec{P_4} \\
+ &(5h^4)\vec{P_5}|
\end{aligned}
\tag{4.16}
$$

$$\frac{dL(h)}{dh}\Big|_{h=1} = |-5\vec{P_4} + 5\vec{P_5}| \tag{4.17}$$

Using eq. 3.46, $\frac{dL(h)}{dh} = \sigma(h)$;

$$\sigma(h)|_{h=1} = |-5\vec{P_4} + 5\vec{P_5}| \tag{4.18}$$

$$\implies L = |-5\vec{P_4} + 5\vec{P_5}| \tag{4.19}$$

$$\therefore |\vec{P_5}| = \frac{L}{5} + |\vec{P_4}| \tag{4.20}$$

Using control points formulations of quintic PH (eqs. 3.89-3.93);

$$\vec{P_4} = \vec{P_0} + \frac{1}{5}A_0\vec{i}A_0^* + \frac{1}{10}(A_0\vec{i}A_1^* + A_1\vec{i}A_0^*) +$$
$$\frac{1}{30}(A_0\vec{i}A_2^* + 4A_1\vec{i}A_1^* + A_2\vec{i}A_0^*) + \frac{1}{10}(A_1\vec{i}A_2^* + A_2^*\vec{i}A_0^*) \tag{4.21}$$

Using eq. (4.21) in (4.20);

$$|\vec{P_5}| = \frac{L}{5} + |\vec{P_0} + \frac{1}{5}A_0\vec{i}A_0^* + \frac{1}{10}(A_0\vec{i}A_1^* + A_1\vec{i}A_0^*) +$$
$$\frac{1}{30}(A_0\vec{i}A_2^* + 4A_1\vec{i}A_1^* + A_2\vec{i}A_0^*) + \frac{1}{10}(A_1\vec{i}A_2^* + A_2^*\vec{i}A_0^*)| \tag{4.22}$$

Equation 4.22 is the FKM equation of the CBHA manipulator which gives the relation $P_5 = f(L)$. This equation can not be solved as we do not have the direction vector at the end point, a prerequisite for the calculation of P_4. The reason is that PH is the curve-based approach and its construction depends on the direction vector, and it is a variable curvature curve. In case of the assumption of constant curvature, the curve can be manipulated from the known information to compute the end-point. But in this case, it is not possible. This is a constraint of this approach.

We just imposed the direction vector from the tracked trajectory, to compute the magnitude of the end-point (P_5) and to see the accuracy in the trajectory tracking in terms of position only. Corresponding to the three lengths of the CBHA manipulator, endpoints of the tubes are calculated. Therefore, using geometry of the endpoints B_1, B_2, B_3, as shown in Fig. 4.2, P_f is calculated. Also, as all of the endpoints B_1, B_2, B_3, P_f lie on the same surface, same direction vector is imposed on all of the endpoints.

4.4.3 Results and Discussions

The trajectory (Fig. 4.4) of the end-point (P_5) of the CBHA manipulator is used to calculate the lengths of the CBHA manipulator using PH-IKM approach. Further, these calculated lengths are introduced as an input to the

FKM of the CBHA which approximates the end-points of each tube and subsequently (P_5) of the backbone end of the CBHA manipulator. As shown in Fig. 4.14, this approximated trajectory of the end-point is compared with the reference trajectory for the validation of the proposed forward kinematic model. Other previously developed FKMs for CBHA: 1) Hybrid Approach [Lakhal 2016], 2) Arc Geometry Approach [Escande 2015], are used for comparison. Fig. 4.14 shows the trajectory tracked using FKMs as well as the reference trajectory.

Table 4.3 shows the error comparison of proposed as well as prior developed FKMs. The results obtained using PH-FKM are accurate. The reason of the accuracy is that the additional input of the direction at the end point is given along with the length.
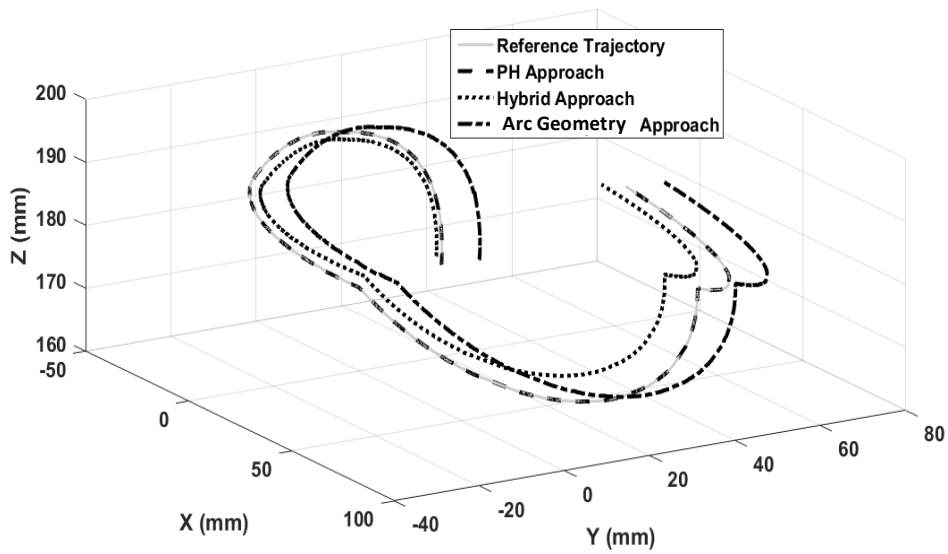
Figure 4.14: Trajectory tracked using FKM

Table 4.3: Error comparison for FKMs in mm

Approaches	Mean Error in Position	Standard Deviation
PH	1.027	0.6559
Arc Geometry	11.7686	9.3256
Hybrid	4.5558	2.0990

4.5 Conclusion of the Chapter

In this chapter, kinematics of soft-continuum manipulators are discussed using PH-based approach. The IKM of soft-continuum manipulators is deduced quantitatively from the PH-based shape reconstruction approach. The performances of the PH-IKM have been tested on the CBHA manipulator. It is discussed in the previous chapter that quintic PH-curves are the best shape representative for the CBHA manipulator. Therefore, the IKM of the CBHA manipulator is computed using quintic PH-curves. The results from the PH-based IKM are compared with the other existing IKMs for the same manipulator realizing the same trajectory. These results conclude that the PH-IKM approach gives the more accurate solution and also it is the most efficient in terms of time cost.

Further, by taking care of the importance of the effect on the shape of the continuum manipulator while it handles masses, the robustness of the shape reconstruction is performed in the case of multiple admissible masses. A qualitative NN approach is used to compute the change in the end effector position of the soft-continuum manipulators according to the amount of mass they are handling. Further, this changed end effector can be used for the shape reconstruction using PH-curves.

PH-curves based IKM of the continuum manipulators also helps us to find the FKM equation of the soft- continuum manipulators. But the PH-based FKM can not be solved without having the direction vector at the end point. The application of FKM is validated on the CBHA manipulator by imposing the direction vector at the end point. Comparison with two existing FKM methods regarding tracking accuracy indicates enhancement of these performances for the same trajectory tracking.

After extending the PH based approach to compute the kinematics of the continuum manipulators, it is interesting to see the performance of the same approach for multi-sectioned or more complex forms of continuum manipulators.

Towards Reconstruction of Soft-continuum Closed Loop Kinematic Chain: PH-based Approach

Contents

5.1   Introduction

In this chapter, a PH-based approach is presented to build multi-section manipulators or to model the shape of the continuum closed loop kinematic chains. Therefore, this work involves the concatenation of PH-curves to describe the kinematics of the soft-continuum links attached in serial or parallel configuration.

5.2   Problem Statement

As discussed in previous chapters, to reconstruct the shape of a single soft-continuum manipulator, four basic input conditions are used. Now, the motive is to model the shape of the manipulators in serial or parallel configuration. Figure 5.1 shows a general case, in which n soft-continuum links are connected
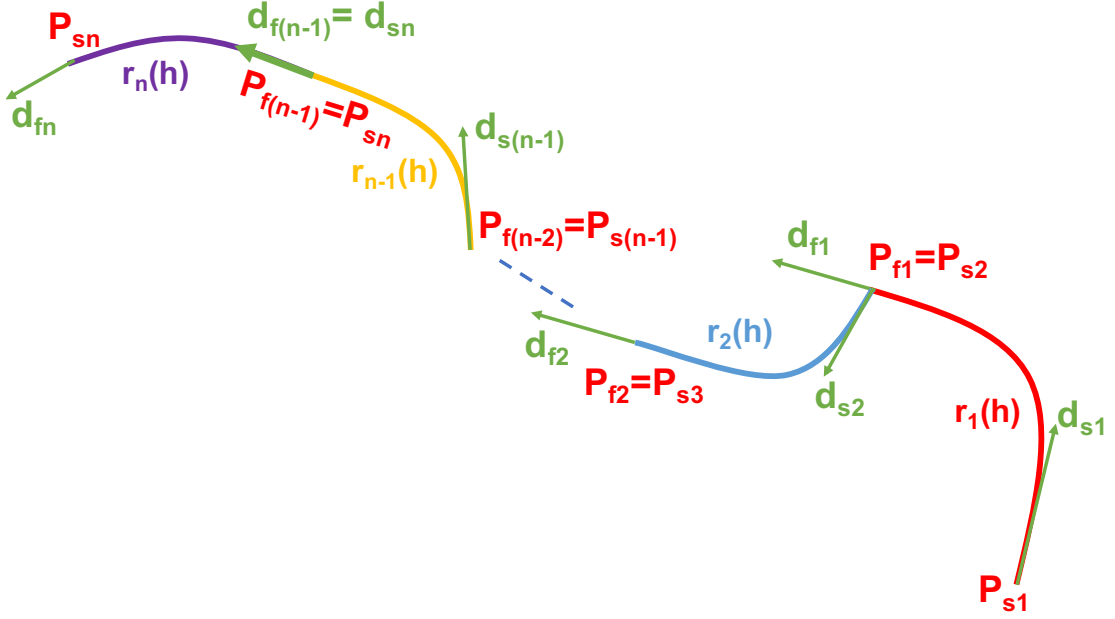
Figure 5.1: General case of n number of soft links connected to form a soft-continuum kinematic chain

to form a kinematic chain. If $r(h)$ is the curve representing the shape of a single soft manipulator, the problem statement to model the n links in a kinematic chain using n curves $r_n(h)$ is stated as:

$$\sum_{i=1}^{n} (P_{s_i}(x_{s_i}, y_{s_i}, z_{s_i}), d_{s_i}(d_{xs_i}, d_{ys_i}, d_{zs_i}) \overset{r_i(h)}{\rightarrow} P_{f_i}(x_{f_i}, y_{f_i}, z_{f_i}), d_{f_i}(d_{xf_i}, d_{yf_i}, d_{zf_i}))$$

(5.1)

Here, h represents the curvilinear coordinate along the curve. $i = 1, 2, ..., n - 1, n$ indicates the link in the kinematic chain. Equation 5.1 represents the concatenation of n PH-curves to form a soft-continuum kinematic chain of n links.

Same as the case of single link, in this case also we need to choose an optimal shape of each link of the kinematic chain to get an optimal shape of the kinematic chain. Therefore the same optimization approach is used as stated in eq. 1.2.

5.3   Concatenation of PH Curves

Sometimes the soft-continuum manipulators are difficult to model with one PH curve due to their complex shape or due to more sections. Also, in the case of soft-continuum closed loop kinematic chains, to model more than one

link, concatenation of PH curves is required. Concatenation of more than one PH curves involves the following two cases:

5.3.1 Case 1: C_1 Continuity

As shown in Fig. 5.2, two PH curves are concatenated. In this case, both of the links are joined with C_1 continuity. Therefore this is the case in which position, as well as velocity, are the same at the junction point. The following conditions need to be used to construct PH curves for this case:
For PH_1,

$$r_1(0) = A \qquad r_1(1) = B \qquad (5.2)$$

$$r_1'(0) = d_s \qquad r_1'(1) = d_m \qquad (5.3)$$

For PH_2,

$$r_2(0) = B \qquad r_2(1) = C \qquad (5.4)$$

$$r_2'(0) = d_m \qquad r_2'(1) = d_f \qquad (5.5)$$
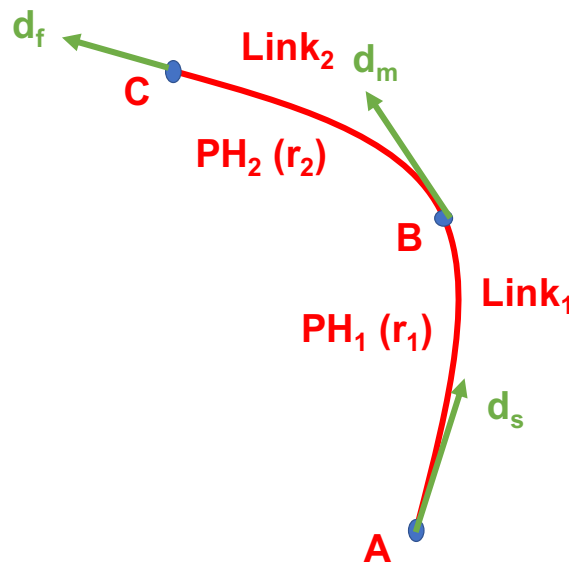
Figure 5.2: Concatenation of two PH curves with C_1 continuity

5.3.2 Case 2: C_0 Continuity

In a soft-continuum kinematic chain, sometimes the links are joined with C_0 continuity having only the position constraint at the junction. Fig. 5.3 shows the concatenation of two PH curves (two links) with C_0 continuity. The

following conditions need to be used to construct PH curves for this case:
For PH_1,

$$r_1(0) = A \qquad r_1(1) = B \tag{5.6}$$

$$r_1'(0) = d_s \qquad r_1'(1) = d_f \tag{5.7}$$

For PH_2,

$$r_2(0) = B \qquad r_2(1) = C \tag{5.8}$$

$$r_2'(0) = d_{ss} \qquad r_2'(1) = d_{ff} \tag{5.9}$$

These two cases are discussed to get the boundary conditions for the soft-
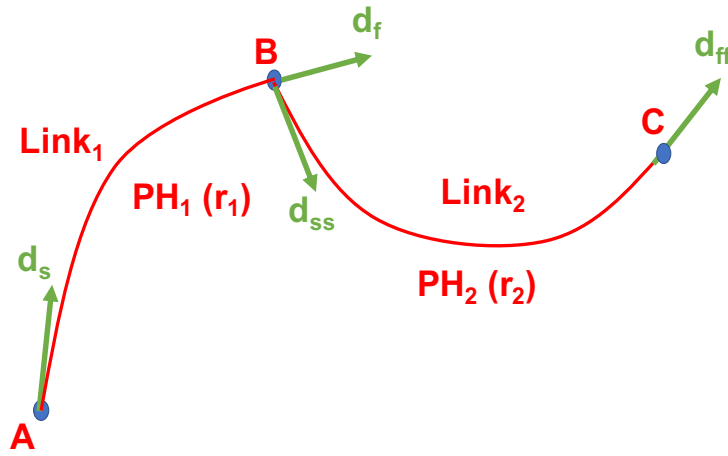
Figure 5.3: Concatenation of two PH curves with C_0 continuity

continuum links concatenated to form the soft-continuum kinematic chain.

5.4 Experimental Validation

5.4.1 Experimental Setup

A continuum closed loop kinematic chain is formed to move towards the application of skipping rope. A CBHA manipulator can move an object like we can move it by hand. Therefore, a continuum closed loop kinematic chain is formed with an assembly of three flexible links. Fig. 5.4 shows the two CBHA arms driving an intermediate flexible rope, forming a closed kinematic chain ABCD. The rope is a passive link, and it is hanging under the condition of its self-weight. Both of the CBHA arms are fixed at their bases. The aim is to model the shape of the soft-continuum kinematic chain using quintic PH-curves. Let us consider that $CBHA_1$ acts as a $link_1$, $rope$ as a $link_2$ and $CBHA_2$ as a $link_3$. A quintic PH-curve is used to reconstruct the shape of
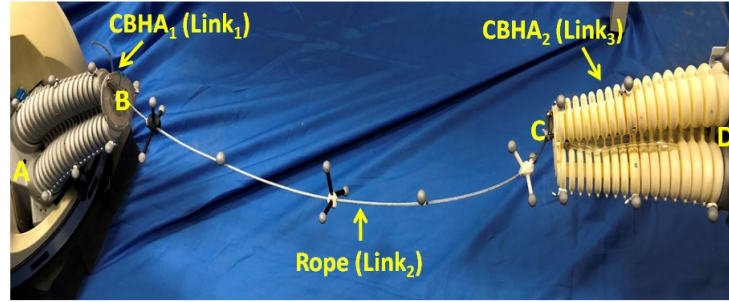
Figure 5.4: Continuum closed loop kinematic chain

each flexible link of the closed kinematic chain (Fig. 5.5). Table 5.1 shows the four initial conditions used to construct the quintic PH-curve for each link. Therefore, three quintic PH-curves are constructed for the considered kinematic chain. Calibrated quintic PH-curves are used in this formulation.

Table 5.1: Initial conditions to construct PH curves for soft-continuum closed loop kinematic chain

	$Link_1$ (PH_1)	$Link_2$ (PH_2)	$Link_3$ (PH_3)
Starting Position	A	B	C
Starting Orientation	$O(A)_{CBHA_1}$	$O(B)_{Rope}$	$O(C)_{CBHA_2}$
Ending Position	B	C	D
Ending Orientation	$O(B)_{CBHA_1}$	$O(C)_{Rope}$	$O(D)_{CBHA_2}$

The markers are attached on all of the three links of the closed kinematic chain: $CBHA_1$, $rope$ and $CBHA_2$ to perform the experimental validation as shown in Fig. 5.4.

5.4.2 Results

Three quintic PH-curves are constructed for the kinematic chain as described in Fig. 5.5. The reconstructed shape of the closed kinematic chain using PH curves is compared with the actual tracked shape (Fig. 5.7). The average errors from the actual shape (tracked markers) for the links $CBHA_1$, $rope$ and $CBHA_2$ are 2.8 mm, 8 mm and 3.1 mm respectively. These results show that PH curves based approach can approximate the shape of the links in a chain.
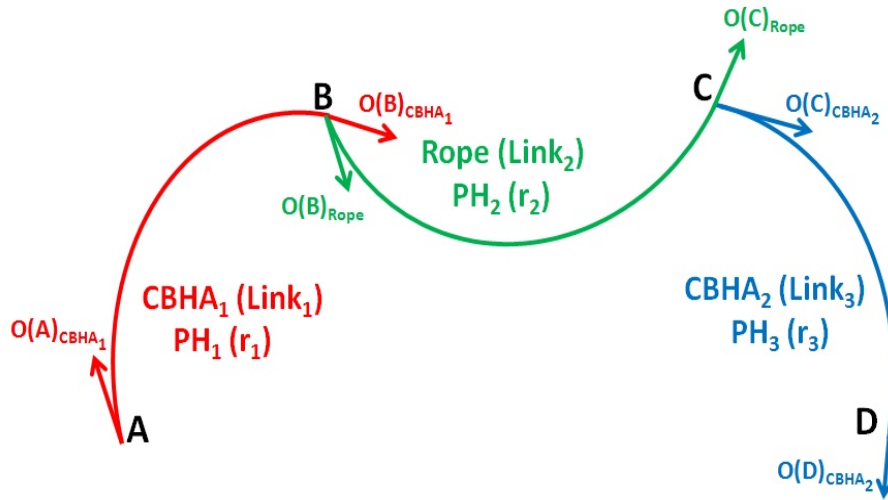
Figure 5.5: Modeling of closed loop kinematic chain using PH curves
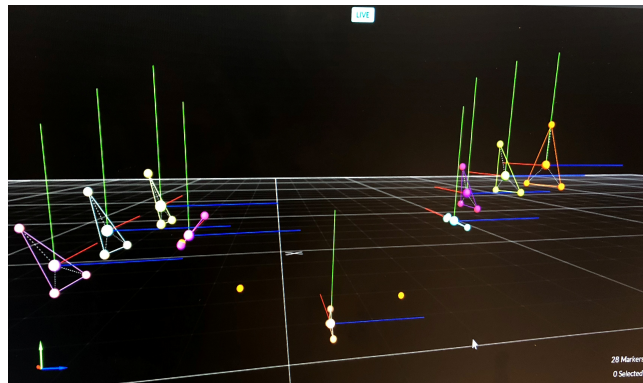
Figure 5.6: Tracking of continuum closed loop kinematic chain
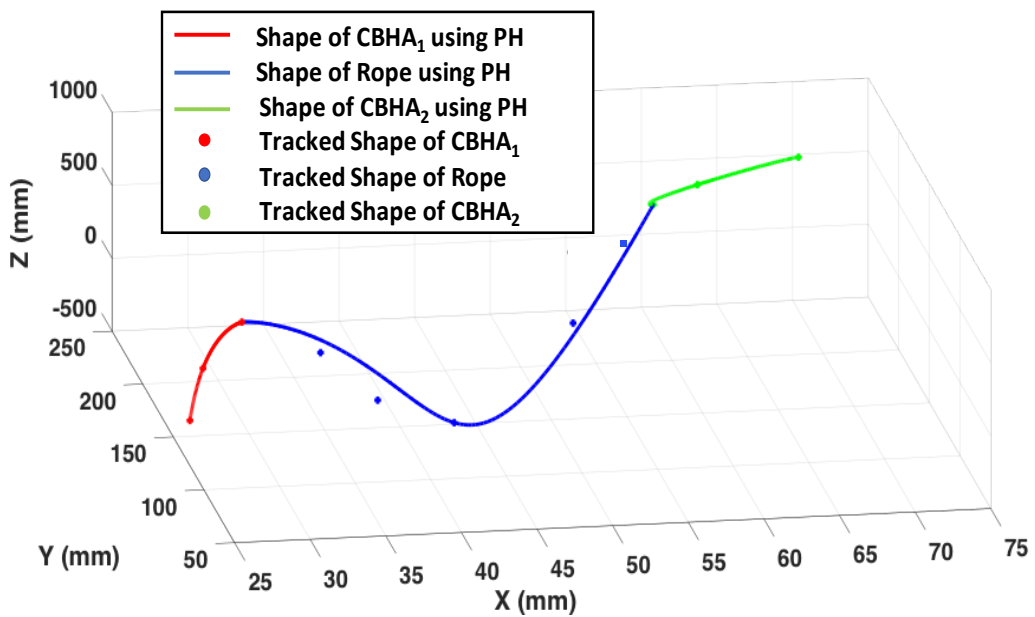
Figure 5.7: Comparison of real shape with shape reconstructed using PH curve for continuum closed loop kinematic chain

Different movements of the kinematic chain are created and tracked using the vision system, and data is recorded for some of the postures during the movement. We tried to reconstruct some postures of the kinematic chain (Fig. 5.8).

From the results, it is clear that quintic PH-curves can model the shape of the soft-continuum kinematic chains. But it is noticed that there are more errors in the shape construction of the different links of the soft-continuum kinematic chain than the errors to model the shape of a single soft-continuum manipulator. The reason for these errors can be:

- The concatenation of two links experience some induced force at the joint. Therefore, it affects the orientation of the links.

- The rope can be more flexible to model using quintic PH curves. That's why there is more error in the shape reconstruction of the rope than the CBHA manipulator.

- Another reason can be the movement of the chain as two CBHAs are moving the rope. PH-based shape reconstruction needs an accurate data of the orientation (direction vector) to model the shape. The orientation tracked during the motion can have some error.

5.5 Conclusion of the Chapter

The improvements in the accuracies in the shape reconstruction and kinematics of the soft-continuum manipulators using PH-based approach leads us to the work of this chapter. This chapter deals with the shape reconstruction of kinematic chains formed using soft-continuum links. A generalized case of a kinematic chain built using n soft-kinematic links is discussed. The shape of each link is reconstructed using a quintic PH-curve. Then the concatenation of these PH-based reconstructed shapes is performed. The optimal shape of each link ensures the optimal shape of the whole kinematic chain after concatenation.

An interesting experimental set-up is created to validate the proposed methodology of modeling soft-continuum kinematic chains. This chain consists of two CBHA manipulators holding a rope. The rope is a passive link here. Therefore, this chain composed of three soft-continuum links is modeled using the discussed methodology. The optimal shape of each link is modeled separately, and then all of the three links are concatenated to reconstruct an optimal shape of the constructed soft-continuum kinematic chain. The results show that the errors in the reconstructed shape are in the acceptable range.

Furthermore, it is noticed that the chain consists of two CBHAs and a rope illustrates that it is a heterogeneous chain due to the presence of two different
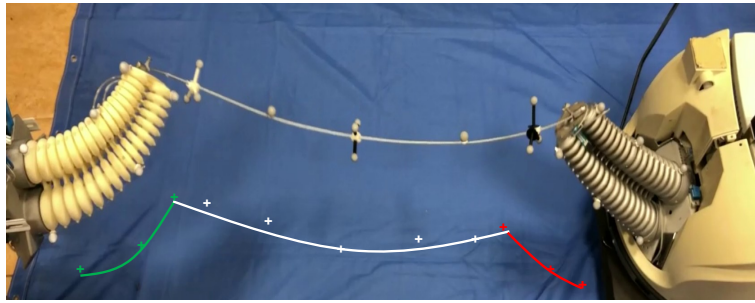
(a)
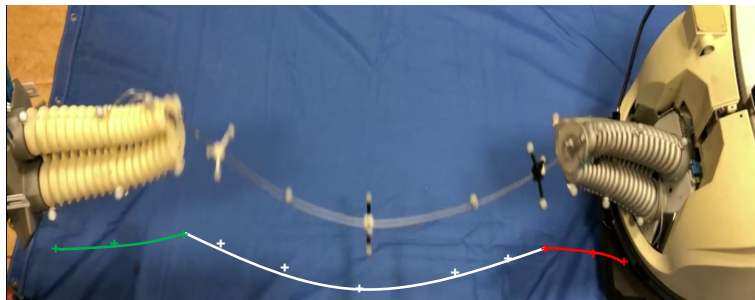
(b)
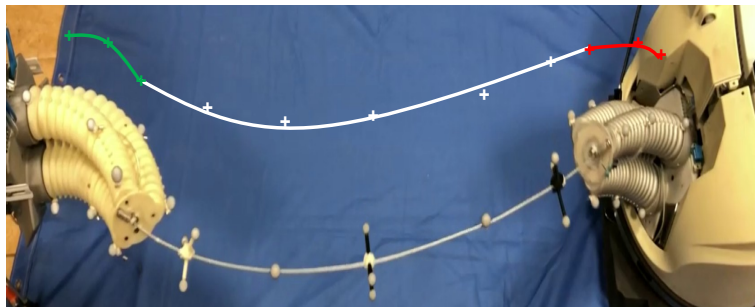
(c)
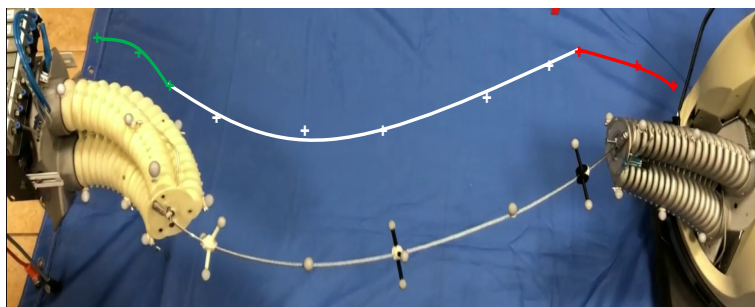
(d)

Figure 5.8: Random postures of the continuum kinematic chain reconstructed using quintic PH-curves

type of links (CBHA and rope) in the chain. Therefore, another interesting conclusion is drawn that the proposed methodology can also model the shapes of the heterogeneous soft-kinematic chains. Also, the single manipulators which are heterogeneous can be modeled using this approach.

Conclusion and Prospective

Contents

The primary objective of this work is to provide a methodology to model the shape of soft, continuum manipulators based on the geometrical curve approach. Pythagorean Hodograph (PH) curves are used to model the optimal shape of the manipulators, starting from the knowledge of their input and end points' poses. This approach of shape reconstruction leads to the calculation of kinematic behavior of the manipulators. The proposed methodology is validated experimentally on the CBHA manipulator, and it is also compared with the existing kinematic approaches for CBHA. The aim is to compare the performances of each kinematic approach applied on the same robot.

6.1   Summary of Conclusions

First, a concise and a complete view of the field of soft manipulators is presented, after discussion of the terminology of soft and continuum manipulators. The main interesting problems addressed in the framework of this Ph.D. thesis are:

1) Shape reconstruction,

2) Kinematic modeling of soft-continuum manipulators.

Due to the soft material properties, the modeling of the shape of soft manipulators plays a vital role. A positioning of PH model-based for the shape reconstruction has been made compared to existing quantitative and qualitative approaches to model the shape as well as the kinematics of the soft-continuum manipulators. Also, the analytical or data models of soft-continuum manipulators need to be validated for simulation of control purposes. The complexity of these models requires a real-time optimization as one of the specifications for the proposed contribution.

The choice of the type of the curve for the shape reconstruction is an important step. The curves can be represented as parametric or non-parametric

form. Further, the parametric curves can be represented as analytical or synthetic form and non-parametric as implicit or explicit form. Different types of curve-based approaches are discussed with their mathematical formulations. Synthetic curves are found more appropriate to model the shape of soft-continuum manipulators due to the presence of control points to control their shape. The mainly used synthetic curves (Hermite, Bezier, B-splines, PH curves) are discussed to reconstruct the shape of soft-continuum manipulators and are compared to choose an appropriate curve as per our requirements. The discussion involves how to approximate the bending along the backbone of soft-continuum manipulators by cubic/quintic polynomial functions describing geometrical curves to reconstruct the shape. Furthermore, a class of soft-continuum manipulators, namely Compact Bionic Handling Assistant (CBHA) is introduced. All of the discussed curve based approaches are applied to this manipulator to reconstruct its shape. The results are compared and discussed regarding accuracy and time cost to choose an optimal real-time approach. Results show that quintic PH curves are the best to reconstruct the postures of the CBHA in 76.50 % of the cases. The remaining 13.50 % postures are better reconstructed using Hermite, Bezier and cubic PH curves. In these 13.50 % of cases, the posture of the CBHA is near to the straight configuration. The advantages of PH curves over the other curves are:

1) PH curves are computationally efficient.

2) Less number of input boundary conditions can generate higher order PH curves.

3) Length of a PH-curve has a closed form solution.

Furthermore, the calibration of the PH based reconstructed shape is performed to accommodate the uncertainties in the structure of the CBHA manipulator using known experimental data. This calibration further improves the accuracy of the PH based reconstructed shape.

Due to the flexible-made structure of the soft-continuum manipulators, their bending is sensitive to the grasped loads. In this case, it is important to evaluate the robustness of the modeling approach especially when the modeling concerns a manipulator, where its main task is the manipulation of objects. External grasped masses by the soft manipulators induce their shape deformation compared to their equivalent in rigid structure. Therefore, both cases: 1) Free load conditions, 2) Loaded conditions, are discussed. A qualitative NN approach is used to compute the change in the end effector position of the soft-continuum manipulators according to the amount of mass they are handling. Further, this changed end effector position can be used for the shape reconstruction using PH-curves.

After the shape reconstruction, the kinematics of the soft-continuum manipulators is discussed by using the Pythagorean Hodograph (PH) curve-based modeling. Forward, as well as, inverse kinematic models can be deduced using

PH curves. Developed kinematic models are tested on the CBHA manipulator, and the results are compared with the existing kinematic approaches for the same manipulator. There is a limitation of finding the FKM using PH curves as we need the orientation of the endpoint of the manipulator as an extra input.

An extension of PH based shape reconstruction approach to a heterogeneous soft-continuum closed loop kinematic chain has been discussed. This study aims to propose a methodology of building heterogeneous multi-section, for designing a soft-continuum parallel manipulator. A test bench has been developed, composed of two CBHA manipulators holding a rope, thereby mimicking the skipping rope application. The overall shape of the three heterogeneous sections is modeled using the PH based shape reconstruction approach, and validated using an external optiTrack vision system. This gives the following two important outcomes: 1) provides the process of the concatenation of PH curves under different conditions, 2) acknowledges the applicability of PH curves as a shape modeling of heterogeneous multi-section manipulators.

As a conclusion of this work, we have shown that the PH based approach can model shape as well as kinematics of the soft-continuum manipulators. It can also be applied to the heterogeneous multi-section manipulators. The other interesting application of this approach is to design manipulators. By obtaining an optimal shape using the PH based shape reconstruction approach of each section, a manipulator can be designed section by section as per our requirement.

6.2 Future Works

The possible extensions in the current work regarding the modeling of soft-continuum manipulators are numerous. Based on our experience with the curve model-based technique, the following prospectives can be taken care of:

1. Dynamic modeling of soft-continuum manipulators:
   The proposed PH-based approach is used to model optimal shape and the kinematics of the soft-continuum manipulators. The prospective is not to keep this approach limited only to the kinematic modeling. The extension of this approach to model dynamics of the soft-continuum manipulators needs a physical interpretation of the PH-curve approach. The main core of the PH-curve reconstruction is the control points. The latter are used to control the shape of the curve, which describes mathematically a quintic polynomial. Now, if this polynomial representation can be described physically by the behavior of a non-redundant rigid manipulator, it can generate an automatic control of the control points. This can be described by using the controlled joints of the rigid manipulator, encapsulating a continuum curve of our soft manipulator. Figure

6.1 illustrates a 2D virtual rigid manipulator made up from the control polygon of the reconstructed PH curve. Therefore, this assumption of the virtual rigid manipulator can help us to compute the velocities and efforts on each control point, which induce the dynamics of the encapsulated soft-continuum manipulator, represented by a PH-curve.
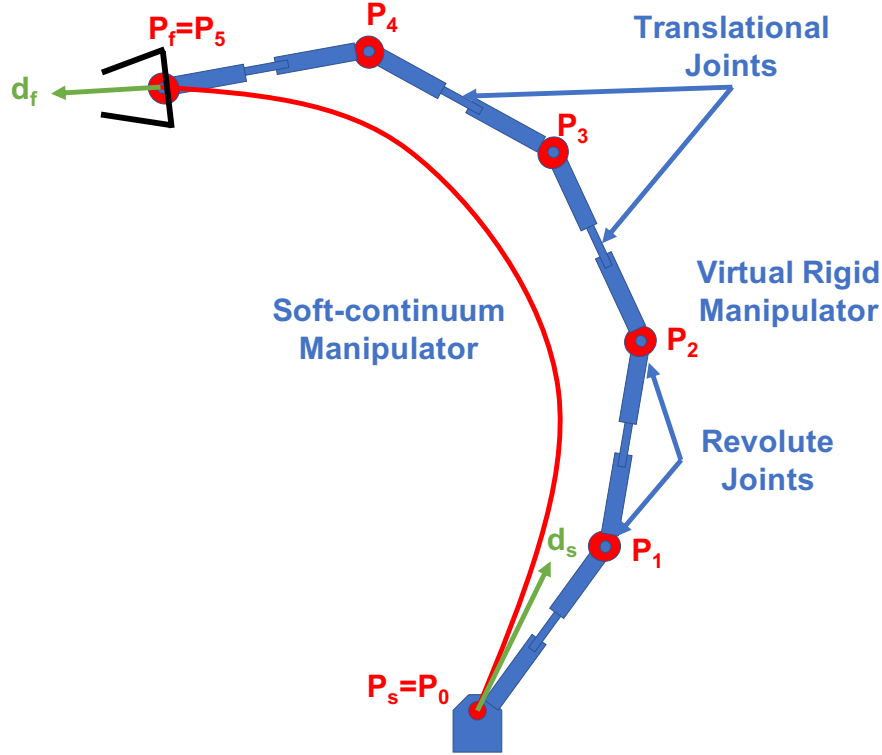
Figure 6.1: Soft-continuum manipulator encapsulated by a virtual 2D rigid manipulator

2. The other main prospective is to use PH-based approach to avoid obstacles. As PH-based shape is the function of its control points $(P_0,...,P_5)$, where the change in the control points will result in the shape-shifting of the soft-continuum manipulator.

$$\text{PH-shape} = f(P_0, P_1, P_2, P_3, P_4, P_5) \tag{6.1}$$

The control points of the PH curve are computed using the minimum potential energy criteria. In case of the presence of obstacles, we do not need to adhere to the minimum energy criteria. Therefore, we can move from minimum to the direction of an increase in the energy until we are enabled to avoid the obstacle. Defining the different types of obstacles and formulating an algorithm to relocate the trajectory of control points in the presence of constraints is required.

3. In future, it would also be interesting to check the performance of PH-based approach to model more non-homogeneous or different types of non-homogeneous continuum structures.

Introduction to Quaternions

A.1 Introduction

Until now we have learned that a 3×3 orthogonal matrix can represent a rotation in $\mathbb{R}^3$ about an axis through the origin with determinant 1. However, the matrix representation seems redundant because only four of its nine elements are independent. Also, the geometric interpretation of such a matrix is not clear until we carry out several steps of calculation to extract the rotation axis and angle. Furthermore, to compose two rotations, we need to compute the product of the two corresponding matrices, which requires twenty-seven multiplications and eighteen additions. Quaternions are very efficient for analyzing situations where rotations in $\mathbb{R}^3$ are involved. A quaternion is a 4-tuple, which is a more concise representation than a rotation matrix. Its geometric meaning is also more evident as the rotation axis, and angle can be trivially recovered. The quaternion algebra to be introduced will also allow us to compose rotations easily. This is because quaternion composition takes merely sixteen multiplications and twelve additions. The development of quaternions is attributed to W. R. Hamilton [Hamilton 1844] in 1843. Legend has it that Hamilton was walking with his wife Helen at the Royal Irish Academy when he was suddenly struck by the idea of adding a fourth dimension in order to multiply triples. Excited by this breakthrough, as the couple passed the Brougham bridge of the Royal Canal, he carved the newfound quaternion equations

$$\hat{\vec{i}}^2 = \hat{\vec{j}}^2 = \hat{\vec{k}}^2 = \hat{\vec{i}}\hat{\vec{j}}\hat{\vec{k}} = -1 \tag{A.1}$$

into the stone of the bridge. This event is marked by a plaque at the exact location today. Hamilton spent the rest of his life working on quaternions, which became the first non-commutative algebra to be studied.

A.2 Quaternion Algebra

The set of quaternions, together with the two operations of addition and multiplication, form a non-commutative ring. The standard orthonormal basis for $\mathbb{R}^3$ is given by three unit vectors $\hat{\vec{i}} = (1, 0, 0)$, $\hat{\vec{j}} = (0, 1, 0)$, $\hat{\vec{k}} = (0, 0, 1)$. A quaternion q is defined as the sum of a scalar q_0 and a vector $\vec{q} = (q_1, q_2, q_3)$,

given as:

$$q = q_0 + \vec{q} = q_0 + q_1\hat{\vec{i}} + q_2\hat{\vec{j}} + q_3\hat{\vec{k}} \tag{A.2}$$

A.2.1 Addition and Multiplication

Addition of two quaternions acts component-wise. More specifically, consider the quaternion q above and another quaternion:

$$p = p_0 + \vec{p} = p_0 + p_1\hat{\vec{i}} + p_2\hat{\vec{j}} + p_3\hat{\vec{k}} \tag{A.3}$$

Then the addition of the two quaternions implies:

$$p + q == (p_0 + q_0) + (p_1 + q_1)\hat{\vec{i}} + (p_2 + q_2)\hat{\vec{j}} + (p_3 + p_3)\hat{\vec{k}} \tag{A.4}$$

Every quaternion q can be represented as a negative $-q$ having components $-q_i$, $i = 0, 1, 2, 3$. The product of two quaternions satisfies these fundamental rules introduced by Hamilton:

$$
\begin{aligned}
\hat{\vec{i}}^2 = \hat{\vec{j}}^2 &= \hat{\vec{k}}^2 = \hat{\vec{i}}\hat{\vec{j}}\hat{\vec{k}} = -1 \\
\hat{\vec{i}}\hat{\vec{j}} &= \hat{\vec{k}} = -\hat{\vec{j}}\hat{\vec{i}} \\
\hat{\vec{j}}\hat{\vec{k}} &= \hat{\vec{i}} = -\hat{\vec{k}}\hat{\vec{j}} \\
\hat{\vec{k}}\hat{\vec{i}} &= \hat{\vec{j}} = -\hat{\vec{i}}\hat{\vec{k}}
\end{aligned}
\tag{A.5}
$$

Now we can give the product of two quaternions p and q:

$$
\begin{aligned}
pq &= (p_0 + p_1\hat{\vec{i}} + p_2\hat{\vec{j}} + p_3\hat{\vec{k}})(q_0 + q_1\hat{\vec{i}} + q_2\hat{\vec{j}} + q_3\hat{\vec{k}}) \\
&= p_0q_0 - (p_1q_1 + p_2q_2 + p_3q_3) + p_0(q_1\hat{\vec{i}} + q_2\hat{\vec{i}} + q_3\hat{\vec{i}}) + q_0(p_1\hat{\vec{i}} + p_2\hat{\vec{i}} + p_3\hat{\vec{i}}) + \\
&\quad (p_2q_3 - p_3q_2)\hat{\vec{i}} + (p_3q_1 - p_1q_3)\hat{\vec{j}} + (p_1q_2 - p_2q_1)\hat{\vec{k}}
\end{aligned}
\tag{A.6}
$$

Whew! It is too long to remember or even to understand what is going on. Fortunately, we can utilize the inner product and cross product of two vectors in $\mathbb{R}^3$ to write the above quaternion product in a more concise form:

$$pq = p_0q_0 - \vec{p} \cdot \vec{q} + p_0\vec{q} + q_0\vec{p} + \vec{p} \times \vec{q} \tag{A.7}$$

In the above, $p = (p1, p2, p3)$ and $q = (q1, q2, q3)$ are the vector parts of p and q, respectively.

Example A.2.1. Suppose the two vectors are given as follows:

$$
\begin{aligned}
p &= 5 + 2\hat{\vec{i}} - \hat{\vec{j}} + \hat{\vec{k}} \\
q &= 2 - 3\hat{\vec{i}} + \hat{\vec{j}} - 5\hat{\vec{k}}
\end{aligned}
$$

We separated out their vector parts, $\vec{p} = (2, -1, 1)$ and $\vec{q} = (-3, 1, -5)$ and calculated their dot and cross products as:

$$\vec{p} \cdot \vec{q} = -12 \tag{A.8}$$

$$\vec{p} \times \vec{q} = \begin{vmatrix} \hat{\vec{i}} & \hat{\vec{j}} & \hat{\vec{k}} \\ 2 & -1 & 1 \\ -3 & 1 & -5 \end{vmatrix} \tag{A.9}$$
$$= 4\hat{\vec{i}} + 7\hat{\vec{j}} - \hat{\vec{k}}$$

Using eq. A.7, the quaternion product is:

$$pq = 10 - (-12) + 5(-3\hat{\vec{i}} + \hat{\vec{j}} - 5\hat{\vec{k}}) + 2(2\hat{\vec{i}} - \hat{\vec{j}} + \hat{\vec{k}}) + (4\hat{\vec{i}} + 7\hat{\vec{j}} - \hat{\vec{k}}) = 22 - 7\hat{\vec{i}} + 10\hat{\vec{j}} - 24\hat{\vec{k}} \tag{A.10}$$

We see that the product of two quaternions is still a quaternion with scalar part $p_0 q_0 - \vec{p} \cdot \vec{q}$ and vector part $p_0 \vec{q} + q_0 \vec{p} + \vec{p} \times \vec{q}$. The set of quaternions is closed under multiplication and addition. It is not difficult to verify that multiplication of quaternions is distributive over addition. The identity quaternion has real part 1 and vector part 0.

A.2.2 Conjugate

Let $q = q_0 + \vec{q} = q_0 + q_1 \hat{\vec{i}} + q_2 \hat{\vec{j}} + q_3 \hat{\vec{k}}$ be a quaternion. The conjugate of q, denoted q^*, is defined as;

$$q = q_0 - \vec{q} = q_0 - q_1 \hat{\vec{i}} - q_2 \hat{\vec{j}} - q_3 \hat{\vec{k}} \tag{A.11}$$

From the definition, we have;

$$(q^*)^* = q_0 - (-\vec{q}) = q$$
$$q + q^* = 2q_0$$
$$q^* q = q q^*$$

A.3 Solution of equation $A\vec{i}A^* = \vec{c}$

In Hermite interpolation problem, we have to solve equation of the form [Farouki 2008]:

$$A\vec{i}A^* = \vec{c} \tag{A.12}$$

Where A is a quaternion of form $A = a_0 + a_x \vec{i} + a_y \vec{j} + a_z \vec{k}$ and $\vec{c} = c_x \vec{i} + c_y \vec{j} + c_z \vec{k}$ is a given vector. Substituting these in (A.12), we get:

$$a_0^2 + a_x^2 - a_y^2 - a_z^2 = c_x \tag{A.13}$$

$$2(a_0 a_z + a_x a_y) = c_y \tag{A.14}$$

$$2(a_x a_z - a_0 a_y) = c_z \tag{A.15}$$

Here, we have three equations with four unknowns, it means solution of (A.12) exhibits one degree of freedom.

Let $v = \frac{\vec{c}}{|\vec{c}|} = (\lambda, \mu, \nu)$ be a unit vector in the direction of $\vec{c}$, then with $a_0 = 0$, a particular solution is easily seen as:

$$A = \pm\sqrt{\frac{1}{2}(1+\lambda)|\vec{c}|}[\vec{i} + \frac{\mu}{1+\lambda}\vec{j} + \frac{\nu}{1+\lambda}\vec{k}] \tag{A.16}$$

Moreover, if Q is any quaternion satisfying the equation

$$Q\vec{i}Q^* = \vec{i} \tag{A.17}$$

The quaternions that satisfy (A.17) are [Farouki 2008] of the form:

$$Q = cos\phi + sin\phi\vec{i} \tag{A.18}$$

$$A\vec{i}A^* = AQ\vec{i}(AQ)^* = AQ\vec{i}Q^*A^* = A\vec{i}A^* \tag{A.19}$$

which implies, AQ must also be a solution of (A.12). Therefore, the most general solution of (A.12), can be parameterized in terms of an angular variable ϕ as:

$$A(\phi) = \sqrt{\frac{1}{2}(1+\lambda)|\vec{c}|}(-\sin\phi + \cos\phi\vec{i} + \frac{\mu\cos\phi + \nu\sin\phi}{1+\lambda}\vec{j} + \frac{\nu\cos\phi - \mu\sin\phi}{1+\lambda}\vec{k}) \tag{A.20}$$

As $sin(\phi + \pi) = -sin\phi$ and $cos(\phi + \pi) = -cos\phi$, the above expression clears the sign ambiguity in (A.16). Therefore, the $\pm$ sign is omitted in this general solution.

ANSYS Model

B.1 FEM Model of CBHA in ANSYS

FEM technique is a very popular and dependable technique for simulating the structural effects of force in a system. FEM model of the CBHA is generated to find the shape of the manipulator under different sets of input pressures. The FEM model is simulated in ANSYS 17.2 (Workbench) (Fig. B.1). The main components of FEM model are:

1. Geometry of manipulator

2. Mesh generation

3. Material assignment

4. Solving technique
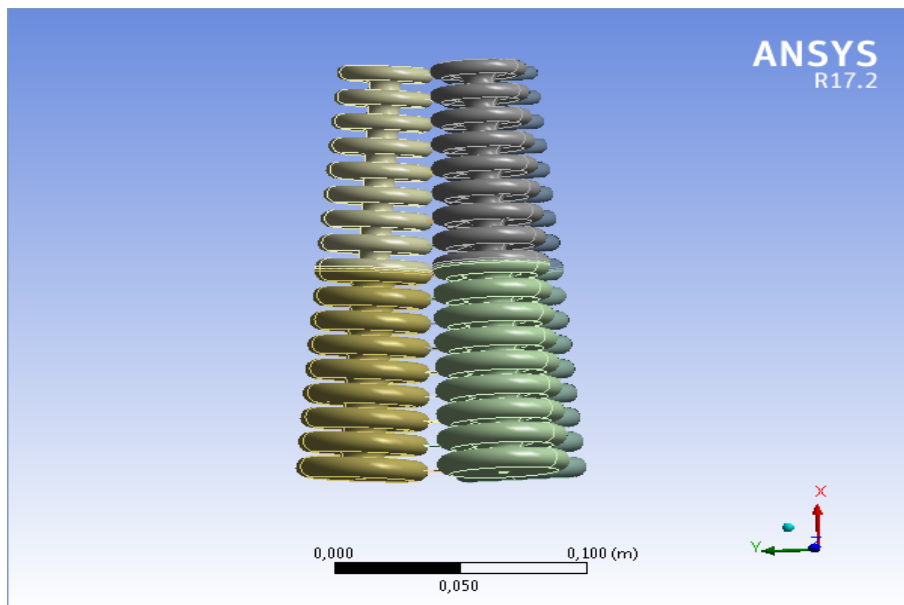
Figure B.1: Contact information between two sections

B.1.1   Contact information between two sections
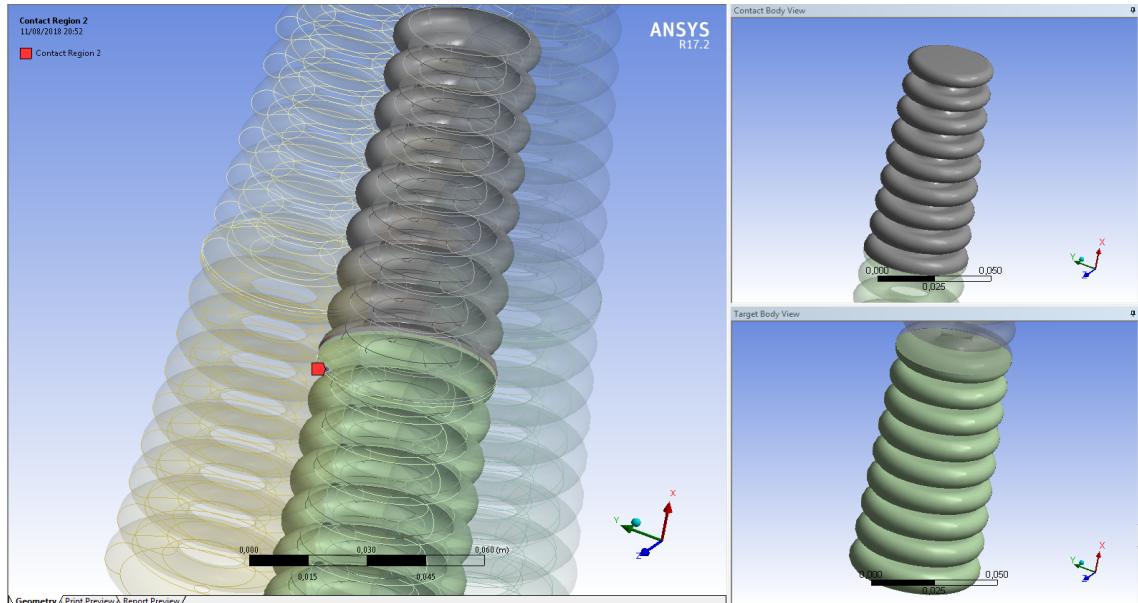
Figure B.2: Contact information between two sections

The manipulator is designed as a surface model in CATIA V5. Various bodies are modeled in design software and connected in ANSYS Design Modeller. The bodies can be divided in two categories:

1. Bellows

2. Connecting bodies

The bellows form the sections of the robots and are connected in series. As two bellows connected in series share contact surface which is retained in the surface model, this surface is used to create a bonded contact. The details of the contact are shown in Fig. B.2.

B.1.2   Connection of three tubes

Three bellows are connected in parallel to form one section of CBHA. However, the geometry looses the contact surface of the connecting bodies that fix them to the bellows. Therefore a line to surface mesh contact is generated. The contact is shown in fig. B.3.
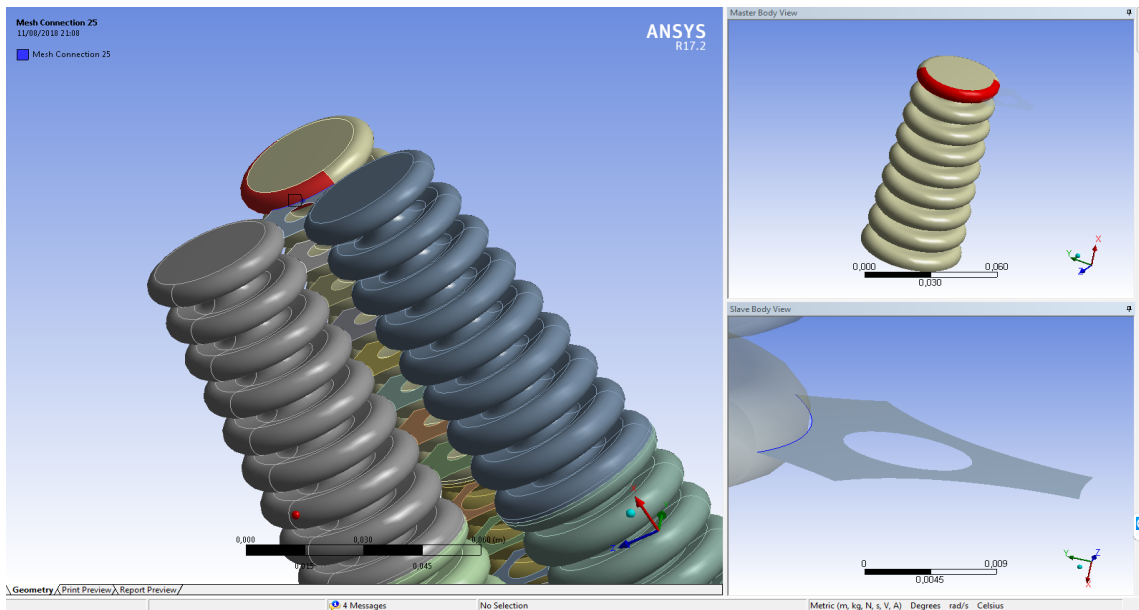
Figure B.3: Connection of three tubes

B.1.3 Material Properties

The nylon polymer used in the manufacturing of CBHA is a nonlinear material. Also most of the operation of CBHA occurs in the region beyond the elastic limit. Therefore linear analysis can not be used for the simulation. Material non- linearities are incorporated by considering the material as bilinear. The strength and other material properties are shown in Fig. B.4. The stress-strain curve of the resulting material is shown in Fig. B.5.

	A	B	C	D
1	Property	Value	Unit	⊗
2	Density	1200	kg m^-3	□
3	⊟ Isotropic Elasticity			□
4	Derive from	Young's Modulu...		
5	Young's Modulus	616	MPa	
6	Poisson's Ratio	0,3		
7	Bulk Modulus	5,1333E+08	Pa	
8	Shear Modulus	2,3692E+08	Pa	
9	⊟ Bilinear Isotropic Hardening			□
10	Yield Strength	27	MPa	
11	Tangent Modulus	6	MPa	
12	Tensile Ultimate Strength	41	MPa	□

Figure B.4: Material properties
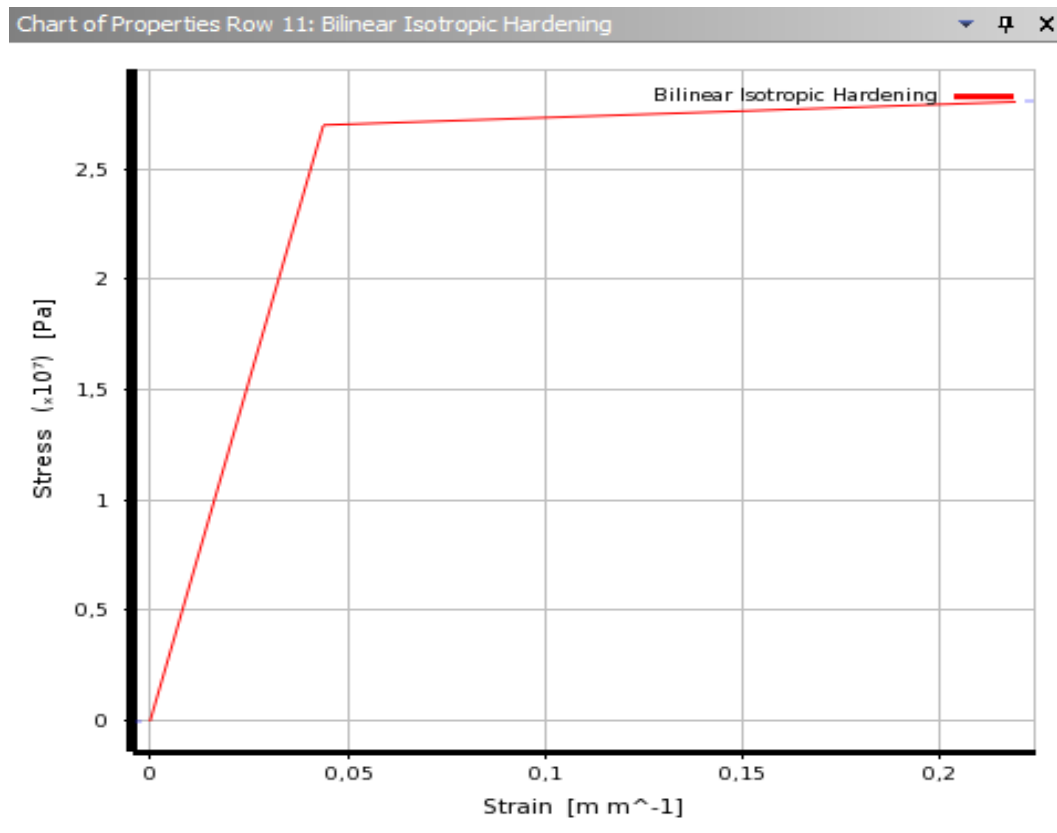
Figure B.5: Stress-strain curve

B.1.4   Mesh

As discussed previously, the bodies are approximated as surfaces so shell elements are used to create a discretized mesh for the structures. A combination of 4 node quad elements and 3 node triangular elements is used to create the mesh. The discretized mesh model of the manipulator is shown in Fig. B.6. To assure an error free approximation of the actual surfaces, Element Quality is used as a mesh metric. The quality shows that most of the elements used to construct the mesh model adhere to the good quality of the mesh, therefore the mesh model is selected without any further corrections.
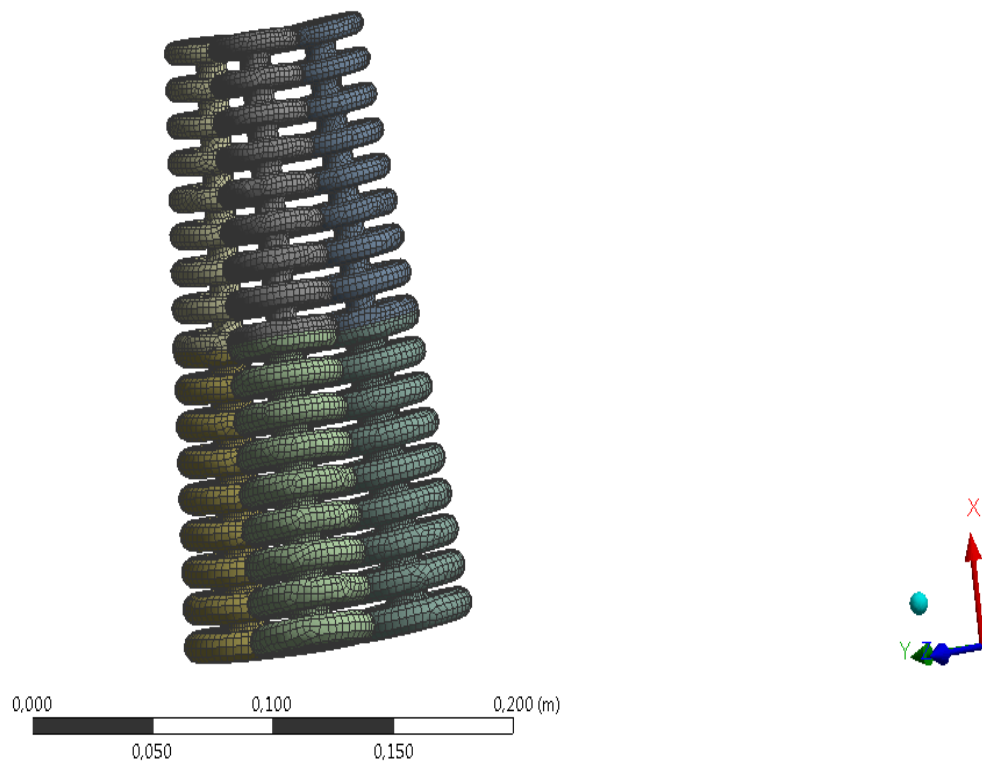
Figure B.6: Mesh generation

B.1.5 Detailing of Mesh

Figure B.7: Detailing of mesh

B.1.6   Input pressure graph of P_1

To simulate the model, one cycle of pressure is applied. A maximum pressure of 1.25 bar is applied to one bellow of the lower section over a time of 30 sec. The cycle is divided into 6 load steps of unequal duration. The load step details are tabulated in Fig. B.9.
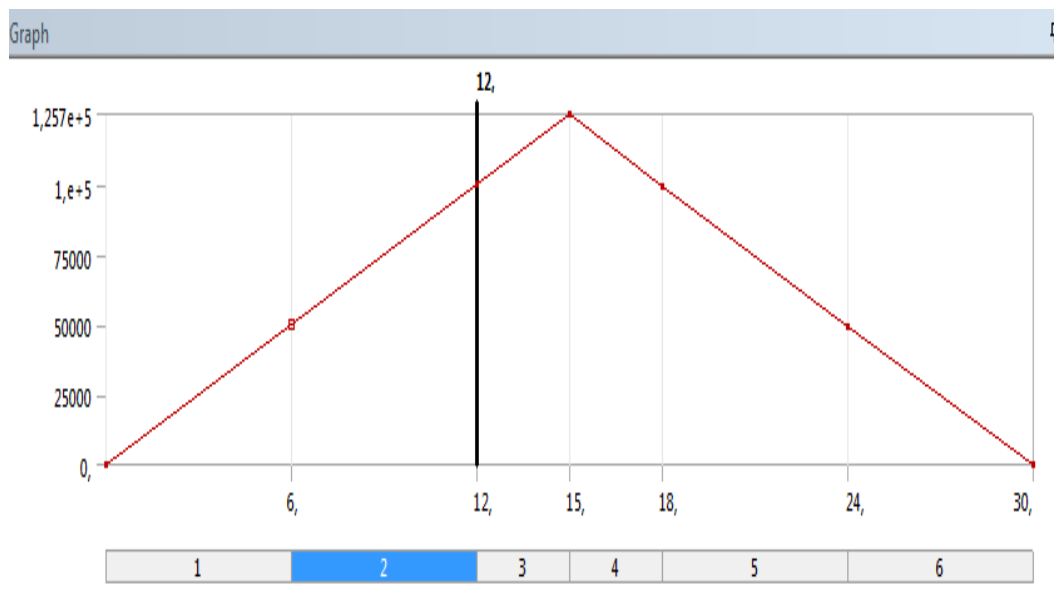
Figure B.8: Input pressure graph of P_1

Figure B.9: Steps of input pressure

B.1.7 Results of Deformation

C: Copy of Copy of Static Structural
Figure
Type: Total Deformation
Unit: m
Time: 15
11/08/2018 20:42

0,16859 Max
0,14985
0,13112
0,11239
0,093658
0,074927
0,056195
0,037463
0,018732
0 Min

0,000   0,100   0,200 (m)
   0,050   0,150
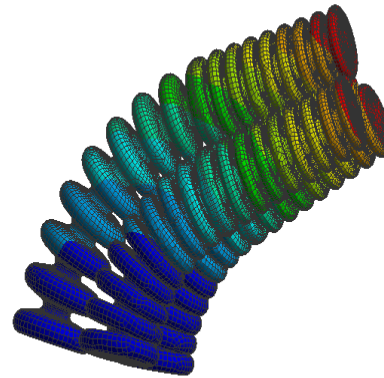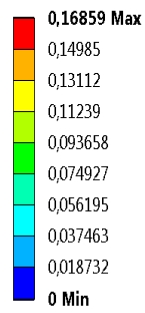
Figure B.10: Soft-continuum manipulator

Bibliography

[Abbas 2017] Ali Abbas and Jianguo Zhao. *Twisted and coiled sensor for shape estimation of soft robots*. In Intelligent Robots and Systems (IROS), 2017 IEEE/RSJ International Conference on, pages 482–487. IEEE, 2017. (Cited on page 19.)

[Alambeigi 2017] Farshid Alambeigi, Yu Wang, Shahriar Sefati, Cong Gao, Ryan J Murphy, Iulian Iordachita, Russell H Taylor, Harpal Khanuja and Mehran Armand. *A curved-drilling approach in core decompression of the femoral head osteonecrosis using a continuum manipulator*. IEEE Robotics and Automation Letters, vol. 2, no. 3, pages 1480–1487, 2017. (Cited on page 11.)

[Aleotti 2005] Jacopo Aleotti, Stefano Caselli and Giuliano Maccherozzi. *Trajectory reconstruction with nurbs curves for robot programming by demonstration*. In Computational Intelligence in Robotics and Automation, 2005. CIRA 2005. Proceedings. 2005 IEEE International Symposium on, pages 73–78. IEEE, 2005. (Cited on page 48.)

[Anderson 1967] Victor C Anderson. *Tensor arm manipulator design*. Trans. ASME, vol. 67, pages 1–12, 1967. (Cited on page 11.)

[Araújo 2001] FM Araújo, LA Ferreira, JL Santos and F Farahi. *Temperature and strain insensitive bending measurements with D-type fibre Bragg gratings*. Measurement Science and Technology, vol. 12, no. 7, page 829, 2001. (Cited on page 14.)

[Ataollahi 2017] Asghar Ataollahi, Kaspar Althoefer, Tobias Richard Schaeffter and Kawaldeep Rhode. *Continuum manipulator*, June 13 2017. US Patent 9,675,781. (Cited on page 14.)

[Bajo 2010] Andrea Bajo and Nabil Simaan. *Finding lost wrenches: Using continuum robots for contact detection and estimation of contact location*. In Robotics and Automation (ICRA), 2010 IEEE International Conference on, pages 3666–3673. IEEE, 2010. (Cited on page 11.)

[Bajo 2016] Andrea Bajo and Nabil Simaan. *Hybrid motion/force control of multi-backbone continuum robots*. The International journal of robotics research, vol. 35, no. 4, pages 422–434, 2016. (Cited on pages ix and 13.)

[Behrens 2012] Roland Behrens, Maik Poggendorf, Erik Schulenburg and Norbert Elkmann. *An elephant's trunk-inspired robotic arm-trajectory de-*

termination and control. In Robotics; Proceedings of ROBOTIK 2012; 7th German Conference on, pages 1–5. VDE, 2012. (Cited on page 11.)

[Berglund 2010] Tomas Berglund, Andrej Brodnik, Håkan Jonsson, Mats Staffanson and Inge Soderkvist. *Planning smooth and obstacle-avoiding B-spline paths for autonomous mining vehicles.* IEEE Transactions on Automation Science and Engineering, vol. 7, no. 1, pages 167–172, 2010. (Cited on page 44.)

[Bieze 2018] Thor Morales Bieze, Frederick Largilliere, Alexandre Kruszewski, Zhongkai Zhang, Rochdi Merzouki and Christian Duriez. *FEM-based kinematics and closed-loop control of soft, continuum manipulators.* 2018. (Cited on pages 6, 26, 91 and 92.)

[Böhm 1984] Wolfgang Böhm, Gerald Farin and Jürgen Kahmann. *A survey of curve and surface methods in CAGD.* Computer Aided Geometric Design, vol. 1, no. 1, pages 1–60, 1984. (Cited on page 42.)

[Bruyninckx 1997] Herman Bruyninckx and Dominiek Reynaerts. *Path planning for mobile and hyper-redundant robots using Pythagorean hodograph curves.* In Advanced Robotics, 1997. ICAR'97. Proceedings., 8th International Conference on, pages 595–600. IEEE, 1997. (Cited on page 48.)

[Burgner-Kahrs 2015] Jessica Burgner-Kahrs, D Caleb Rucker and Howie Choset. *Continuum robots for medical applications: A survey.* IEEE Transactions on Robotics, vol. 31, no. 6, pages 1261–1280, 2015. (Cited on pages 11 and 12.)

[Chawla 2018] Anant Chawla, Chase Frazelle and Ian Walker. *A Comparison of Constant Curvature Forward Kinematics for Multisection Continuum Manipulators.* In 2018 Second IEEE International Conference on Robotic Computing (IRC), pages 217–223. IEEE, 2018. (Cited on page 23.)

[Chen 2010] Xianfeng F Chen, Chi Zhang, David Webb, Kyriacos Kalli and Peng Gang-Ding. *Highly sensitive bend sensor based on Bragg grating in eccentric core polymer fiber.* IEEE Photonics Technology Letters, vol. 22, no. 11, 2010. (Cited on page 15.)

[Chirikjian 1994] Gregory S Chirikjian and Joel W Burdick. *A modal approach to hyper-redundant manipulator kinematics.* IEEE Transactions on Robotics and Automation, vol. 10, no. 3, pages 343–354, 1994. (Cited on pages ix and 20.)

[Chirikjian 2015] Gregory S Chirikjian. *Conformational modeling of continuum structures in robotics and structural biology: A review.* Advanced Robotics, vol. 29, no. 13, pages 817–829, 2015. (Cited on pages 14 and 23.)

[Choi 2002] Hyeong In Choi, Doo Seok Lee and Hwan Pyo Moon. *Clifford algebra, spin representation, and rational parameterization of curves and surfaces.* Advances in Computational Mathematics, vol. 17, no. 1-2, pages 5–48, 2002. (Cited on page 55.)

[Cianchetti 2013] Matteo Cianchetti, Tommaso Ranzani, Giada Gerboni, Iris De Falco, Cecilia Laschi and Arianna Menciassi. *STIFF-FLOP surgical manipulator: mechanical design and experimental characterization of the single module.* In Intelligent Robots and Systems (IROS), 2013 IEEE/RSJ International Conference on, pages 3576–3581. IEEE, 2013. (Cited on page 11.)

[Conrad 2013] Benjamin L Conrad, Jinwoo Jung, Ryan S Penning and Michael R Zinn. *Interleaved continuum-rigid manipulation: An augmented approach for robotic minimally-invasive flexible catheter-based procedures.* In Robotics and Automation (ICRA), 2013 IEEE International Conference on, pages 718–724. IEEE, 2013. (Cited on page 11.)

[Dahlquist 2008] G Dahlquist and A Björck. *Numerical Methods in Scientific Computing, ser.* Numerical Methods in Scientific Computing. Philadelphia, PA: Society for Industrial and Applied Mathematics (SIAM), vol. 1, 2008. (Cited on page 62.)

[De Boor 1962] Carl De Boor. *Bicubic spline interpolation.* Journal of mathematics and physics, vol. 41, no. 1-4, pages 212–218, 1962. (Cited on page 39.)

[Dietz 1993] Roland Dietz, Josef Hoschek and Bert Jüttler. *An algebraic approach to curves and surfaces on the sphere and on other quadrics.* Computer Aided Geometric Design, vol. 10, no. 3-4, pages 211–229, 1993. (Cited on page 50.)

[Elbanhawi 2015] Mohamed Elbanhawi, Milan Simic and Reza N Jazar. *Continuous path smoothing for car-like robots using B-spline curves.* Journal of Intelligent & Robotic Systems, vol. 80, no. 1, pages 23–56, 2015. (Cited on page 44.)

[Escande 2015] Coralie Escande, Taha Chettibi, Rochdi Merzouki, Vincent Coelen and Pushparaj Mani Pathak. *Kinematic calibration of a multisection bionic manipulator.* IEEE/ASME transactions on mechatron-

ics, vol. 20, no. 2, pages 663–674, 2015. (Cited on pages ix, 6, 24, 25, 26, 91 and 104.)

[Farin 1987] Gerald Farin, Gerhard Rein, Nikolas Sapidis and Andrew J Worsey. *Fairing cubic B-spline curves.* Computer Aided Geometric Design, vol. 4, no. 1-2, pages 91–103, 1987. (Cited on page 44.)

[Farin 2000] Gerald Farin and Dianne Hansford. The essentials of cagd. AK Peters/CRC Press, 2000. (Cited on page 42.)

[Farin 2002] Gerald Farin. *A history of curves and surfaces.* Handbook of computer aided geometric design, vol. 1, 2002. (Cited on page 42.)

[Farouki 1990] Rida T Farouki and Takis Sakkalis. *Pythagorean hodographs.* IBM Journal of Research and Development, vol. 34, no. 5, pages 736–752, 1990. (Cited on pages 48, 51 and 54.)

[Farouki 1995] Rida T Farouki and C Andrew Neff. *Hermite interpolation by Pythagorean hodograph quintics.* Mathematics of computation, vol. 64, no. 212, pages 1589–1609, 1995. (Cited on pages 51 and 54.)

[Farouki 1996] Rida T Farouki. *The elastic bending energy of Pythagorean-hodograph curves.* Computer Aided Geometric Design, vol. 13, no. 3, pages 227–241, 1996. (Cited on page 59.)

[Farouki 2002] Rida T Farouki, Mohammad al Kandari and Takis Sakkalis. *Hermite interpolation by rotation-invariant spatial Pythagorean-hodograph curves.* Advances in Computational Mathematics, vol. 17, no. 4, pages 369–383, 2002. (Cited on pages 53, 56, 57 and 59.)

[Farouki 2008] Rida T Farouki. Pythagorean-hodograph curves. Springer, 2008. (Cited on pages 3, 49, 53, 56, 60, 125 and 126.)

[Farvardin 2016] Amirhossein Farvardin, Ryan J Murphy, Robert B Grupp, Iulian Iordachita and Mehran Armand. *Towards real-time shape sensing of continuum manipulators utilizing fiber bragg grating sensors.* In Biomedical Robotics and Biomechatronics (BioRob), 2016 6th IEEE International Conference on, pages 1180–1185. IEEE, 2016. (Cited on page 16.)

[fes 2018] *Website of the Festo subsidiary : Festo-Didactic*, 2018. (Cited on pages 3 and 63.)

[Fraś 2015] J Fraś, Jan Czarnowski, M Maciaś, J Główka, Matteo Cianchetti and Arianna Menciassi. *New STIFF-FLOP module construction idea for improved actuation and sensing.* In Robotics and Automation (ICRA), 2015 IEEE International Conference on, pages 2901–2906. IEEE, 2015. (Cited on page 11.)

[Fraś 2016] Jan Fraś, Sebastain Tabaka and Jan Czarnowski. *Visual Marker Based Shape Recognition System for Continuum Manipulators*. In Challenges in Automation, Robotics and Measurement Techniques, pages 435–445. Springer, 2016. (Cited on pages ix and 18.)

[Fraś 2017] Jan Fraś. *Depth-Map-Based Shape Recognition of Soft Continuum Manipulator Body*. In International Conference Automation, pages 300–307. Springer, 2017. (Cited on pages ix, 16 and 17.)

[Gasca 2000] Mariano Gasca and Thomas Sauer. *Polynomial interpolation in several variables*. Advances in Computational Mathematics, vol. 12, no. 4, page 377, 2000. (Cited on page 39.)

[Godage 2011] Isuru S Godage, Emanuele Guglielmino, David T Branson, Gustavo A Medrano-Cerda and Darwin G Caldwell. *Novel modal approach for kinematics of multisection continuum arms*. In Intelligent Robots and Systems (IROS), 2011 IEEE/RSJ International Conference on, pages 1093–1098. IEEE, 2011. (Cited on page 23.)

[Gordon 1974] William J Gordon and Richard F Riesenfeld. *Bernstein-Bézier methods for the computer-aided design of free-form curves and surfaces*. Journal of the ACM (JACM), vol. 21, no. 2, pages 293–310, 1974. (Cited on page 42.)

[Gravagne 2000] Ian A Gravagne and Ian D Walker. *Kinematic transformations for remotely-actuated planar continuum robots*. In Robotics and Automation, 2000. Proceedings. ICRA'00. IEEE International Conference on, volume 1, pages 19–26. IEEE, 2000. (Cited on page 19.)

[Gravagne 2001] Ian A Gravagne, Christopher D Rahn and Ian D Walker. *Good vibrations: a vibration damping setpoint controller for continuum robots*. In Robotics and Automation, 2001. Proceedings 2001 ICRA. IEEE International Conference on, volume 4, pages 3877–3884. IEEE, 2001. (Cited on pages ix and 13.)

[Grzesiak 2011] Andrzej Grzesiak, Ralf Becker and Alexander Verl. *The bionic handling assistant: a success story of additive manufacturing*. Assembly Automation, vol. 31, no. 4, pages 329–333, 2011. (Cited on page 64.)

[Hamilton 1844] William Rowan Hamilton. *Ii. on quaternions; or on a new system of imaginaries in algebra*. The London, Edinburgh, and Dublin Philosophical Magazine and Journal of Science, vol. 25, no. 163, pages 10–13, 1844. (Cited on page 123.)

[Hannan 2005] Michael W Hannan and Ian D Walker. *Real-time shape estimation for continuum robots using vision.* Robotica, vol. 23, no. 5, pages 645–651, 2005. (Cited on pages ix, 16 and 17.)

[Hashemian 2017] Ali Hashemian, Seyed Farhad Hosseini and S Nader Nabavi. *Kinematically smoothing trajectories by NURBS reparameterization–an innovative approach.* Advanced Robotics, vol. 31, no. 23-24, pages 1296–1312, 2017. (Cited on page 48.)

[Hirose 2004] Shigeo Hirose and Makoto Mori. *Biologically inspired snake-like robots.* In Robotics and Biomimetics, 2004. ROBIO 2004. IEEE International Conference on, pages 1–7. IEEE, 2004. (Cited on page 10.)

[Hornik 1989] Kurt Hornik, Maxwell Stinchcombe and Halbert White. *Multilayer feedforward networks are universal approximators.* Neural networks, vol. 2, no. 5, pages 359–366, 1989. (Cited on page 98.)

[Immega 1995] Guy Immega and Keith Antonelli. *The KSI tentacle manipulator.* In Robotics and Automation, 1995. Proceedings., 1995 IEEE International Conference on, volume 3, pages 3149–3154. IEEE, 1995. (Cited on pages ix and 13.)

[Jalel 2015] Sawssen Jalel, Philippe Marthon and Atef Hamouda. *Optimized NURBS Curves Modelling Using Genetic Algorithm for Mobile Robot Navigation.* In International Conference on Computer Analysis of Images and Patterns, pages 534–545. Springer, 2015. (Cited on page 48.)

[Jolly 2009] KG Jolly, R Sreerama Kumar and R Vijayakumar. *A Bezier curve based path planning in a multi-agent robot soccer system without violating the acceleration limits.* Robotics and Autonomous Systems, vol. 57, no. 1, pages 23–33, 2009. (Cited on page 42.)

[Jones 2006] Bryan A Jones and Ian D Walker. *Three-dimensional modeling and display of continuum robots.* In Intelligent Robots and Systems, 2006 IEEE/RSJ International Conference on, pages 5872–5877. IEEE, 2006. (Cited on pages ix, 21 and 22.)

[Jordan 1992] Michael I Jordan and David E Rumelhart. *Forward models: Supervised learning with a distal teacher.* Cognitive science, vol. 16, no. 3, pages 307–354, 1992. (Cited on page 23.)

[Kato 2013] Takahisa Kato, Ichiro Okumura, Sang-Eun Song and Nobuhiko Hata. *Multi-section continuum robot for endoscopic surgical clipping of intracranial aneurysms.* In International Conference on Medical Image Computing and Computer-Assisted Intervention, pages 364–371. Springer, 2013. (Cited on pages ix and 11.)

[Kato 2016] Takahisa Kato, Ichiro Okumura, Hidekazu Kose, Kiyoshi Takagi and Nobuhiko Hata. *Tendon-driven continuum robot for neuroendoscopy: validation of extended kinematic mapping for hysteresis operation*. International journal of computer assisted radiology and surgery, vol. 11, no. 4, pages 589–602, 2016. (Cited on pages ix and 13.)

[Keys 1981] Robert Keys. *Cubic convolution interpolation for digital image processing*. IEEE transactions on acoustics, speech, and signal processing, vol. 29, no. 6, pages 1153–1160, 1981. (Cited on page 39.)

[Komoriya 1989] Kiyoshi Komoriya and Kazuo Tanie. *Trajectory design and control of a wheel-type mobile robot using B-spline curve*. In Intelligent Robots and Systems' 89. The Autonomous Mobile Robots and Its Applications. IROS'89. Proceedings., IEEE/RSJ International Workshop on, pages 398–405. IEEE, 1989. (Cited on page 44.)

[Lakhal 2016] Othman Lakhal, Achille Melingui and Rochdi Merzouki. *Hybrid approach for modeling and solving of kinematics of a compact bionic handling assistant manipulator*. IEEE/ASME Transactions on Mechatronics, vol. 21, no. 3, pages 1326–1335, 2016. (Cited on pages ix, 6, 28, 30, 31, 91, 92, 93 and 104.)

[Lekkas 2014] Anastasios M Lekkas and Thor I Fossen. *Integral LOS path following for curved paths based on a monotone cubic Hermite spline parametrization*. IEEE Transactions on Control Systems Technology, vol. 22, no. 6, pages 2287–2301, 2014. (Cited on page 39.)

[Li 2017] Jinglin Li, Zhou Teng and Jing Xiao. *Can a continuum manipulator fetch an object in an unknown cluttered space?* IEEE Robotics and Automation Letters, vol. 2, no. 1, pages 2–9, 2017. (Cited on page 11.)

[Liming 1944] Roy A Liming. *Practical analytic geometry with applications to aircraft*. Macmillan, 1944. (Cited on page 39.)

[Liu 2015] Hao Liu, Amirhossein Farvardin, Sahba Aghajani Pedram, Iulian Iordachita, Russell H Taylor and Mehran Armand. *Large deflection shape sensing of a continuum manipulator for minimally-invasive surgery*. In IEEE International Conference on Robotics and Automation: ICRA:[proceedings] IEEE International Conference on Robotics and Automation, volume 2015, page 201. NIH Public Access, 2015. (Cited on pages ix and 16.)

[MacPherson 2006] William N MacPherson, M Silva-Lopez, James S Barton, AJ Moore, JDC Jones, D Zhao, Lin Zhang, Ian Bennion, Nicole Metje,

DN Chapman *et al. Tunnel monitoring using multicore fibre displacement sensor.* Measurement Science and Technology, vol. 17, no. 5, page 1180, 2006. (Cited on page 14.)

[Mahl 2014] Tobias Mahl, Alexander Hildebrandt and Oliver Sawodny. *A variable curvature continuum kinematics for kinematic control of the bionic handling assistant.* IEEE transactions on robotics, vol. 30, no. 4, pages 935–949, 2014. (Cited on page 27.)

[Mahoney 2016] Arthur W Mahoney, Patrick L Anderson, Philip J Swaney, Fabien Maldonado and Robert J Webster. *Reconfigurable parallel continuum robots for incisionless surgery.* In Intelligent Robots and Systems (IROS), 2016 IEEE/RSJ International Conference on, pages 4330–4336. IEEE, 2016. (Cited on page 11.)

[Melingui 2015] Achille Melingui, Othman Lakhal, Boubaker Daachi, Jean Bosco Mbede and Rochdi Merzouki. *Adaptive neural network control of a compact bionic handling arm.* IEEE/ASME Transactions on Mechatronics, vol. 20, no. 6, pages 2862–2875, 2015. (Cited on pages 6, 23 and 24.)

[Mochiyama 1998] Hiromi Mochiyama, Etsujiro Shimemura and Hisato Kobayashi. *Shape correspondence between a spatial curve and a manipulator with hyper degrees of freedom.* In Intelligent Robots and Systems, 1998. Proceedings., 1998 IEEE/RSJ International Conference on, volume 1, pages 161–166. IEEE, 1998. (Cited on pages ix, 19 and 20.)

[Orekhov 2016] Andrew L Orekhov, Caroline B Black, John Till, Scotty Chung and D Caleb Rucker. *Analysis and validation of a teleoperated surgical parallel continuum manipulator.* IEEE Robotics and Automation Letters, vol. 1, no. 2, pages 828–835, 2016. (Cited on page 11.)

[Qu 2016] Tingyu Qu, Jie Chen, Shen Shen, Zhen Xiao, Zhe Yue and Henry YK Lau. *Motion control of a bio-inspired wire-driven multibackbone continuum minimally invasive surgical manipulator.* In Robotics and Biomimetics (ROBIO), 2016 IEEE International Conference on, pages 1989–1995. IEEE, 2016. (Cited on page 11.)

[Robinson 1999] Graham Robinson and J Bruce C Davies. *Continuum robots - a state of the art.* In Robotics and Automation, 1999. Proceedings. 1999 IEEE International Conference on, volume 4, pages 2849–2854. IEEE, 1999. (Cited on page 11.)

[Roesthuis 2014] Roy J Roesthuis, Marco Kemp, John J van den Dobbelsteen and Sarthak Misra. *Three-dimensional needle shape reconstruction using an array of fiber bragg grating sensors.* IEEE/ASME transactions

on mechatronics, vol. 19, no. 4, pages 1115–1126, 2014. (Cited on page 15.)

[Roesthuis 2016] Roy J Roesthuis and Sarthak Misra. *Steering of multi-segment continuum manipulators using rigid-link modeling and FBG-based shape sensing*. IEEE transactions on robotics, vol. 32, no. 2, pages 372–382, 2016. (Cited on pages ix and 21.)

[Rolf 2012] Matthias Rolf and Jochen J Steil. *Constant curvature continuum kinematics as fast approximate model for the Bionic Handling Assistant*. In Intelligent Robots and Systems (IROS), 2012 IEEE/RSJ International Conference on, pages 3440–3446. IEEE, 2012. (Cited on pages ix, 13, 26 and 28.)

[Rolf 2014] Matthias Rolf and Jochen J Steil. *Efficient exploratory learning of inverse kinematics on a bionic elephant trunk*. IEEE transactions on neural networks and learning systems, vol. 25, no. 6, pages 1147–1160, 2014. (Cited on page 24.)

[Schoenberg 1969] IJ Schoenberg. *Cardinal interpolation and spline functions*. Journal of Approximation theory, vol. 2, no. 2, pages 167–206, 1969. (Cited on page 39.)

[Searle 2013] Thomas C Searle, Kaspar Althoefer, Lakmal Seneviratne and Hongbin Liu. *An optical curvature sensor for flexible manipulators*. In Robotics and Automation (ICRA), 2013 IEEE International Conference on, pages 4415–4420. IEEE, 2013. (Cited on page 18.)

[Shah 2010] MA Shah and N Aouf. *3d cooperative pythagorean hodograph path planning and obstacle avoidance for multiple uavs*. In Cybernetic Intelligent Systems (CIS), 2010 IEEE 9th International Conference on, pages 1–6. IEEE, 2010. (Cited on page 48.)

[Shanmugavel 2007] Madhavan Shanmugavel, Antonios Tsourdos, Rafal Zbikowski and Brian White. *3D path planning for multiple UAVs using Pythagorean hodograph curves*. In AIAA Guidance, navigation and control conference and exhibit, page 6455, 2007. (Cited on page 48.)

[Siciliano 2016] Bruno Siciliano and Oussama Khatib. Springer handbook of robotics. Springer, 2016. (Cited on page 10.)

[Singh 2017] Inderjeet Singh, Othman Lakhal, Yacine Amara, Vincent Coelen, Pushparaj Mani Pathak and Rochdi Merzouki. *Performances evaluation of inverse kinematic models of a compact bionic handling assistant*. In Robotics and Biomimetics (ROBIO), 2017 IEEE International Conference on, pages 264–269. IEEE, 2017. (Cited on pages 26, 91, 92 and 93.)

[Škrjanc 2010] Igor Škrjanc and Gregor Klančar. *Optimal cooperative collision avoidance between multiple robots based on Bernstein–Bézier curves*. Robotics and Autonomous systems, vol. 58, no. 1, pages 1–9, 2010. (Cited on page 42.)

[Song 2010] Baoye Song, Guohui Tian and Fengyu Zhou. *A comparison study on path smoothing algorithms for laser robot navigated mobile robot path planning in intelligent space*. Journal of Information and Computational Science, vol. 7, no. 1, pages 2943–2950, 2010. (Cited on page 83.)

[Song 2015a] Shuang Song, Zheng Li, Max Q-H Meng, Haoyong Yu and Hongliang Ren. *Real-time shape estimation for wire-driven flexible robots with multiple bending sections based on quadratic Bezier curves*. IEEE Sensors Journal, vol. 15, no. 11, pages 6326–6334, 2015. (Cited on pages 18, 63 and 83.)

[Song 2015b] Shuang Song, Zheng Li, Haoyong Yu and Hongliang Ren. *Electromagnetic positioning for tip tracking and shape sensing of flexible robots*. IEEE Sensors Journal, vol. 15, no. 8, pages 4565–4575, 2015. (Cited on pages 18 and 42.)

[Spooner 2002] Jeffrey T Spooner, Manfredi Maggiore, Raul Ordonez and Kevin M Passino. Frontmatter and index. Wiley Online Library, 2002. (Cited on page 98.)

[Su 2012] Benyue Su and Liping Zou. *Manipulator trajectory planning based on the algebraic-trigonometric hermite blended interpolation spline*. Procedia Engineering, vol. 29, pages 2093–2097, 2012. (Cited on page 39.)

[Tonapi 2014] Manas M Tonapi, Isuru S Godage and Ian D Walker. *Next generation rope-like robot for in-space inspection*. In Aerospace Conference, 2014 IEEE, pages 1–13. IEEE, 2014. (Cited on page 11.)

[Trivedi 2014] Deepak Trivedi and Christopher D Rahn. *Model-based shape estimation for soft robotic manipulators: The planar case*. Journal of Mechanisms and Robotics, vol. 6, no. 2, page 021005, 2014. (Cited on page 18.)

[Unser 1993] Michael Unser, Akram Aldroubi, Murray Eden *et al.* *B-Spline Signal Processing: Part I Theory*. IEEE transactions on signal processing, vol. 41, no. 2, pages 821–833, 1993. (Cited on page 44.)

[Vandini 2017] Alessandro Vandini, Christos Bergeles, Ben Glocker, Petros Giataganas and Guang-Zhong Yang. *Unified tracking and shape es-*

timation for concentric tube robots. IEEE Transactions on Robotics, vol. 33, no. 4, pages 901–915, 2017. (Cited on page 16.)

[Vujović 2016] Milica Vujović, Aleksandar Rodić and Ilija Stevanović. *Design of Modular Re-configurable Robotic System for Construction and Digital Fabrication*. In International Conference on Robotics in Alpe-Adria Danube Region, pages 550–559. Springer, 2016. (Cited on pages ix and 10.)

[Wagner 2010] Petr Wagner, Jiri Kotzian, Jan Kordas and Viktor Michna. *Path planning and tracking for robots based on cubic hermite splines in real-time*. In Emerging Technologies and Factory Automation (ETFA), 2010 IEEE Conference on, pages 1–8. IEEE, 2010. (Cited on page 39.)

[Walker 2013] Ian D Walker. *Continuous backbone "continuum" robot manipulators*. Isrn robotics, vol. 2013, 2013. (Cited on pages ix, 10 and 23.)

[Wang 2017] Jie Wang, Yi Lu, Changchun Zhang, Shuang Song and Max Q-H Meng. *Pilot study on shape sensing for continuum tubular robot with multi-magnet tracking algorithm*. In Robotics and Biomimetics (ROBIO), 2017 IEEE International Conference on, pages 1165–1170. IEEE, 2017. (Cited on page 18.)

[Webster III 2010] Robert J Webster III and Bryan A Jones. *Design and kinematic modeling of constant curvature continuum robots: A review*. The International Journal of Robotics Research, vol. 29, no. 13, pages 1661–1683, 2010. (Cited on page 23.)

[Wilkening 2017] Paul Wilkening, Farshid Alambeigi, Ryan J Murphy, Russell H Taylor and Mehran Armand. *Development and experimental evaluation of concurrent control of a robotic arm and continuum manipulator for osteolytic lesion treatment*. IEEE robotics and automation letters, vol. 2, no. 3, pages 1625–1631, 2017. (Cited on page 11.)

[Yang 2013] Gil Jin Yang and Byoung Wook Choi. *Smooth trajectory planning along Bezier curve for mobile robots with velocity constraints*. International Journal of Control and Automation, vol. 6, no. 2, pages 225–234, 2013. (Cited on page 42.)

[Yi 2007] Xinhua Yi, Jinwu Qian, Linyong Shen, Yanan Zhang and Zhen Zhang. *An innovative 3D colonoscope shape sensing sensor based on FBG sensor array*. In Information Acquisition, 2007. ICIA'07. International Conference on, pages 227–232. IEEE, 2007. (Cited on page 15.)

[Zeid 2004] Ibrahim Zeid. *Mastering cad/cam with engineering subscription card*. McGraw-Hill Science/Engineering/Math, 2004. (Cited on pages 35 and 48.)

[Zhao 2010] Qiang Zhao and Fang Gao. *Design and analysis of a kind of biomimetic continuum robot.* In Robotics and Biomimetics (ROBIO), 2010 IEEE International Conference on, pages 1316–1320. IEEE, 2010. (Cited on pages 4 and 11.)

[Zheng 2014] Tianjiang Zheng, Yawei Yang, David T Branson, Rongjie Kang, Emanuele Guglielmino, Matteo Cianchetti, Darwin G Caldwell and Guilin Yang. *Control design of shape memory alloy based multi-arm continuum robot inspired by octopus.* In Industrial Electronics and Applications (ICIEA), 2014 IEEE 9th Conference on, pages 1108–1113. IEEE, 2014. (Cited on pages 4 and 11.)

Curve Based Approach for Shape Reconstruction of Continuum Manipulators

Abstract: This work provides a new methodology to reconstruct the shape of continuum manipulators using a curve based approach. Pythagorean Hodograph (PH) curves are used to reconstruct the optimal shape of continuum manipulators using minimum potential energy (bending and twisting energy) criteria. This methodology allows us to obtain the optimal kinematics of continuum manipulators. The models are applied to a continuum manipulator, namely, the Compact Bionic Handling Assistant (CBHA) for experimental validation under free load manipulation. The calibration of the PH-based shape reconstruction methodology is performed to improve its accuracy to accommodate the uncertainties due to the structure of the manipulator. The proposed method is also tested under the loaded manipulation after combining it with a qualitative Neural Network approach. Furthermore, the PH-based methodology is extended to model multi-section heterogeneous bodies. This model is experimentally validated for a closed loop kinematic chain formed using two CBHA manipulating jointly a rope.
Keywords: Continuum manipulators, Shape reconstruction, Pythagorean Hodograph, Continuum kinematics.

Modélisation par des courbes pour la reconstruction des formes de manipulateurs continuums

Résumé: Ce travail de thèse propose une nouvelle méthode de modélisation et de reconstruction de la forme d'une classe de manipulateurs continuum, basée sur la géométrie des courbes. Les Hodographes Pythagoriens (courbes HP) sont utilisées pour reconstruire des formes optimales pour ce type de robots, par une optimisation des énergies potentielles de flexion et de torsion. Cette méthode nous permis de déduire la cinématique optimale des bras manipulateurs continuum. La validation de la méthode proposée a été réalisée sur le robot dit trompe d'éléphant 'Compact Bionic Handling Assistant (CBHA)'. Une calibration a été réalisée sur la méthode de reconstruction afin d'améliorer les performances en terme de précision et de prendre en considération les incertitudes dues à la structure du bras manipulateur. La méthode proposée est également testée dans le cas de la préhension, en s'appuyant sur une approche qualitative à base de réseaux de neurones. De plus, l'approche HP est étendue à la modélisation des structures de robots hétérogènes avec plusieurs sections. Ce dernier a été validé pour une chaîne cinématique fermée, composée de deux manipulateurs CBHA, manipulant conjointement une corde flexible.
Mots clés: Manipulateurs continuums, Reconstruction des formes, Pythagorean Hodograph, Cinématiques continuums.